Investigating the effects of climate change and sea level rise on the coastal processes of the Beaufort Sea, Yukon Territory

by

Jennifer Turner

Department of Geography, McGill University, Montreal
June 2004

A thesis submitted to McGill University in partial fulfillment of the requirements of the degree of Master of Science

Your file Votre référence
ISBN: 0-494-06464-1
Our file Notre référence
ISBN: 0-494-06464-1

ABSTRACT

High latitude areas have been identified in most GCMs as regions where global warming will appear earliest and be the greatest. Since much of Canada's north is underlain by permafrost, a warming of 3-5°C could cause widespread erosion and thermokarst. The Arctic coastal zone is particularly vulnerable, as it lies at the interface between terrestrial systems dominated by permafrost, and marine systems dominated by sea ice and wave action. This study aims at understanding some mechanisms of arctic coastal erosion, such as thermoerosional niches and block failure. The final goal of this research is to identify the areas of Herschel Island, Yukon Territory, which are likely to experience the greatest magnitude of change in the near future. This information is then coupled with a climate change scenario in order to predict future coastal erosion in the area.

RÉSUMÉ

Les hautes latitudes ont été identifiées par la plupart des modèles de circulation climatique comme les régions où le réchauffement climatique sera le plus important et le plus rapide. Le nord du Canada étant majoritairement une zone de pergélisol, un réchauffement de 3°C à 5°C pourrait entraîner de vastes dynamiques d'érosion et de thermokarst. La zone côtière arctique y est particulièrement vulnérable, se trouvant à l'interface entre les systèmes terrestres dominés par le pergélisol, et les systèmes marins dominés par la glace de mer et l'action des vagues. Cette étude vise à décrire et comprendre certains mécanismes de l'érosion côtière en milieu arctique, tels que l'écroulement de blocs et la thermo-érosion. L'objectif final de cette recherche étant d'identifier les régions de l'île d' Herschel, territoire du Yukon, qui sont susceptibles d'éprouver le plus grand changement à court terme. Cette information sera alors couplée à un scénario de changement climatique afin de prévoir la future érosion côtière dans le secteur.

ACKNOWLEDGEMENTS

During the preparation and writing of this thesis, numerous people have lent me their guidance and assistance. To all of you who helped me get through the past two years, I would like to acknowledge the time you spent with me, the knowledge you shared with me, and the support you gave me when I needed it most.

Foremost, I would like to thank my supervisor Dr. Wayne Pollard for his patience, wisdom, and understanding over the past two years. Wayne has shared with me both his love of – and enthusiasm for – working in the Arctic landscape, and it is something that I hope to impart to others in my future endeavours. He was also instrumental in providing me with the means to travel to my field site on Herschel Island, where I was able to truly appreciate the beauty inherent in the northern landscape.

To those organizations that contributed funding for this research: McGill University (Eben Hopson Bursary/Award for Study at McGill), the McGill Institute for the Study of Canada (Banque Nationale Master's Fellowship), the McGill Centre for Climate and Global Change Research (C^2GCR), the Arctic Institute of North America (Grants-in-Aid), the Department of Indian and Northern Affairs (Northern Scientific Training Program), and the Aurora Research Institute in Inuvik, NWT, for laboratory support and use of equipment while I was in the field.

I would also like to thank my other committee member, Michel Lapointe, for his suggestions regarding my thesis; Steven Solomon and David Atkinson of the Atlantic Division of the Geological Survey of Canada for their many insightful suggestions throughout my research. Thank you as well to Curt Dixon and David Willis for painstakingly finding datasets and bathymetric maps that were useful for this work. Md. Azharul Hoque (or just Hoque) was indispensable during the numerical modeling stage, and Hugues Lantuit was a good person to have around for both fieldwork and the creation of a GIS map of Herschel Island (and some really good laughs along the way). My fieldwork could not have been completed without the help and guidance of Nicole Couture – thank you for all your suggestions and insight.

To my fellow graduate students in the Department of Geography, I want to thank you for lending sympathy during the "downs" (especially to Jamie), and for partying with me during all the "ups". I'm glad that something good came out of my computer crashing at the beginning of my degree (Delia learned the importance of making backups – and so did I!) Barcelona was a blast (Tim, Hugues and Greg), and I'll carry those memories with me forever. A special "thank you" to Camellia Ibrahim, who was always making me laugh with her crazy antics during the summer of 2003, and who gave me expert advice for how to survive the "thesis crunch", and to Chad Davey who made BH 427 a really great place to work. To team "Geogs" (later known as the "Scramblers") – thanks for all the awesome co-rec volleyball games (especially Dana's dancing)! Simon... words can't express how much I've appreciated your companionship over the last 8 months. Thank you for listening when I needed someone to talk to, and for lending me your shoulder when I was so tired that I didn't think I'd be able to go on. To anyone else I haven't mentioned... it's not because you've been forgotten. Thank you.

I'd also like to thank the administrative staff of the Geography Department. Maria, I missed you while you were away (the department nearly fell apart!) and I'm glad that you're back. I've enjoyed all of our discussions over the past two years, and appreciated your advice during the crazy submittal process. Thank you also to Angie Mansi, Paul Wrigglesworth, Gordon Ewing and George Wenzel for your support and guidance.

Finally, and most importantly, thanks go to my family. Without your unconditional support over the past two years, I would have never completed this degree. To my parents, you are a source of inspiration to me. Your love and patience has, at times, been the only thing that has kept me going. You have taught me that pride in myself is more important than seeking approval from others, and (besides my thesis), that may be the most important lesson I have learned over the past two years. Even though these words do not begin to express my gratitude for everything you have done for me – *thank you.*

TABLE OF CONTENTS

LIST OF FIGURES

LIST OF TABLES

NOTATION

A	parameter related to equilibrium beach profiles [$\approx 0.1\ m^{1/3}$ for sand]
a	empirical parameter for wave-induced melting [0.5 for unidirectional flow]
B	thickness of the unfrozen beach sediment [$B = B_b$ at $t = 0$]
B_b	initial thickness of the unfrozen beach sediment [m]
B_c	initial thickness of the unfrozen cliff sediment [m]
C_w	volumetric heat capacity of the seawater
D	vertical melting depth of the frozen beach sediment (m)
d	depth of water (feet)
d_b	fixed seaward boundary before the storm [0.04 m]
d_c	still water depth at the toe of the cliff [$d_c = (S + d_b + E - W \cdot \tan\theta_b)$]
d_r	wave depth [m]
E	total vertical eroded depth on the beach [$E = (B_b - B + D)$]
F	parameter depending on whether the turbulent boundary layer flow is hydraulically smooth or fully rough
$\hat{F}$	available fetch (miles)
f_w	wave friction factor at the melting surface
H	cliff height above its toe [$H = (H_c + d_b + E - W \cdot \tan\theta_b)$]
h_b	convective heat transfer coefficient on the exposed frozen beach sediment [$J/(s \cdot m^2 \cdot °C)$]
H_c	height of the cliff above MSL [m]
h_c	convective heat transfer coefficient on the exposed frozen cliff sediment [$J/(s \cdot m^2 \cdot °C)$] between T_w and L_c
h'_c	critical depth for deep slips [m]
H_r	wave height [m]
k_b	equivalent sand roughness of the frozen beach sediment
k_c	equivalent sand roughness of the frozen cliff sediment
k_r	linear wave number based on T_r and d_r
K_w	thermal conductivity of the seawater
L_b	volumetric latent heat of fusion per unit volume of the frozen beach sediment [$L_b = n_b \cdot \rho_i \cdot L_i$]

L_c volumetric latent heat of fusion of the frozen cliff sediment [$L_c = n_c \cdot \rho_i \cdot L_i$] ($J/m^3$)

L_i latent heat of fusion per unit mass [3.3×10^5 J/kg]

n_b ice volume per unit volume of frozen beach sediment

n_c ice volume per unit volume of frozen cliff sediment

P_b coarse sediment volume per unit volume of the unfrozen beach sediment

P_c coarse sediment volume per unit volume of the unfrozen cliff sediment

q_b offshore coarse sediment transport rate at the seaward boundary where water depth is given by [$S + E + d_b$] during the storm

q_c offshore coarse sediment transport rate at the cliff toe

q_{melt} coarse sediment supply rate due to the melting of the frozen beach sediment over the width W

q_p the potential coarse sediment transport rate, or the upper limit of q_b

R horizontal retreat of the cliff [m]

R_u wave runup on the cliff face [m]

s change in shear strength

S increase in water level above MSL during a storm [m]

S_w ambient seawater salinity in parts per thousand (ppt)

t time [hrs]

T_m melting temperature of the ice embedded in the frozen beach and cliff sediment [$\approx -0.06S_w$ for $S_w < 35$ ppt]

T_r wave period [s]

T_w ambient seawater temperature [°]

U average wind speed (miles per hour)

U_b representative fluid velocity immediately outside the boundary layer

v kinematic viscosity of the seawater

v_b coarse sediment volume per unit volume of the frozen beach sediment

v_c coarse sediment volume per unit volume of the frozen cliff sediment

W beach width from the fixed seaward boundary to the cliff toe [m] [$W = (R + W_b + db/\tan\theta_b)$]

W_b beach width above MSL [m]

z	depth below the ground surface
ℓ_c	inclined length of the frozen cliff sediment [m]
θ	angle of the slope [°]
θ_b	beach slope angle [°]
θ_c	seaward cliff slope angle [°]
ρ_i	ice density [920 kg/m^3]
α	empirical parameter [0.01 m$^{1.5}$/s for ice-free sand beaches]
τ	change in shear stress
γ	total weight of the overlying soil

CHAPTER 1 – INTRODUCTION

1.1 Overview

Permafrost landscapes are some of the most beautiful – and least understood – landscapes on Earth. The Canadian Arctic is no different; since the earliest explorers ventured there over a hundred years ago, countless studies have been conducted in order to understand the geomorphic and climatic agents that affect the evolution of the landscape (Mackay 1959, 1963, 1972*a*,*b*; Washburn 1973; Ramseier *et al.* 1974; McRoberts and Morgenstern 1974; Lewis and Forbes 1974; Shah 1978; Aré 1983; Hill *et al.* 1985; Harry *et al.* 1985; Pinchin and Nairn 1987; Walker 1988; Aré 1988; Harper *et al.* 1988; Dallimore *et al.* 1988; Pollard and Dallimore 1988; Fulton 1989; Harper 1990; Pollard 1990; Héquette and Barnes 1990; Pollard 1991; Mackay and Dallimore 1992; Burn 1994; French 1994; Héquette *et al.* 1995; French 1996; Komar 1998; Nairn *et al.* 1998; Kobayashi *et al.* 1999; Héquette *et al.* 2001; Hudak and Young 2002; Solomon and Gareau 2003; Grechishchev 2003). Although much is known about this region, there are still many unanswered questions. The modern era of exploration involved mostly summer expeditions, lead by the US and Canadian military and government during WWII, which opened previously inaccessible land to settlers and researchers alike. It was also during this time that some of the first comprehensive studies were conducted in order to understand the geomorphic nature of permanently frozen ground, and the effects of large-scale disturbance to this sensitive medium.

However, few studies have been conducted involving the geomorphology of arctic coasts. In areas of continuous permafrost, the combined effects of wave action, the open water season, storm surge, and thaw control the amount of annual coastal retreat. Even though the summer thaw season is brief, lasting only 3-4 months, these factors can cause extensive coastal backwasting in a very short period of time. Any change in one or more of these variables will result in a corresponding change in coastal erosion patterns. Global warming is expected to increase storm wave activity by increasing the length of the open water season, increasing effective fetch length, and increasing storm activity as well as warming the permafrost. There is an immediate need to address how soon these changes will affect rates of coastal erosion. Therefore, the overall aim of this study is to investigate the added effects of a warming climate on wave-related coastal retreat, in

order to assess the impact of climate change on arctic coasts. This information is valuable not only to the 10,000 inhabitants of the southern coast of the Beaufort Sea, and to the oil and gas companies with investments in the region, but also to researchers and managers studying the impacts of climate change on environmental ecosystems in the region.

1.2 Background

1.2.1 Permafrost and Ground Ice

Permafrost is defined as soil or rock that remains at or below 0°C for at least two consecutive years (IPA 1998). In Canada, permafrost underlies approximately 50% of the total landmass (Mackay 1972*a*) and is divided into zones of continuous and discontinuous permafrost, based on its spatial pattern (Figure 1). Permafrost is also found in alpine regions, and relict subsea permafrost may be found within the continental slope of the Arctic Ocean. In the continuous zone, permafrost underlies all exposed ground and extends from several to hundreds of metres in depth. However, beneath some bodies of water where temperatures cannot penetrate from the surface, permafrost may be absent. These permafrost-free regions are known as *taliks*. In the discontinuous zones, permafrost may only reach several centimetres in thickness, and is easily disturbed by anthropogenic activities. In these areas, the permafrost is often confined to peatlands, where it is well insulated (Gold *et al.* 1972).

Permafrost forms due to the propagation of extremely cold air temperatures from the ground surface. The layer of ground that thaws each summer season is termed the *active layer* (Figure 2). Its thickness can range from tens of centimetres in the high arctic to over a metre in the subarctic (French 1996; Couture 2000). Usually the base of the active layer corresponds with the upper limit of the permafrost table, where the maximum annual temperature nears 0°C (Brown 1963). Below 15 to 30 metres, permafrost temperatures begin to increase as they are affected by geothermal heat from the Earth's interior (Brown 1963). At some depth between 15 and 30 metres, annual surface climatic conditions cease to affect the thermal properties of the permafrost; this is known as the *level of zero annual amplitude.* It is only long-term climatic fluctuations that will affect any changes below this point (Brown 1963).

Many surface and terrain factors such as vegetation, soil, snow cover, and topographical orientation affect the surface energy balance and thus the amount of cold that is allowed to penetrate into the ground surface. The thicker the vegetative or snow cover, the warmer the ground surface will remain during the winter season (Brown 1963). The presence of vegetation protects surficial sediments from the direct effects of solar insulation. Organic layers in the active layer also add degrees of insulation to the

underlying permafrost. Snow banks and/or snow patches which remain throughout the majority of the summer in localized depressions play an important role in the propagation of colder temperatures into the soil, and thus aid in the growth of permafrost. Solar radiation also plays an important role in ground surface temperature; therefore, aspect is another factor influencing permafrost growth and degradation. Temperatures on exposed southeast slopes are often warmer than on the opposite side, therefore permafrost may exist on northward-facing slopes, but not on adjacent southward-facing ones (Brown 1963; French 1996).

The water content of soils also plays a large part in the mechanics of permafrost formation and degradation. The diffusivity, conductivity and heat capacity of the soil depends on its type, density, water content and temperature. The transfer of heat occurs not only through simple conduction, but also through the transfer of water in the soil profile (Gold *et al.* 1972). Unfrozen water will begin to freeze at different temperatures, depending on the size of the pore spaces between individual grains of sediment and on the pressures that exist at the freezing plane. As the freezing front extends downwards, unfrozen water is drawn upwards, causing the formation of segregated ice lenses, which can result in heaving of the overlying sediments (Gold *et al.* 1972; French 1996).

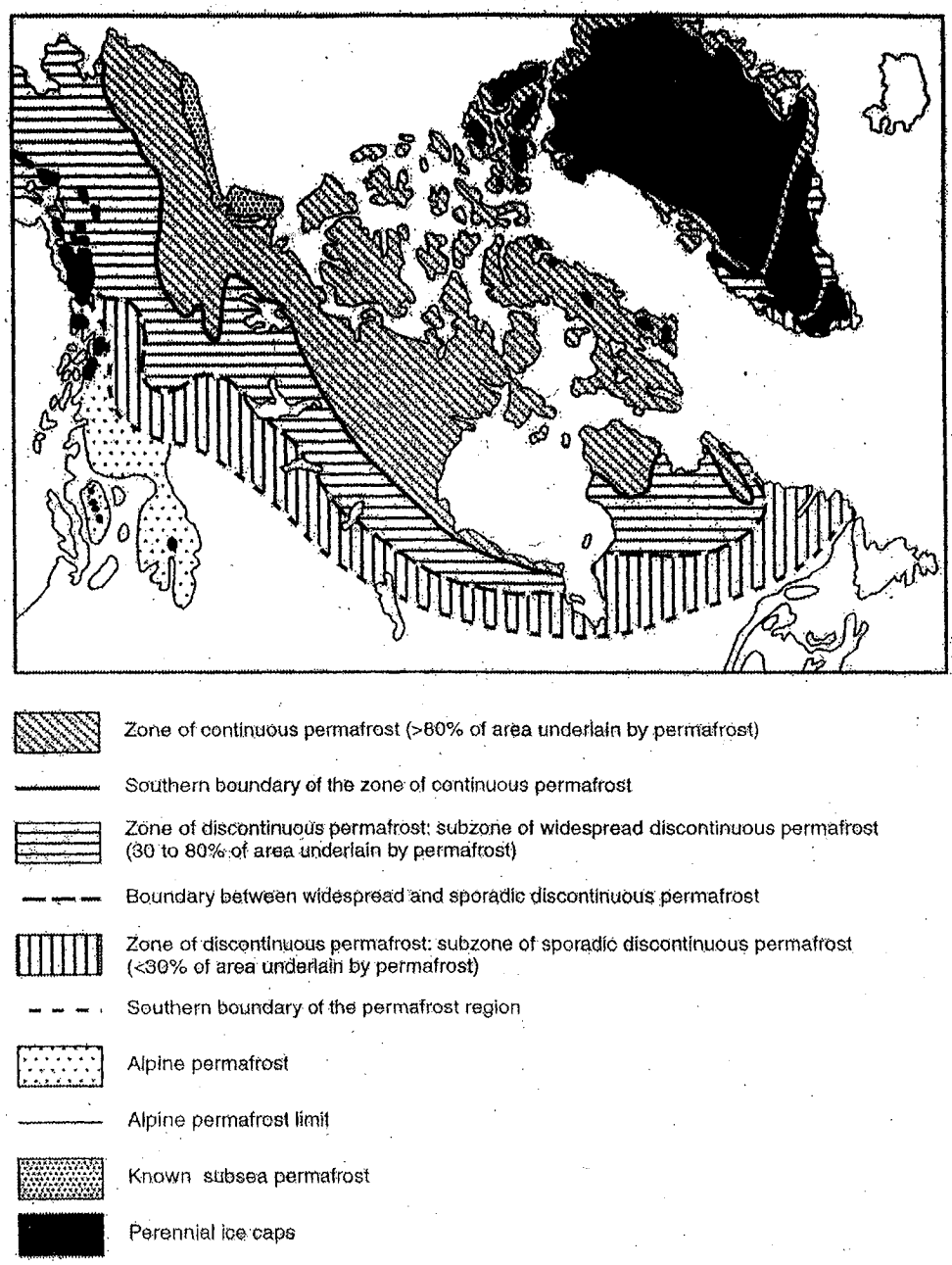

Figure 1: **Distribution of permafrost in Canada (from the Association of Canadian Geographical Researchers 1988).**

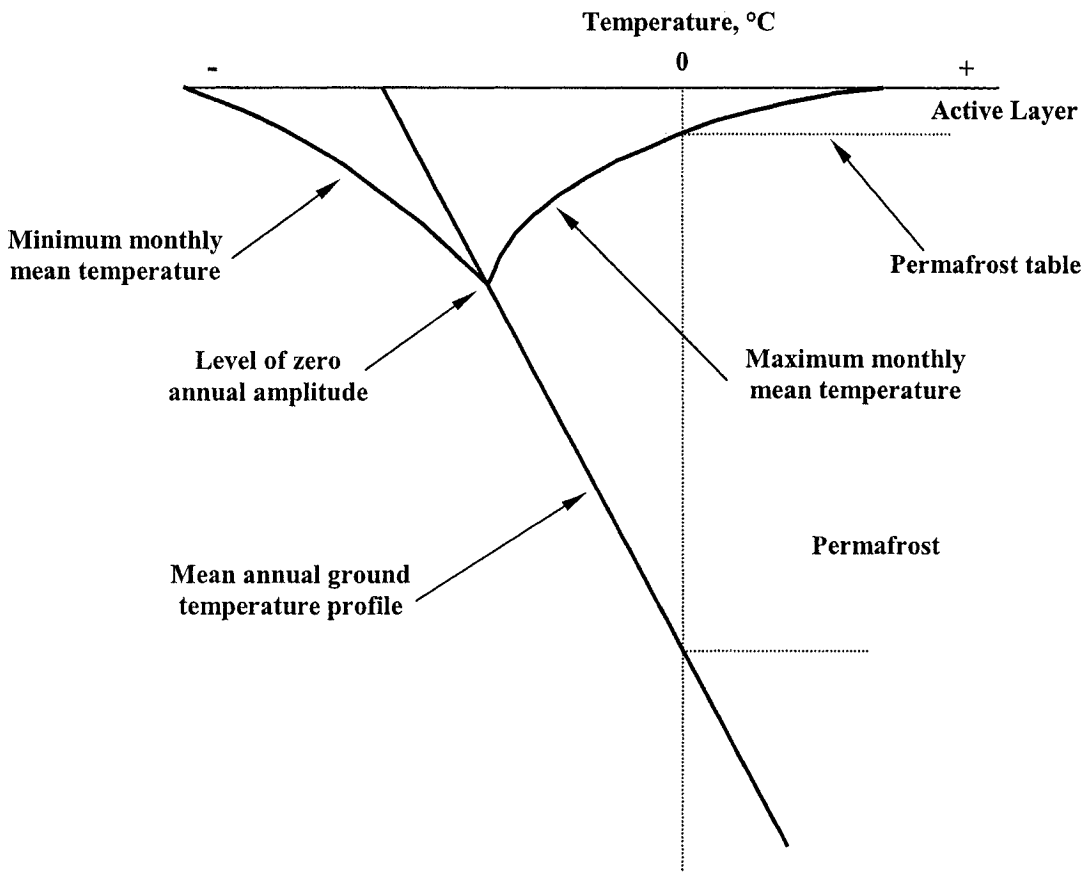

Figure 2: **Idealized ground temperature profile in areas where permafrost exists (from Andersland and Anderson 1978). Temperature profile decreases with depth.**

Ground ice occurs in pores, cavities or voids in soil or rock and includes massive ice (Mackay 1972*a*). One of the main criteria for the classification of ground ice is the source of water prior to freezing, and the second is the transfer of water during the freezing process (Mackay 1972*a*; Pollard and French 1980). There are several ways of looking at ice contained in soil. Ice content is by far the most important variable, and can be measured volumetrically (ice volume as a percentage of the soil volume) or gravimetrically (either ice weight as a percentage of total sample weight or ice weight as a percentage of the dry weight of the soil fraction). Another method examines the amount of 'excess ice', which refers to the volume of supernatant water present when a sample of soil is thawed (French 1996), or simply the volume of water in excess of the saturated portion.

As soil freezes, it attracts water from above and below the freezing plane (Gold *et al.* 1972; Mackay 1989). The growth of ice lenses into larger bodies of segregated ice can cause visible uplift and heaving of the ground surface (Gold *et al.* 1972; Mackay 1989). The distribution of ice in permafrost is dependent upon factors such as soil type and water availability; therefore, segregation is more likely to occur in clays and silts (having a grain size of 0.01 mm in diameter or less) (Taber 1929, 1930). A classification based on ground ice formation is provided in Figure 3 (Mackay 1972*a*).

When ice forms *in situ*, it is generally termed *epigenetic* ice, as it is younger than the surrounding sediments. Ice formed at the same time as sediment deposition is called *syngenetic*. Pore ice is responsible for bonding individual grains of soil together. In finer grained sediments, pore ice may aggrade into segregated ice. The distinction between these two types of ice lies in the overall water content of the soil and secondary redistribution of water in response to freezing. As pore ice and/or segregated ice melts, the water is reabsorbed into the surrounding sediments. The ground may experience some loss of cohesion, but its bearing strength should remain quite high (Mackay 1972*a*). However, subsidence problems associated with the melt of excess ice in the upper layers of permafrost have caused numerous problems in the continued settlement and development of the north (French 1994, 1996; Wolfe *et al.* 1998; Johnson *et al.* 2003).

Ice wedges constitute one of the most common types of ice in the Arctic, and form distinct landforms (Figure 4). Frozen ground cracks due to the thermal contraction

of the ground in winter. During the spring thaw, these cracks are filled with melt water which then freezes. Repeated cracking at the same site over several years and the incremental addition of veins can produce a v-shaped body of ice called an ice wedge, which may range in size from 1 m to 10 m (Mackay 1972*a*; French 1996). When viewed aerially, networks of ice wedges form a polygonal pattern of troughs flanked by low ridges, with the trough of the polygon underlain by an ice wedge (Figure 5). Ice wedges can be epigenetic, synergetic and episyngenetic, and form most often in poorly drained areas of the continuous permafrost zone (French 1996).

Massive ground ice is defined gravimetrically when its moisture content exceeds 250% dry weight, or 85-90% by volume (Harry *et al.* 1988; Mackay 1989; Mackay and Dallimore 1992; Pollard 1990, 2000). This ice may form *in situ* (such as ice wedges, pingo ice, and large ice lenses), or it may be buried ice (such as glacier ice, sea ice, lake ice, river ice, snowbank ice, or buried river icings) (Mackay 1972*a*; IPA 1998). Buried ice is not often discussed in North American literature as it is quite uncommon, therefore most descriptions of massive ice revolve around epigenetic ice (Mackay 1972*a*).

Massive ice will only form in soils of high water content in continuous permafrost zones. One of the most massive ice-rich areas in Canada can be found along the western Arctic coast (Mackay 1966; Rampton 1982; Pollard & Dallimore 1988; French 1996). Bodies of massive ice are often tens of metres thick (Figure 6), and may extend over several kilometres; they are generally underlain by sandy sediments and overlain by clay-grade sediments (Mackay & Dallimore 1992; French 1996; IPA 1998).

Knowledge of ground ice formation and evolution is necessary for understanding past landscape regimes, and for understanding the future geomorphic effects of both natural and anthropogenic change. The degradation of massive ice is responsible for thermokarst in both coastal and inland regions; therefore, a more comprehensive understanding of paleoclimates and paleogeomorphology may aid in understanding the future geomorphic effects of climate change (Pollard 2000).

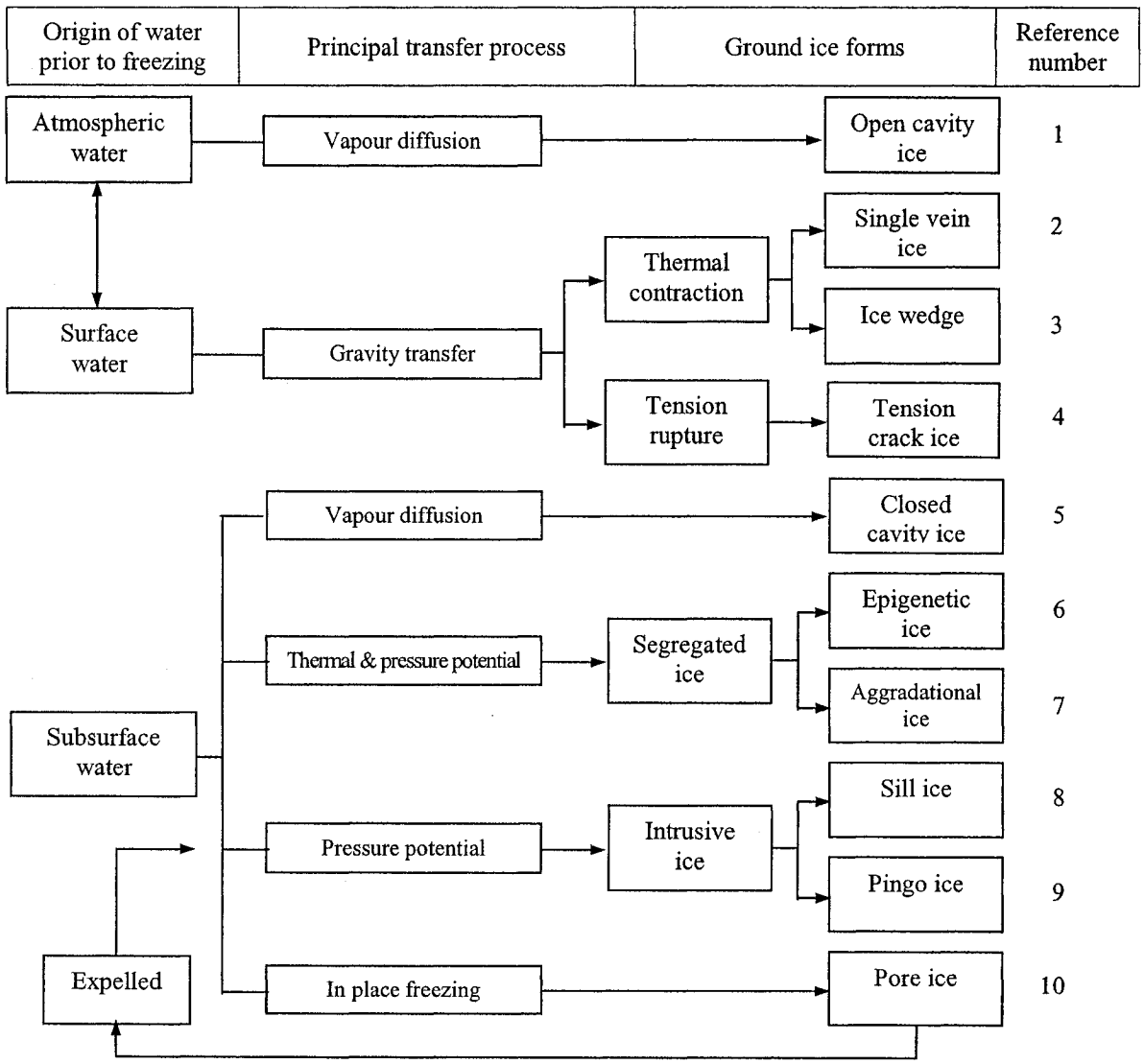

Figure 3: **A genetic classification of ground ice (from Mackay 1972*a*).**

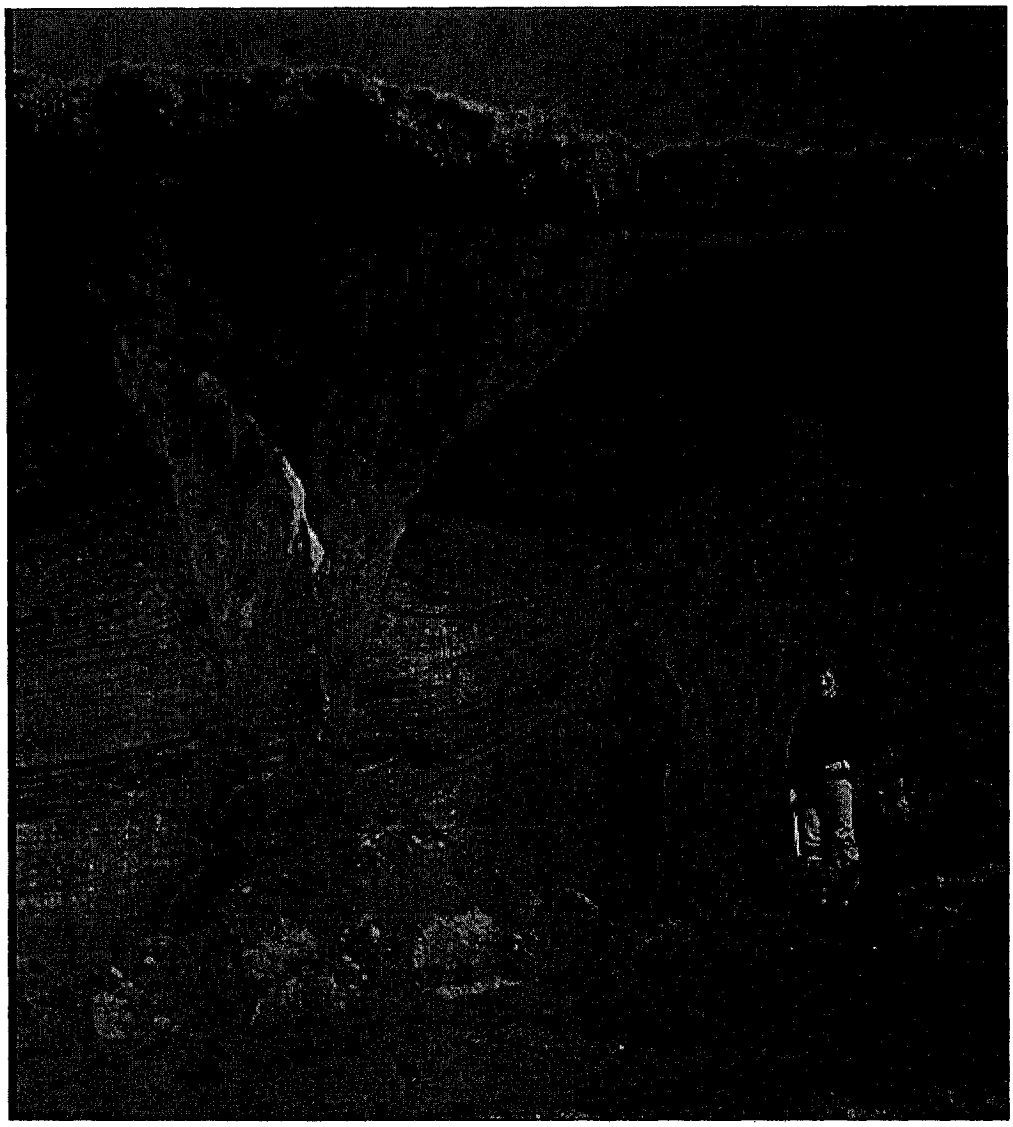

Figure 4: **Active (left) and truncated (right) ground ice wedges, Herschel Island. Man is approximately 175 cm. (Photo taken in 1986).**

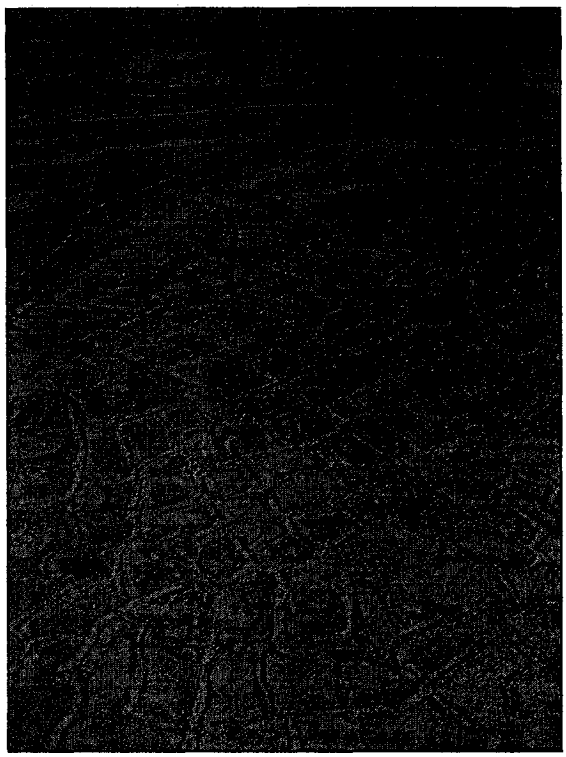

Figure 5: **Ice wedge polygons, southern coast of the Beaufort Sea (2003). Each side of the polygon corresponds to an ice wedge.**

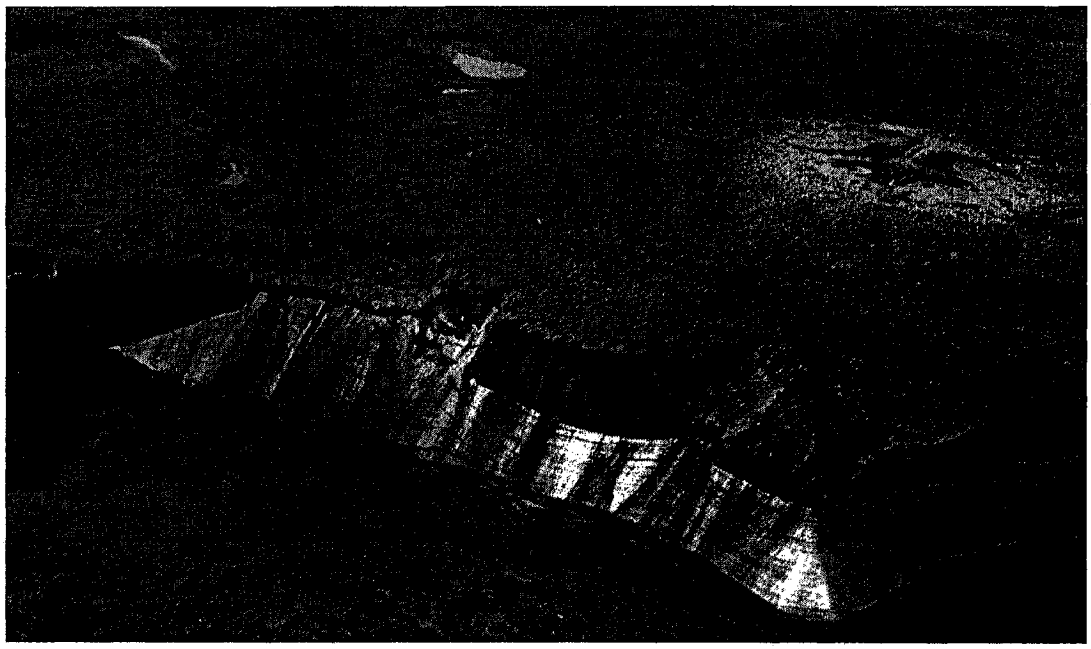

Figure 6: **Massive ice near Tuktoyaktuk, NWT. Ice measures greater than 20 m thick × greater than 500 m long. 1984.**

1.2.2 Wave Climate

The wave climate of the southern Beaufort Sea (Figure 13) is dominated by a seasonal ice cover which lasts from mid-October to early June (Hill and Solomon 1999; Hudak and Young 2002). Sloping gently away from the coastline is the Beaufort Shelf, which reaches a maximum depth of 70 m. This gently sloping bathymetry influences the coastal dynamics of the area through the attenuation of wave energy along the rough sea bottom (Harry 1982; Héquette and Barnes 1990). Coastal dynamics in the region are also affected by the winter sea-ice cover, which limits the growth and power of waves. During the open water season, winds generally originate from the east and southeast (Hudak & Young 2002). Storm winds from the northwest, often greater than 40 km/h, may cause storm surges up to 2.4 m in height (Harper and Penland 1982; Harper *et al.* 1988; Eid & Cardone 1992; Solomon *et al.* 1994; Hill and Solomon 1999). As the Beaufort Sea lies in a microtidal zone, these storm surges affect the coast more than regular tidal activity, which is usually less than 0.5 m in range (Harper and Penland 1982; Hill and Solomon 1999).

While storm surge is one of the most critical factors affecting coastal erosion in the southern Beaufort Sea, most surges occur only late in the season when available fetch is at a maximum. It is at this point that the partially thawed cliff sediments are most vulnerable to wave attack (Harry 1982). Two of the largest storms on record occurred during September 13-16 and September 21-22, 1976 on southwest Banks Island. These storms represented the peak in a 10-year period for both duration and kilometres of wind run. They are also responsible for some of the largest waves on record, measuring 3.5 m (Harry 1982).

Coastal sediments are moved through the nearshore zone by longshore currents. These currents flow along the shore and are generated by waves breaking while approaching the coast obliquely. There are two main components which affect longshore currents: (1) the surf zone and the contours of the coast and bottom bathymetry, and (2) winds, tides, and large horizontal eddies (Zenkovich 1967). Currents which form as a result of the second component move in the same direction over long distances and are more stable, however weaker, than those formed by the first component. Typical velocities of longshore currents measure approximately 1 m/s on natural beaches

(Zenkovich 1967). Because of their strength, longshore currents are important for the evolution of natural beaches. At Herschel Island, sediment that is entrained from the beach and nearshore zones is transported both offshore and around the island due to longshore currents.

The effects of climate change in this sensitive environment may have extremely negative effects on the stability of the northern coastline. Warmer seasonal temperatures will reduce the amount of permanent and seasonal sea ice, resulting in a greater fetch. This will allow for the creation of larger waves and higher water levels, which will result in greater amounts of coastal erosion (Kobayashi and Vidrine 1995).

1.2.3 Coastal Erosion

Various coastal erosion studies have been undertaken in this region of the Beaufort Sea over the past 30 to 40 years (Mackay 1963; Lewis and Forbes 1974; Harper *et al.* 1978; Aré 1983, 1988; Harry *et al.* 1985; Dallimore *et al.* 1988; Harper *et al.* 1988; Héquette and Barnes 1990; Dyke 1991; Kobayashi and Vidrine 1995; Dallimore *et al.* 1996; Hill and Solomon 1999; Kobayashi *et al.* 1999; Héquette *et al.* 2001; Brown 2003), however to date no published study has addressed the potential effects of climate change in this sensitive environment.

Recent coastal erosion studies have been based on analysis using aerial photographs and satellite imagery (Lantuit 2002). These types of analyses are excellent for determining the extent of erosion along a coastline, however they do not provide a clear idea about the processes involved. Other studies focus on the energy transfer between air and ground thermal regimes, and on the classical hydrodynamic factors that affect coastal stability. Recent numerical models have incorporated both the thermal and mechanical aspects of coastal erosion (Kobayashi and Vidrine 1995; Nairn *et al.* 1998; Kobayashi *et al.* 1999; Héquette *et al.* 2001). However, incorporating all necessary data, such as mapping ground ice content, collecting multiyear data, geophysical data and drilling information has not been attempted due to the lack of accurate information in these fields.

Coastal erosion in the Beaufort Sea is driven mainly by low frequency, high magnitude events. Low magnitude storms throughout the spring and summer season transport small amounts of sediment away from the beach zone. However, it is the two or three late-season storms that affect 80-90% of coastal change (Solomon *et al.* 1994; Wolfe *et al.* 1998).

The majority of coastal sediments in the Canadian Arctic are composed of medium- to fine-grained sediments, which promotes the growth of segregated ice lenses and/or bodies of massive ice parallel to the ground surface (French 1996). High rates of coastal erosion therefore, are due to the melting of these icy accumulations (Dallimore *et al.* 1996). In their study of the sediments of North Head, Dallimore *et al.* (1996) created a table showing the contribution of ground ice to the total volume of cliff and nearshore materials of six coastal segments (Table 1). Data includes onshore segments and material in the upper 3 m of offshore sediments. Pore ice contributes the largest volume of ice in this region, followed by massive ground ice in both onshore and offshore environments.

High rates of coastal erosion are produced during and after large storm events due to wave action and storm surge. These downwasting mechanisms are known as thermoerosion and block failure (Hill and Solomon 1999). After thawed sediments are removed from the cliff face, frozen sediments are carved from the toe, creating a thermoerosional niche at the base of the cliff. These eroded sediments are carried away from the source through the action of longshore and offshore currents. When the overburden pressure exceeds the tensile strength of the coastal section, downwasting of the eroded segment occurs through block failure (Hill and Solomon 1999). Discontinuities in the permafrost, specifically those associated with the presence of massive ice bodies and/or ice wedges provide an ideal slip surface for block failure. This failed block of predominantly frozen sediment will then act as a shield for that portion of the coast, protecting it from further erosion until all of the sediment therein has been transported in suspension away from the nearshore zone (Harry 1982; Aré 1983; French 1996).

In ice-rich environments, cliffs that consist of ice cemented homogeneous sediment (such as silts and fine sands) can also fail through active layer detachment sliding or through retrogressive thaw slumping (Lewkowicz 1992; Harris and Lewkowicz

1993, 2000). Eroding cliffs follow a seasonal, temperature-related cycle. In the winter cold temperatures refreeze the active layer, extending the freezing front well into the ground. During the spring and summer, heat conduction from regular wave action acts as a catalyst, causing erosion of the cliff face. The rate of retreat is dependent upon sediment removal in the nearshore zone; as more sediment is removed, the potential for erosion increases. Slope failure ceases when either the ice content of the material is reduced, or when wave action is no longer sufficient to actively transport the sediments, resulting in stabilization of the headwall (French 1996).

Thaw settlement is also considered a major contributor to coastal erosion; if the removal (thaw) of the excess pore ice in the coastal sediments exceeds a critical value, then their complete thawing results in subsidence of the ground to water (sea) level. At this point, coastal erosion will continue unchecked until the coastal sediments retreat beyond the water line, or the amount of pore ice in the remaining sediments rests below the critical value (Aré 1983).

Coastal Segment	Wedge Ice (%)		Pore Ice (%)		Ground Ice (%)		Total Ice (%)		Excess Ice (%)	
	Onshore	Offshore	Onshore	Offshore	Onshore	Offshore	Onshore	Offshore	Onshore	Offshore
A	2.3	0.0	56.0	56.0	20.0	20.0	78.3	76.0	38.3	36.0
B	6.9	1.8	43.3	47.5	0.0	7.5	50.2	56.8	10.2	16.8
C	3.0	0.0	45.9	39.5	6.0	0.0	54.9	39.5	14.9	1.5
D	0.0	9.1	0.0	45.3	0.0	0.0	0.0	54.4	0.0	14.4
E	2.7	0.0	42.2	39.5	0.0	0.0	44.9	39.5	4.9	1.5
F	3.3	0.0	45.6	39.5	4.5	0.0	53.4	39.5	13.4	1.5

Table 1: **Taken from Dallimore *et al.* (1996). Volume of ground ice in coastal and nearshore sediments, North Head, Richards Island, N.W.T.**

1.2.4 Climate Change

It has long been known that Earth's climate is changing, and that it is affected by human activities (Brown 1963; Gold *et al.* 1972; McRoberts and Morgenstern 1974; Barry 1988; Cohen 1997; Burn 1994, 1998; IPCC 2001). Before the Industrial Revolution, the impact of these activities on both local and regional climate regimes was minimal. However, since the mid 18th century, change has been detected on a global scale. Some blame these changes on human activities, while others attribute it to natural climate variability. In all likelihood it may also be a combination of both these processes. At this stage of knowledge, the global climate model is still too complex to be fully understood.

The 2001 IPCC report documents changes in near-surface temperatures from the instrumental record since the early 1900's. These changes include a global increase in temperature of 0.6°C, acceleration in the rise of sea surface temperatures in the North Atlantic, an increase in global ocean heat content of 0.037°C/decade, a reduction in the diurnal temperature range (with minimum temperatures increasing at twice the rate of maximum temperatures), a decrease in the extent of continental and alpine glaciers, a decrease in lake and river ice cover in the Northern Hemisphere, a decrease in snow cover in the Northern Hemisphere, a 10 to 15% reduction in sea ice extent in the Arctic spring and summer, and a 40% reduction in Arctic sea ice thickness. In areas that have seen an increase in precipitation, an increase in extreme events is likely, with the opposite being true for arid environments. Changes in hurricane, tropical storm, tornado and monsoon patterns have not been analyzed due to the sporadic nature of these events; therefore it is not known how these will change. It is expected, however, that a changing climate will have its greatest impacts in northern environments.

Figure 7 demonstrates 30-year average temperatures in Tuktoyaktuk, NWT, a region that is experiencing the effects of increased coastal erosion and climate warming. This settlement was built on a peninsula which extends into the southern portion of the Beaufort Sea. As a result, aerial photographs between 1950 and 1972 have shown 40 m (130 feet) of coastal erosion (Shah 1978). Figure 7 includes a trend line showing that overall temperatures have been increasing. This data corresponds well with similar data

collected from borehole measurements in northern Alaska, which show an approximate warming of 3°C over the past 125 years (Lachenbruch *et al.* 1988; Lachenbruch 1994).

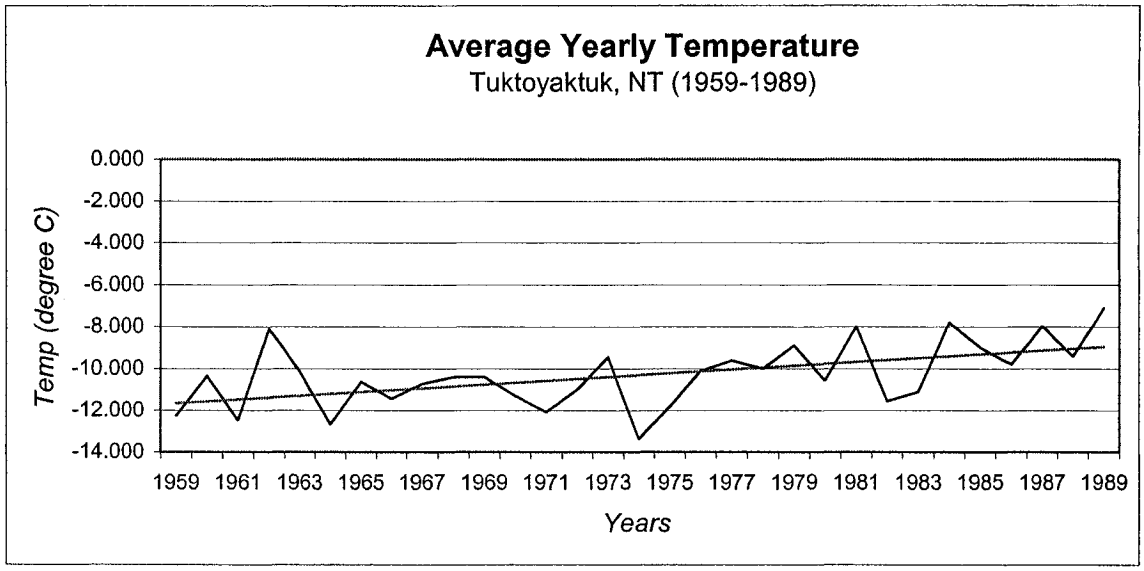

Figure 7: **Average yearly temperatures at Tuktoyaktuk, NT (1959-1989). Although yearly averages seem to be quite sporadic, there is a general increase in temperature through the decades. (Source: Canadian Monthly Climate Data and 1961-1990 Normals, Environment Canada 1994 cd-rom).**

1.3 Thesis Objectives

The primary purpose of this study is to investigate the potential for increased coastal erosion related to climate change, and to understand the mechanisms of block failure and thermoerosional niche development in the vicinity of Herschel Island. There is a strong correlation between storm surge and coastal erosion in the southwest Beaufort Sea (Solomon *et al.* 1993). Factors such as amount of fetch, depth of water, wind speed and duration, and wind direction control surge and wave heights and thus determine the effect of storms on the coast and nearshore zone (Hudak and Young 2002). Anticipating storm frequency, storm intensity, and rates of coastal erosion is beneficial to the 10,000 inhabitants along the southern coast of the Beaufort Sea, as well as the companies associated with oil and gas exploration in the area. Sediment erosion and entrainment in the nearshore zone will also affect local marine ecology; therefore, understanding these processes is also beneficial to this area of study (Dyke 1991).

This study will test the hypothesis that coastal erosion occurs mainly through a range of distinct mass wasting processes such as retrogressive thaw slumping, thermoerosional niche development, and block failure. Primary goals of this study include: (1) identification of coastal erosion processes on Herschel Island; (2) improved understanding of thermoerosional niche and block failure processes as they affect ice-rich coastal sediments; and (3) improved understanding of both the benefits and drawbacks of the numerical model developed by Kobayashi *et al.* (1999). Secondary goals of this study include: (1) forming a climate change factor and adding it to a storm database in order to predict storm intensity; (2) comparing these results to estimated IPCC 2001 climate change predictions in order to validate current models; and (3) the creation of a detailed digital map of Herschel Island, identifying areas of greatest risk to wave-induced coastal erosion.

CHAPTER 2 – STUDY AREA

2.1 Herschel Island

2.1.1 Geomorphological History of the Area

A feature of the Yukon Coastal Plain, Herschel Island (69°36'N, 139°04'W) lies approximately 60 km east of the international border (Alaska) and 2.5 km north of the Yukon coast (Figure 8). It formed as an ice-push feature during the Late Wisconsinan, and is composed of glacial and post-glacial lacustrine deposits; evidence of this can be found in some bodies of massive ice that are common to the area (Mackay 1959; Rampton 1982; Pollard 1990). Herschel Island rises 183 m above sea level, and is the only major feature of the southern Beaufort coastline that interrupts wind and water currents. The climate of the northern Interior Plains is polar continental. Average temperatures at Komakuk Beach, YT are -21.5°C in winter and 6°C in summer, with an average yearly precipitation of 154 mm. Conditions further east at Shingle Point, YT are quite similar, with average temperatures of -22°C in winter and 7°C in summer, and average yearly precipitation values of 232 mm (Figure 8) (Environment Canada). Due to the predominant nival runoff regime, vegetation is sparse and in the northern regions consists of high Arctic tundra (Fulton 1989).

2.1.2 Herschel Island Physiography & Surficial Geology

The sediments of Herschel Island are comprised mainly of sands, silts, and silty clays of the Pleistocene Epoch or earlier (Mackay 1959). The island was formed by a lobe of the Laurentide Ice Sheet, forming an ice-push structure. A likely source for this large volume of sediment is Herschel Basin, which lies just southeast of the island, as it is elongated in the inferred northwest-southeast direction of ice movement (Mackay 1959). Most of the beds on Herschel Island demonstrate a folded, tilted and thrust-faulted configuration due to the *in situ* formation of a glacial-tectonic ridge (Mackay 1959, 1971). Sub-vertical shear planes occur in abundance in the coastal clay sediments, and are responsible for much of the erosion that occurs through block failure (Mackay 1959).

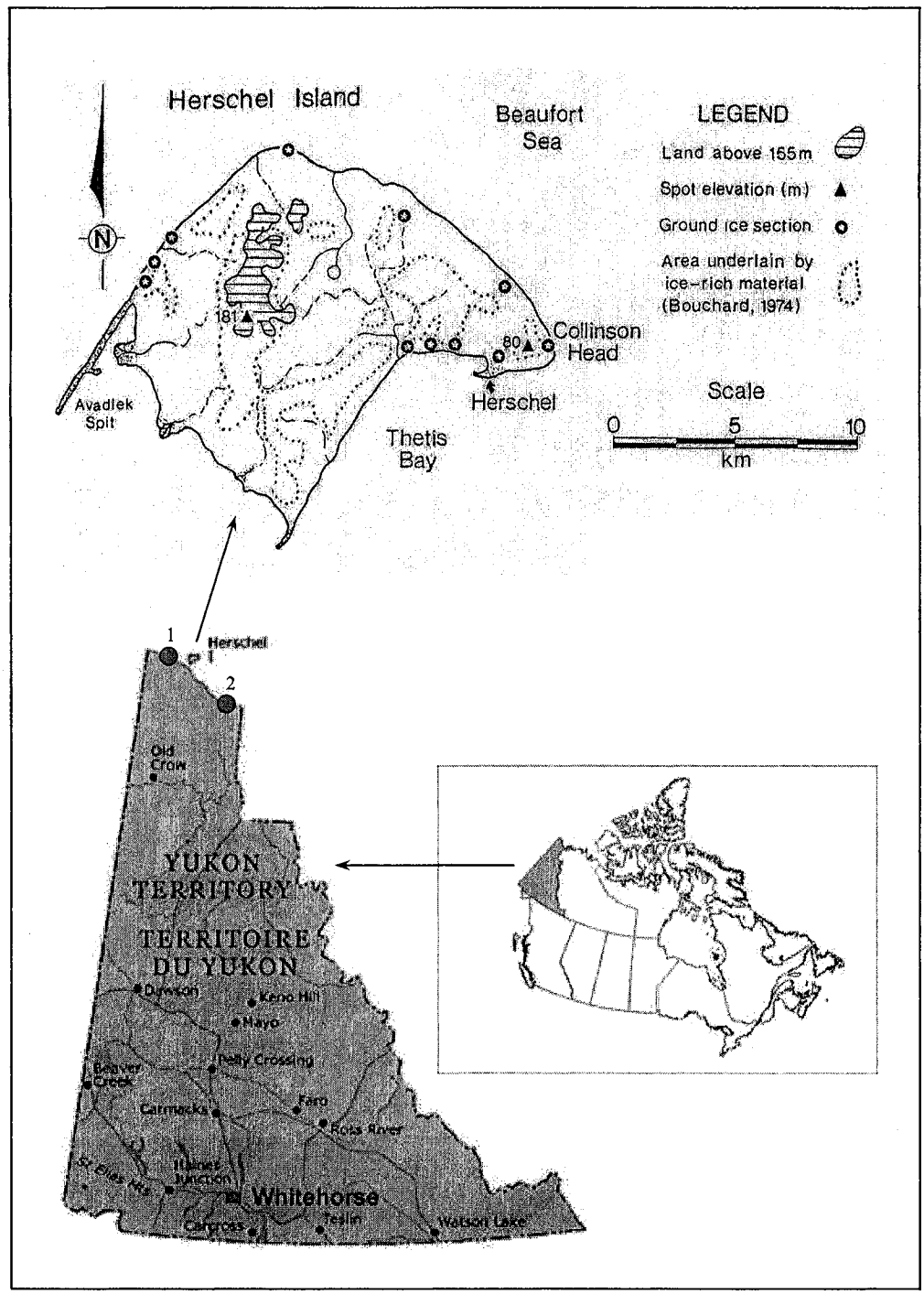

Figure 8: **Location of Herschel Island, Yukon Territory. Ground ice locations from Pollard (1990). Climate data are presented for Komakuk Beach (1) and Shingle Point (2) DEW line stations (images courtesy of Pollard 1990 and the Canadian Government).**

Herschel Island has a unique physiography that distinguishes it from the surrounding Yukon Coastal Plain. The highest point on the island reaches 183 m above sea level, and the waters surrounding the island do not exceed 3 m depth (Mackay 1959; Bouchard 1974). The island's topography is gently rolling, however there are clear differences between the southeastern and northwestern parts of the island. Steeply sloping bluffs that rise nearly vertically out of the Beaufort Sea characterize the northern and western parts of the island. Within this landscape are a series of asymmetric ridges and gullies running parallel to each other (Bouchard 1974). This ridge and valley sequence is interpreted as glacially ice-thrust in origin (Mackay 1959). Along the coastline, erosion occurs through the development of a thermoerosional niche and subsequent block failure (Aré 1983, 1988; Walker 1988).

The southern and eastern parts of the island are also dominated by rolling topography, however ridges and gullies are absent. High levels of solar radiation cause continual slumping, resulting in more gently angled slopes (Bouchard 1974). However, the main differences concern the coastal morphologies; longshore currents have formed two gravel spits along the southeastern and southwestern tips of the island (Figure 8), with Avadlek Spit (southwestern) being the larger of the two at roughly 6 km in length (Lantuit 2002).

Thermokarst processes are responsible for most of the coastal erosion along the southern aspects of Herschel Island. The term *thermokarst* was first used in 1932 by M.M. Ermolaev to describe "... irregular, hummocky terrain due to the melting of ground ice" (French 1996). Considered one of the main types of thermokarst on Herschel Island, retrogressive thaw slumps (Figure 9) may extend 200-300 metres inland, and will only stabilize with either a change in soil type and/or ice content, or a stabilization of slope (<3-4°) (Harry 1988; de Krom 1990; French 1996; Murton 2001). The rate at which they progress depends largely on the ice content of the underlying materials (Mackay 1966). On Herschel Island, ground ice constitutes up to 60-70% of the upper 10-12 m of permafrost, and massive ice bodies consist of ice wedges, buried snowbank ice, injection ice, segregated ice, and glacier ice (Figure 3) (Walker 1988; Pollard 1990).

Retrogressive thaw slumps are widespread on the south and eastern coasts of Herschel Island, producing bowl-shaped depressions characterized by well-developed

headwalls and mudflows through the base. De Krom (1990) documented maximum scarp retreat rates on Herschel Island of 5 m/yr. Retrogressive thaw slumps form through: (1) ablation and thermal erosion of the cliff face; (2) block failure of the overlying active layer and surface vegetation; (3) sliding of material off the cliff face; and (4) mudflows within the slump floor.

Active layer detachment failures differ from retrogressive thaw slumps in that they are "gravity induced downslope movements of weathered debris" (Permafrost Subcommittee 1988), which can be activated by periods of warmer weather and/or heavier rainfall events (Harris and Lewkowicz 1993). The eroded mass of sediment and vegetation flows over a slip surface. These blocks retain their form and structure, and are deposited at some point downslope from the headwall. Typical failures measure 20-40 m parallel to the coast, 10-20 m perpendicular to the coast, and occur on slopes of 10-15° (Harris and Lewkowicz 1993). Several active layer detachment failures were identified by de Krom (1990) in the Thetis Bay region of Herschel Island.

Other forms of thermokarst present on the southern coast of the Beaufort Sea include thaw lakes. These ponds are generally shallow (<3 m depth) and circular to elliptical in shape, forming in flat terrain underlain by silty-clay sediment with high ice contents (French 1996). Often the development of these thaw lakes is in association with the maturing of ice wedges / polygonal ground topography (Figure 10). However, they may also form due to terrain disturbance (natural or anthropogenically induced), such as a change in vegetation cover (French 1996). Along the southern coast of the Canadian Beaufort Sea, thermokarst lakes are often visible near actively eroding shorelines (Figure 11), and may contribute large quantities of additional sediment to the beach and nearshore zones if breached during the thaw season.

Thermokarst lakes are dynamic features that are common to the Arctic landscape. Draining of the lake can occur either slowly (2000-3000 years) or rapidly (days) (French 1996). Rapid draining may occur through tapping along ice-wedge margins or truncation due to coastal retreat. In the case of ice wedge drainage, the resulting exposed surface undergoes ice segregation and frost heave as cold air temperatures penetrate from the surface downwards. Solifluction (downslope movement of saturated sediments) and mass wasting occur near the banks of the former lake, moving sediment from the margins

towards the centre, effectively erasing all traces of the former thermokarst depression (Andersson 1906; French 1996). The slow disappearance of a thermokarst lake may occur due to gradual infilling and sedimentation. In this case, examination of ^{14}C dates at the site may provide information regarding climate and vegetation over a period of several thousands of years.

Figure 9: **Thermal erosion (retrogressive thaw slump), southern Beaufort Sea Coast, Yukon Territory, 2003.**

Figure 10: **Thaw lakes associated with ice wedge terrain, southern Beaufort Sea coast, Yukon Territory, 1985 (A26779-15).**

Figure 11: **A drained thaw lake located near active coastal erosion, southern Beaufort Sea coast, Yukon Territory. Dashed line delineates a thaw lake.**

2.2 The Beaufort Sea

The Beaufort Sea is a southern extension of the Arctic Ocean (Figure 12). The smallest ocean in the world (13,986,000 km^2), the Arctic Ocean includes Baffin Bay (Canada), the Barents Sea (Russia), the Beaufort Sea (Canada & US), the Chukchi Sea (Russia & US), the East Siberian Sea (Russia), the Greenland Sea (Norway), Hudson Bay (Canada), Hudson Strait (Canada), the Kara Sea (Russia), the Laptev Sea (Russia), the Northwest Passage (Canada), and other tributary water bodies. The Beaufort Sea itself is bordered on the south and east by the Yukon and Northwest Territories and on the southwest by Alaska (Hudak and Young 2002). The total area of the Beaufort Sea equals approximately 450 000 km^2 and is covered by sea ice for most of the year. Thaw occurs in late June and the open water season extends into October (Hudak and Young 2002). Average seawater temperatures between Herschel Island and King Point have been recorded at –1.2°C to –1.6°C (Mackay 1972*b*).

The southern coast of the Beaufort Sea is composed of unconsolidated alluvial and glacial sediments, not rock, as are many of the coasts in more southern latitudes. Permafrost has been aggregating in this region for approximately 40,000 years, and in some areas is more than 600 m thick. Sea level rise in the region has been documented at approximately 2.5 mm/a over the past 3000 years, with a maximum of approximately 4.4 mm/a (Hill *et al.* 1993). As much of the coast remained unglaciated during the Late Wisconsinan, it is believed that recent sea level changes are due mainly to eustatic fluctuations in sea level, and not isostatic rebound (Mackay 1972*b*).

The Beaufort Sea is a unique environment (Figure 13). It contains five bathymetric components: (1) the coast, (2) the Mackenzie River and Delta, (3) the continental shelf, (4) the Mackenzie Canyon, and (5) the continental slope (Arctec 1987). Each of these components brings an element of individuality to this environment, which has been identified as an area most likely to experience the strongest effects of climate change (IPCC 2001).

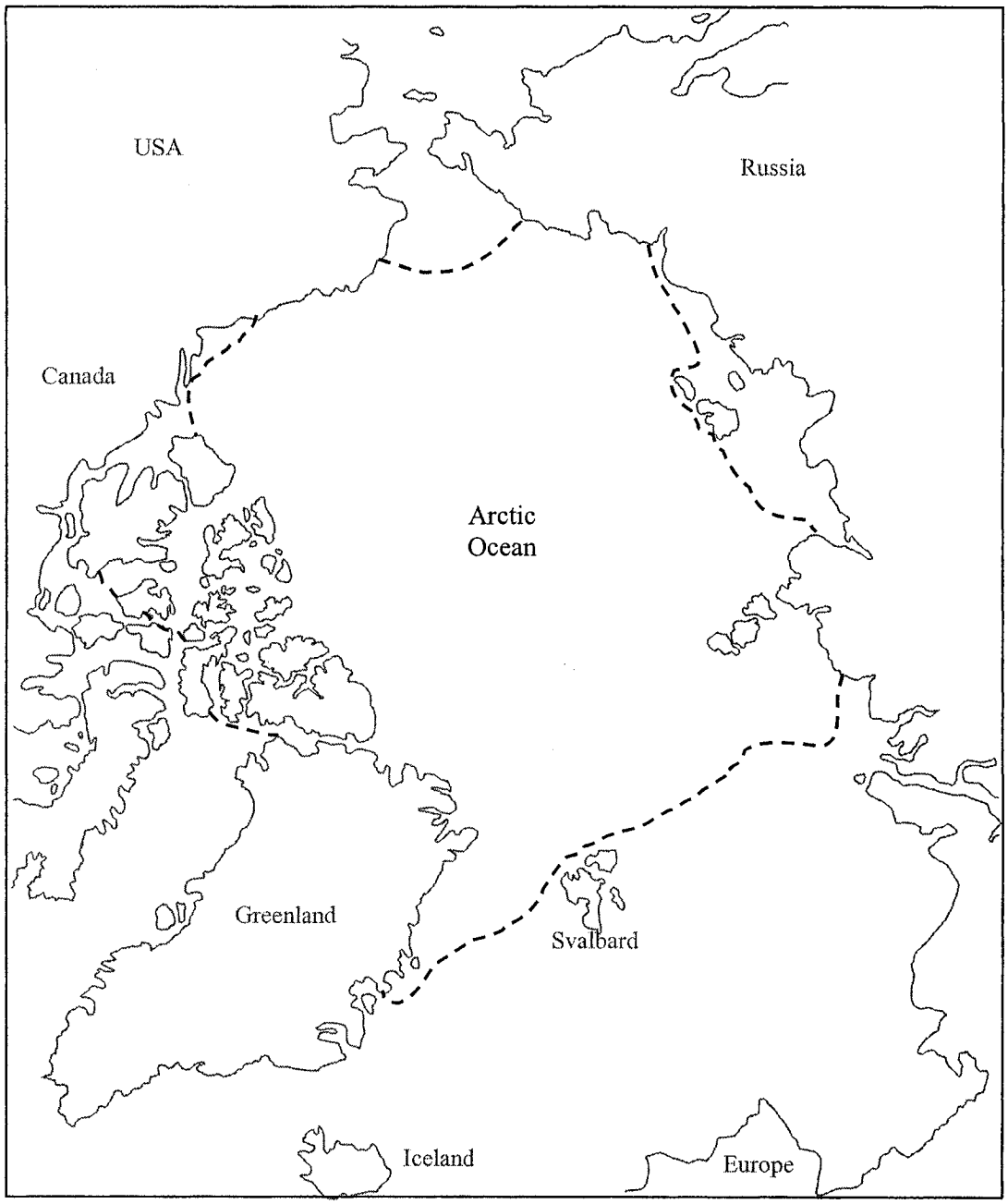

Figure 12: **The Arctic Ocean. Dashed line represents the average maximum sea ice extent. (Modified from Smith, W.O. 1990).**

2.2.1 Ocean Currents

The Beaufort Gyre is a clockwise rotation of currents in the Arctic Ocean, driven by both the Coriolis Force (acceleration due to the rotation of the Earth), and winds that form due to high-pressure systems in the northern latitudes. These currents are responsible for the movement of the permanent ice pack, which completes a full rotation every 7-10 years (Milne 1973). Tides do not affect oceanic circulation patterns in the Arctic Ocean, as the area is microtidal in nature (<30 cm) (Sater 1969).

Two dominant currents exchange water between the Arctic Ocean and other world oceans through the Fram Straight, which lies between Greenland and Svalbard, Norway. The first is the West Spitsbergen Current (WSC), which flows northward from the Atlantic Ocean carrying warm water into the Arctic Ocean. The second current is the East Greenland Current (EGC), which is responsible for transporting colder water from the Arctic Ocean into the Norwegian Sea (Smith 1990).

Upon entering the Arctic Ocean, the WSC encounters the Transpolar Drift. This current transports surface waters and ice from the western (Eurasian basin) to eastern side of the Arctic basin (Smith 1990). As the warmer water of the WSC meets the colder current, the sensible heat serves to melt the ice floes, resulting in a cooler upper layer of water (Smith 1990). The ECG carries not only colder water away from the Arctic Ocean along the eastern coast of Greenland, but it is also responsible for carrying icebergs into the Atlantic Ocean in the order of 4000 – 5000 km^3 of ice each year (Smith 1990).

2.2.2 Sea Ice

Sea ice in the Arctic Ocean generally begins forming in early- to mid-October, with complete ice cover occurring by the end of the same month. Ice remains until break-up occurs mid-June (Arctec 1987).

Ice cover consists of several types of ice, including first year ice, multi-year ice, and ice floes. First year ice forms as a skim on the surface of the water and expands in a downward direction; maximum thickness reaches 2 m in the Arctic Ocean. Multi-year ice is composed of ice that has not completely thawed through the summer season, and can reach a maximum thickness of 4 m (Arctec 1987). Ice floes consist of old sea ice that

has been broken into large sections through wave action, but which are too large to melt completely during the thaw season; they are reintegrated into the winter ice cover (Arctec 1987).

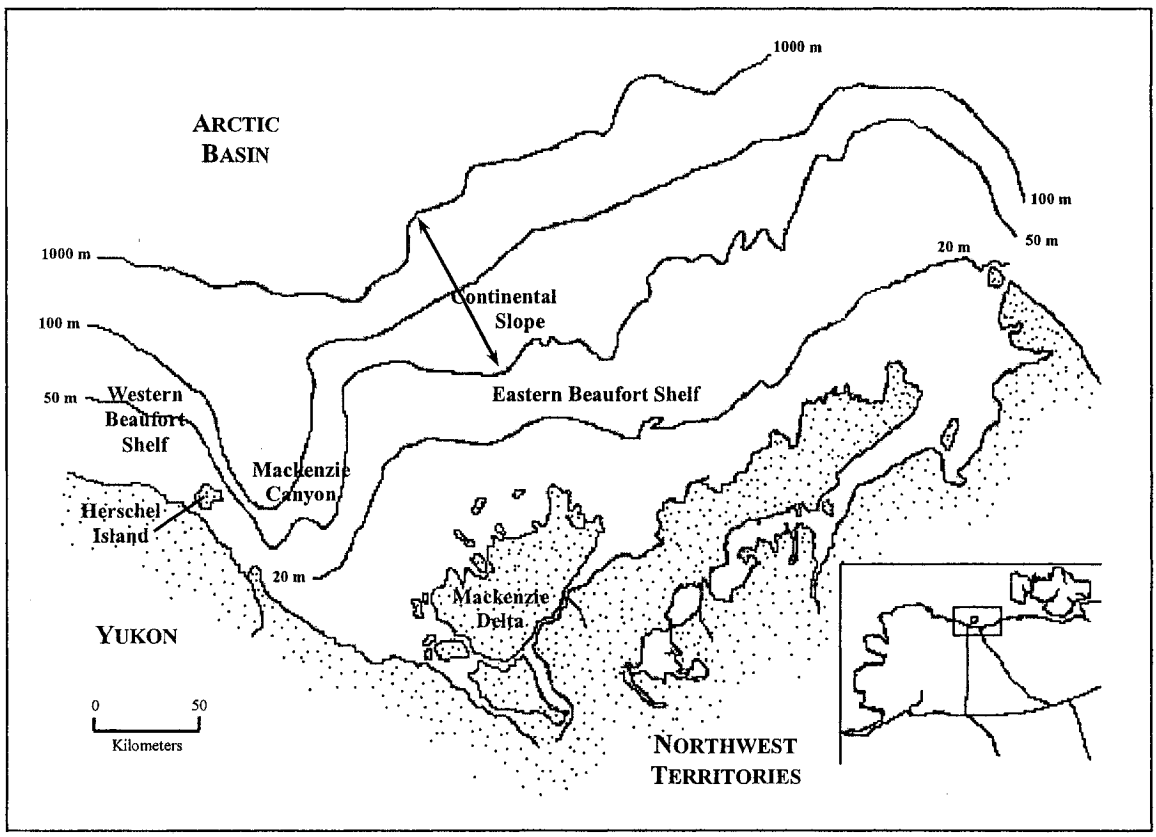

Figure 13: Morphology of the Beaufort Sea (modified from Hill *et al.* 1991).

There are several ice zones in the Beaufort Sea, including: (1) polar pack ice, (2) seasonal zone, (3) shear zone, and (4) landfast zone (Arctec 1987).

Polar pack ice consists of ice in the central region of the Beaufort Sea, which is subject to the clockwise circulation associated with the Beaufort Gyre. The Gyre covers most of the western portion of the Beaufort Sea, as well as portions of the Chukchi and East Siberian seas. It is also affected by the Transpolar Drift, which is responsible for moving ice from the western to the eastern side of the Arctic Ocean (Smith 1990). Ice in this zone is relatively thick, and consists mainly of old sea ice (Arctec 1987).

The seasonal zone contains a higher percentage of first-year ice than does the polar pack zone, also drifting in a clockwise direction due to the influence of the Beaufort

Gyre. Its dimensions depend on the prevailing wind direction and the seaward growth of ice in the landfast zone (Arctec 1987).

The shear zone is the area between the seasonal ice zone and the stable landfast ice. It contains a mixture of ice types, severe ridging, and variable amounts of open water that are season dependent. The shear zone affects the coastal zone primarily through the development of ridge keels, which become frozen to the sea bottom during the winter months and which may effect major amounts of erosion during the thaw season (Arctec 1987).

The landfast zone has the greatest impact on coastal evolution, and plays a crucial role to sediment transport in the nearshore zone (Figure 14). This zone is located next to the shore along most of the Beaufort coast, and has open water conditions throughout the summer season. Movement of ice during the winter period is due to thermal contraction and expansion of the continuous ice sheet, and is generally limited to 10 m (Arctec 1987). Ice in the landfast zone adheres to the seafloor, protecting it from erosion associated with wave, current and ice abrasion during the winter period (Arctec 1987).

2.2.3 The Beaufort Shelf

The Canadian Beaufort Shelf stretches from the Alaskan Peninsula to the Canadian Arctic Archipelago, and extends northward approximately 150 km from the coastal zone, ending in 80 m water depth at the continental shelf margin (Sater 1969; Harper 1990; Hill *et al.* 1991; Hebert 2002). Cutting through the Beaufort Shelf east of Herschel Island is the Mackenzie Trough, a glacial valley 200-300 m deep, formed during the Early Wisconsinan glaciation (Hill *et al.* 1991). The shelf is composed of unconsolidated clays and silts mainly deposited by the Mackenzie River during the past 15,000 years (Harper 1990). Permafrost underlies much of the shallow coastal zone, as this area has undergone rapid transgression since the last glacial maximum (~ 40 000 BP) when sea levels were approximately 140 m lower than at present (Hill and Solomon 1999).

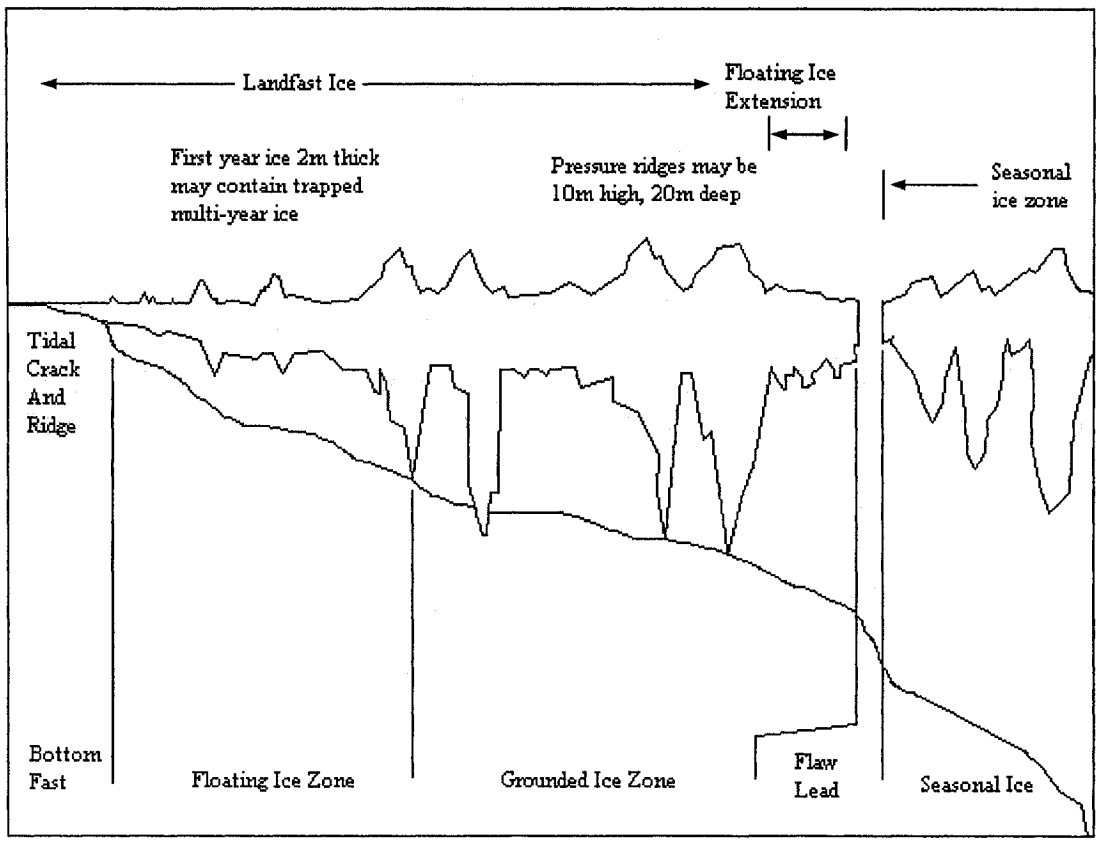

Figure 14: Landfast ice morphology (modified from Arctec, 1987).

The unique geology of the Beaufort Shelf has created an ideal trap for oil and gas deposits (Harper 1990). Perhaps the most valuable of these accumulations are natural gas hydrates, which are water molecules containing frozen gas molecules (such as methane). One unit volume of gas hydrate is equal to 160 times the volume of liquid methane. The depth to the top of subsea permafrost is dependent upon several factors, such as erosion, sedimentation, and water temperature, therefore exploratory drilling in this area is problematic due to the risks involved with a blowout of such volatile material (Mackay 1972*b*; Smith and Judge 2003). As well, in offshore areas with high ice content, thermal disturbance may result in hydrate sublimation, releasing vast quantities of methane directly into the atmosphere (Milne 1973).

2.3 The Coastal Zone

The coastal zone includes cliffs, dunes and estuaries above the water line, as well as sediment transport in the littoral zone to a depth of 10-20 m (Komar 1998). The *littoral zone* is defined as the environment in its entirety, beginning at the beach and continuing through to a water depth at which sediment is less actively transported by wave action (Komar 1998). Exact terminology for the coastal and nearshore zones has differed over time; coastal engineers and traditional geomorphologists may use different terms for the same feature or zone, therefore describing this environment can be quite challenging. Figure 15 outlines the main features of the coastal zone.

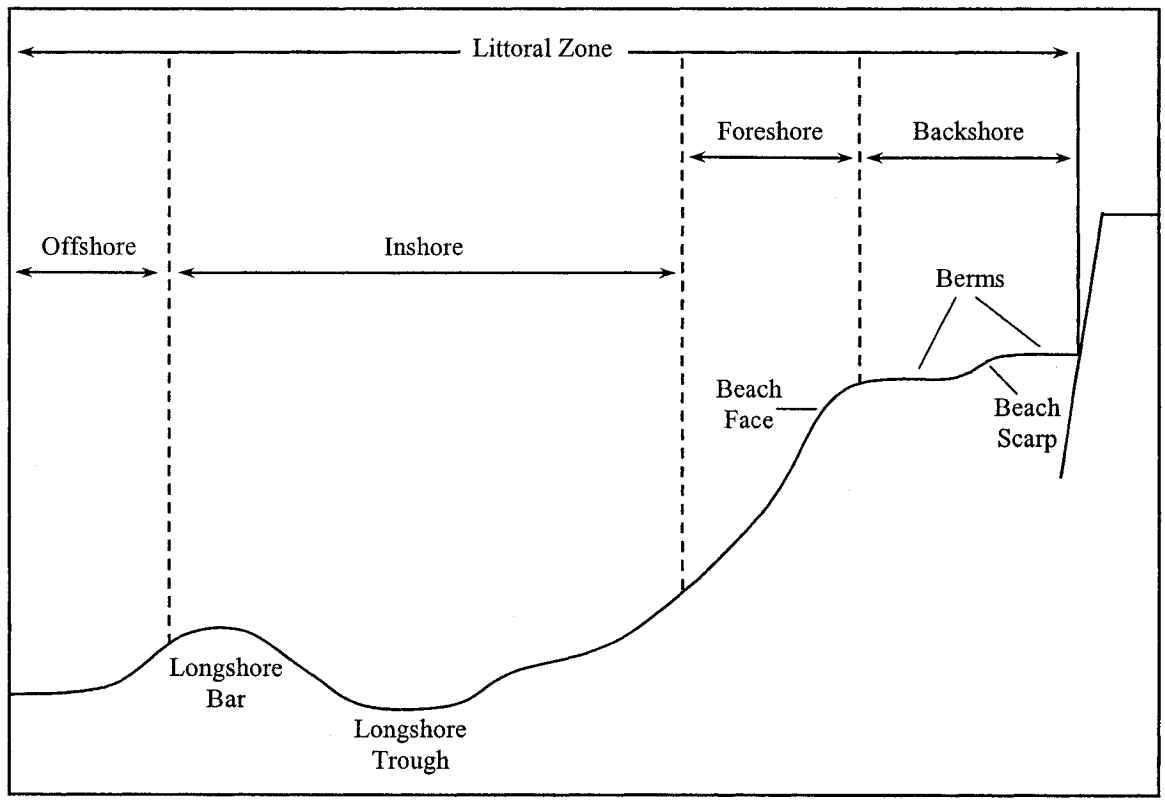

Figure 15: The coastal zone (after Komar 1998, p.46).

There is a close relationship between the coastal zone and the nearshore zone, each with elements common to the other. Sediments deposited in the coastal zone due to cliff erosion are transported through the surf and swash zones into the longshore currents of the nearshore zone (Komar 1998). Therefore a dynamic relationship exits between differing zones in the littoral environment, each contributing to processes in the other.

As defined by Komar (1998), the components of the coastal zone are as follows. First, the *backshore* is the zone that extends from the foreshore to either the beginning of vegetative growth, or to a change in physiography of the beach environment. In permafrost environments, the sediments of this zone are ice-bonded in nature, allowing for the formation of steeply angled coastal bluffs. The *foreshore* is the sloping portion of the beach resting between the upper limit of wave swash at high tide and the watermark associated with low tide. This term is interchangeable with *beach face*, but is more often used. Sediments in this region are composed mainly of sands or small pebbles, and form an unfrozen layer protecting the underlying frozen sediments from thermal erosion. Due to the minimal wave power in this zone, these sediments are not entrained and carried into the nearshore zone unless driven by a storm system. A *berm*, or ridge structure, is formed parallel to the shore due to the deposition of sediment from extensive wave action; a *beach scarp* separates several berms. In Arctic environments, wind-driven sea ice can form berm-like structures. In some cases, these ice-push features significantly modify the nearshore and backshore profiles as ice can be moved tens of metres inland, overtopping existing spit and bar structures. The *inshore zone* extends from the foreshore to just past the point of breaking or shoaling waves, and the *offshore zone* extends from the limit of the inshore zone to the edge of the continental shelf. Permafrost often extends into the offshore zone, but is difficult to map due to problems associated with drilling in the continental slope region. *Longshore bars* and *longshore troughs* are ridges and gullies of sand that lie parallel to each other in the inshore and offshore zones, running parallel to the shoreline. Often, breaks in longshore bars are due to sediment transport by rip currents, which run perpendicular to the shoreline (Walker and Plint 1992).

The coastal sediments of the southern Beaufort Sea are composed almost entirely of unconsolidated medium- to fine-grained sediments high in ice content, which are

highly susceptible to coastal erosion (Harper 1990). The Mackenzie River contributes approximately 150×10^6 tonnes of silt- and clay-sized sediment to the nearshore zone, most of which is carried eastwards by longshore currents to be deposited along the continental shelf (Harper 1990).

Beaufort Sea coastal sediments have been roughly categorized into four classes, which include (Harper *et al.* 1988):

(1) Ice Poor Cliffs – coastal cliffs composed of sand- and gravel-sized sediments, fronted by a beach zone measuring 15 m or less.

(2) Ice Rich Cliffs – coastal cliffs composed of sand- and mud-sized sediments, fronted by a beach zone measuring 15 m or less. The upper segments of the cliff demonstrate thermokarst processes such as retrogressive thaw slumps, with resulting mudflows extending across the beach zone.

(3) Low Tundra Cliffs – coastal cliffs are low, fronted by narrow beaches composed of sand- and gravel-sized sediments; log lines deposited through storm surge and wave action extend inland.

(4) Inundated Tundra – coastal cliffs are low, beaches are extremely narrow or nonexistent, with submerged tundra extending into the shore zone. This is an organic-rich area with high rates of coastal retreat.

Coastal systems are highly influenced by wind and water processes for three to four months a year. However, during the winter freeze-up ice becomes cemented to the shore and bottom sediments. During the spring thaw, this landfast and bottom-fast ice causes (*a*) erosion in the nearshore zone through the offshore transportation of sediment frozen within the ice, and (*b*) the creation of deep troughs (*ice scours*) as wave action and longshore currents pull the ice out into the offshore zone. These two processes constitute an important part of coastal zone morphology in the Beaufort Sea (Harper 1990; Hill 1990; Héquette and Barnes 1990; Ruz *et al.* 1992; Héquette *et al.* 1995).

2.4 The Nearshore Zone

The nearshore zone (Figure 16) lies between the shoreline and extends just past the region where waves break (Komar 1998). It often contains many different geologic materials that are constantly being altered through coastal processes (Dallimore *et al.* 1988). The nearshore zone includes the *breaker zone*, where incoming waves become unstable and break; there is often more than one breaker zone associated with a naturally occurring beach. The *surf zone* is characterized by the curling that occurs after a wave breaks. The *swash zone* is alternatively covered by the run-up of waves and exposed by backwash (Komar 1998).

The breaker zone and surf zone are the most important components of the nearshore zone, for this is where both fine and coarse sediment is first introduced into the water column through the action of wave breaking. The ability of a wave to pick-up coarser grained sediment is dependent upon the energy of that wave, expressed as

[1] $$E = \frac{1}{8}\rho g H^2$$

where E is the total wave-energy density, ρ is the density of water, g is the acceleration of gravity, and H is the wave height (Komar 1998). The surf zone is also where currents occur, such as longshore and rip currents. When water depth is less than or equal to half the wavelength, the waves begin to shoal (Komar 1998). Depending on the slope of the nearshore zone, three distinct types of breakers may result. *Spilling breakers* form on a nearly horizontal beach, *plunging breakers* form on a fairly steep beach, and *surging breakers* form on a very steep beach. Knowledge of the nearshore morphology is vital to understanding how wave energy will dissipate, thus influencing nearshore currents and the transportation of suspended sediment (Komar 1998).

In the vicinity of Herschel Island, suspended sediment is carried around the island in two directions by longshore currents (Figure 17). These currents have created two distinct aggradational spits, Avadlek Spit extending from the southwest corner of the island, and Osborne Point extending from the southeast corner.

Under normal conditions, there exists an equilibrium between onshore wave action and erosion of the beach face. However, during storm conditions, there is a net offshore transport of sediments due to the increased velocity of bottom currents (Héquette

and Hill 1993; Komar 1998). After the storm has dissipated, a proportion of this sediment may again return to the beach zone, dependent upon the depth of the water column and the capacity of the waves to transport large volumes of sediment during fair conditions (Héquette and Hill 1993). Therefore the transport of sediment from the coastal zone is highly variable, and in this region of the Beaufort Sea is dependent upon high-energy conditions (Héquette and Hill 1993).

Field data of erosion mechanics, wave energy and sediment transport are extremely difficult to acquire and even more so in the Arctic. Accordingly, there is little or no information on Arctic coastal sediment transport rates (Héquette and Hill 1993). As hydrocarbon exploration in this region is expected to increase in the coming years, coupled with temperature increases due to climatic warming, further investigations are highly warranted.

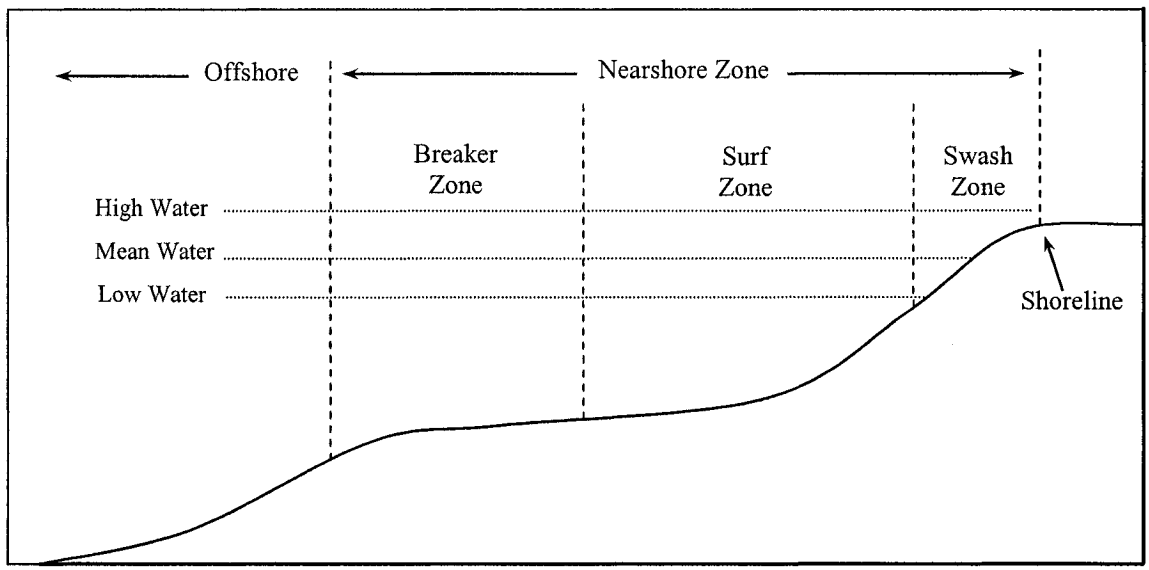

Figure 16: **The nearshore zone, including high, average and low water levels (after Komar 1998, p.46).**

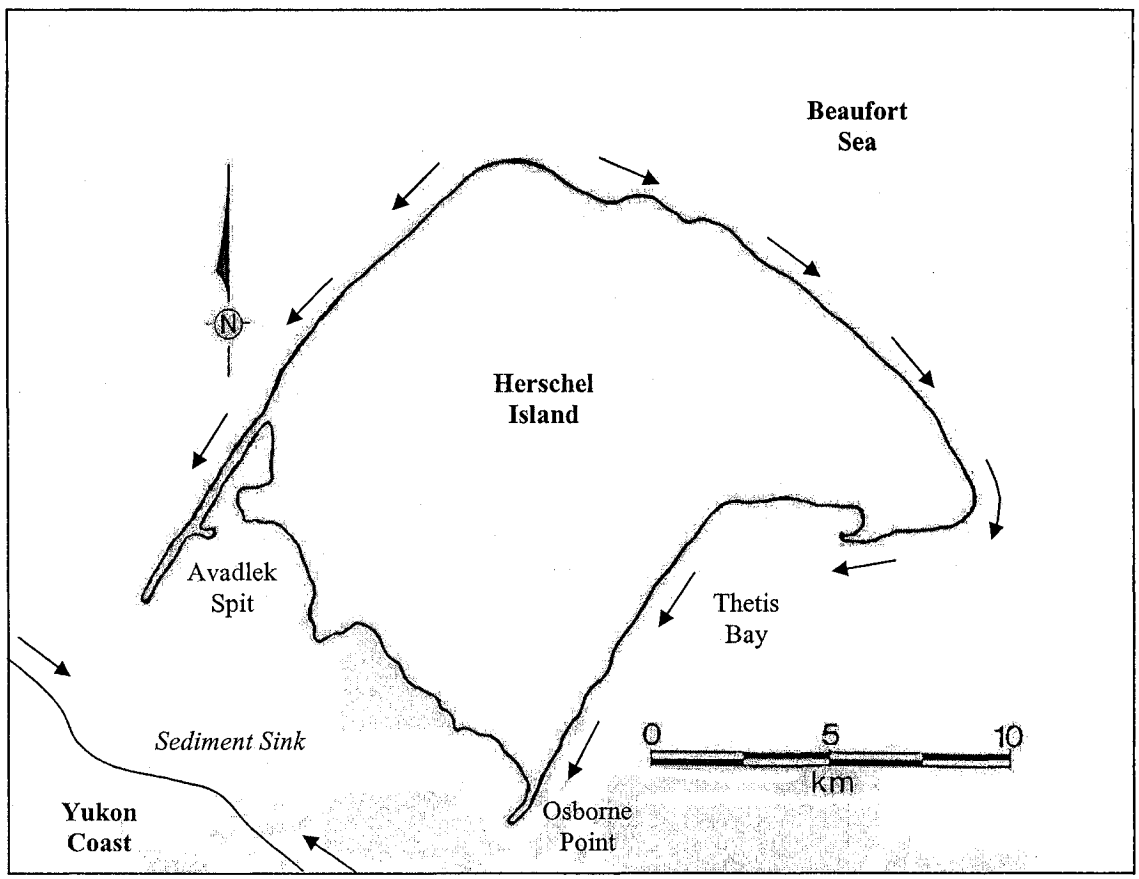

Figure 17: **Longshore currents surrounding Herschel Island, based on airphoto interpretation.**

CHAPTER 3 – METHODOLOGY & ANALYSIS

3.1 Introduction

In order to evaluate how erosional processes such as thermoerosional niche development affect rates of coastal retreat on Herschel Island, a combination of fieldwork and modeling techniques were used. Specifically, a numerical model developed by Kobayashi *et al.* (1999) was utilized to both hindcast rates of coastal erosion in the period 1970-2000, and to predict future erosion based on a climate change scenario. Validation of the model output was then obtained by comparing the results of the hindcast data with rates based on the analysis of remotely sensed images (Lantuit 2002, 2004).

The dominant variables affecting the rate of retreat along the Canadian Beaufort Sea coast were derived from an exhaustive literature search. Statistical information on the climatic, geomorphic, and oceanographic variables was compiled. Previous studies involving the measurement of coastal erosion rates in the Beaufort Sea were analyzed for commonalties. To this end, a wind and wave database from the previous 30 years was compiled from existing datasets. These included reports by the Atmospheric and Environment Service (AES), reports requested by hydrocarbon exploration companies (such as Shell), and individual articles published in refereed journals (Appendix A—1 and A—2). This produced a fairly comprehensive database which was then analyzed against a personal database created using wind speed, wind direction, and air pressure data procured from the Atmospheric Environment Service out of Tuktoyaktuk, NWT (Appendix A—3). Storms identified in existing reports were compared against this original dataset in order to obtain a measure of accuracy. All data was then run through a basic statistical analysis to determine general wind direction, wind speed, resulting wave heights, and storm duration. The results of this analysis are provided later in Chapter 3.

Remote sensing has been used to quantify the amount of coastal retreat that has occurred on Herschel Island, Yukon Territory over the past 35 years (Lantuit 2002, 2004). An attempt to quantify coastal evolution of the southern Beaufort Sea has also been reported in studies by Mackay (1963); Henry (1974); Harper *et al.* (1978); Kobayashi and Atkan (1986); Walker (1988); Héquette and Barnes (1990); Hill (1990); Ruz *et al.* (1992); Solomon *et al.* (1994); Dallimore *et al.* (1996); Wolfe *et al.* (1998);

Kobayashi *et al.* 1999); Hill and Solomon (1999); Héquette *et al.* (2001) and Brown *et al.* (2003).

Examining coastal erosion in the Canadian Beaufort Sea is troublesome due to the scarcity of comprehensive data, not to mention confounding variables such as wave attenuation due to ice floes. Even though an attempt has been made in the last 5-10 years to collect and record data in a more consistent manner, there still remains the need for greater communication between individuals and agencies to ensure that varying datasets can be compared on a basic level (Solomon and Hart 1999).

3.2 Fieldwork

Brief fieldwork was conducted in September 2003 on Herschel Island, Yukon Territory in order to identify active coastal erosion processes, and to possibly observe thermoerosional niche formation and subsequent block failure. An aerial survey of coastal conditions was undertaken, as well as a series of site-specific measurements of ground ice content.

A Trimble 4700 GPS system was also used during this field season. The base was set up just to the rear of the main building on Herschel Spit, and readings were taken around the island at select sites, allowing accurate comparisons of coastal positions to be made from year-to-year.

The predominant method of data collection during this field season was oblique photography taken from the helicopter between King Point and Herschel Island, as well as on Herschel Island. This data is used to visually record the conditions of the island both during and after the storm of September 21-23, 2003.

Figure 18: Sample site #1, Herschel Island, Yukon Territory (2003).

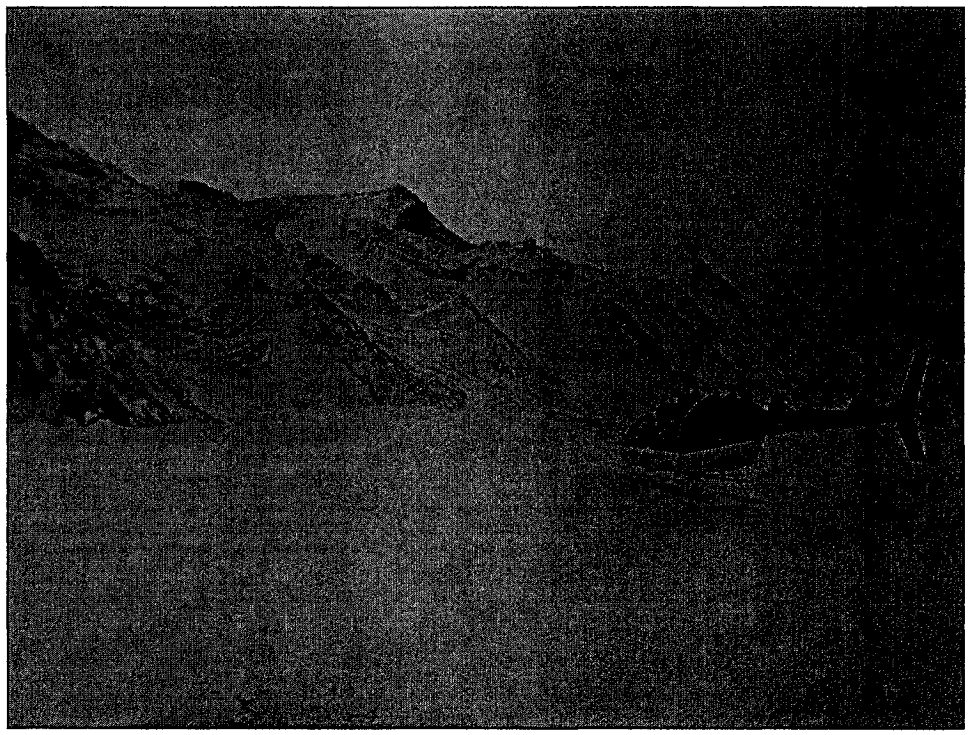

Figure 19: **Sample site #2, Herschel Island, Yukon Territory (2003).**

Figure 20: **Sample site #3, Herschel Island, Yukon Territory (2003).**

3.3 Data Analysis

3.3.1 Storm Selection

Storm selection followed the criterion that was outlined in several existing reports – Murray and Maes (1986); Eid and Cardone (1992); Solomon *et al.* (1994), based on wind speed and storm duration. An event was considered a storm if the minimum wind speed reached 37 km/h for a minimum of 6 hours. The database compiled in the Solomon *et al.* (1994) report was originally obtained by the Atmospheric Environment Service (AES) from the Tuktoyaktuk DEW-line station, which has records extending back to 1958. Based on hourly observations, 211 storms meeting the above criteria between the years 1959 and 1992 were identified (Solomon *et al.* 1994). Often storm climate studies use data obtained from wave hindcast models, which obtain their base data from wind records for the region. In the creation of an original storm database, this method was also utilized.

This inventory was compared with datasets obtained in other reports and papers. For example, Henry (1974) recorded all storm surges at Tuktoyaktuk greater than 0.91 m (3 feet) between 1962 and 1973. These 23 surge events were compared with those of Solomon *et al.* (1994), who showed 38 storms with wave heights of >0.91 m for that same period. Only 43% of storms recorded in both reports correlated. Of the remaining, 22% were ±1 day of the storms as reported in Solomon *et al.* (1994). The other 35% showed >1 days difference.

The data presented by Eid and Cardone (1992) are slightly different from the data presented in Solomon *et al.* (1994) given that the measurements were taken offshore. Consequently, the storm signals appear to be both more severe and longer lasting than coastal signals (Solomon *et al.* 1994). There is a difference of 1.5 between the maximum observed wind speeds between the Eid and Cardone (1992) report, and the values presented in the Solomon *et al.* (1994) report.

3.3.2 Storm Database Statistics

A summary of the Eid and Cardone (1992) dataset is presented in Table 3. Yearly storm frequency was calculated (Figure 21), and rose plots were created to demonstrate the storm wind vectors (Figure 22).

	Storm Duration hours	Max Wind knots	Max Wind km/h	Mean Direction degrees	Wave Height metres	Wave Period seconds
Mean	121.46	40.68	75.33	206.10	4.14	6.47
Median	99.5	40	74	245	4.0	6.0
Mode	72	45	83.4	280	4.0	6.0
Std Dev	65.606	7.386	13.678	104.008	1.593	2.363
Min	38	22	40.7	30	0.5	0.0
Max	295	63	116.7	360	9.5	16.0

Table 2: Storm database statistics (Eid and Cardone 1992).

Of the 50 storms presented in this report, the average storm lasted 121.5 hours with an average maximum wind velocity of 75.3 km/h, an average wind direction of 206° (SW), and an average wave height of 4.1 m. Standard deviation values clearly illustrate that both storm duration and wind direction showed the greatest amount of scattering in the data. Appendix A—1 contains the raw data used in this analysis. A peak wave height of 9.5 m is associated with a large storm event in 1962. As Figure 21 demonstrates, this storm represents a peak for major storm activity until the early 1970's, when another large storm was reported. This was again followed by a lull until the 1980's when high-magnitude storm activity peaked (Solomon *et al.* 1994).

Figure 22 shows the storm wind vector averages for the 50 storms reported in Eid and Cardone (1992). Wind vectors were first grouped into 15° classes, and then into 10° classes. The purpose of this was to see if there would be a significant change in the distribution of the wind vectors, based on how the data was organized. Results showed no notable change in the distribution when the data was grouped in this manner. Based on 139 individual storm readings collected and analyzed from the Environment Canada On-line Climate Archive (1970-2000), wind direction shifted an average of 20° during a storm. The importance of wind vectors to the growth of ocean waves is not well documented in the literature. Komar (1998) briefly mentions the negative effect of "contrary winds" to wave growth (p. 179-183), however this idea is not elaborated on.

For this study, it will be assumed that the effect of contrary winds is minimal, and therefore will not be considered.

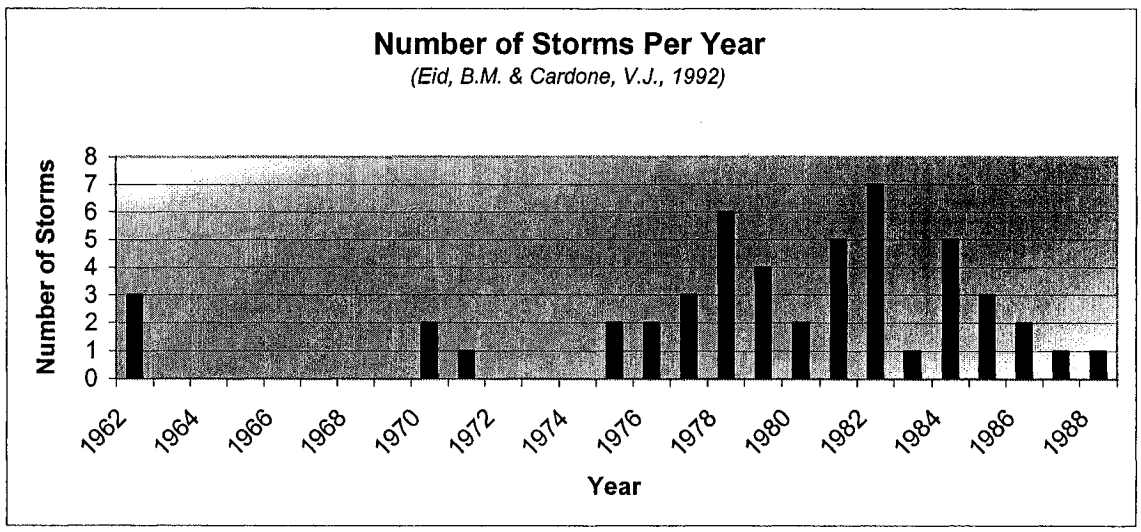

Figure 21: **Storm frequency in the Canadian Beaufort Sea (1962-1988).**

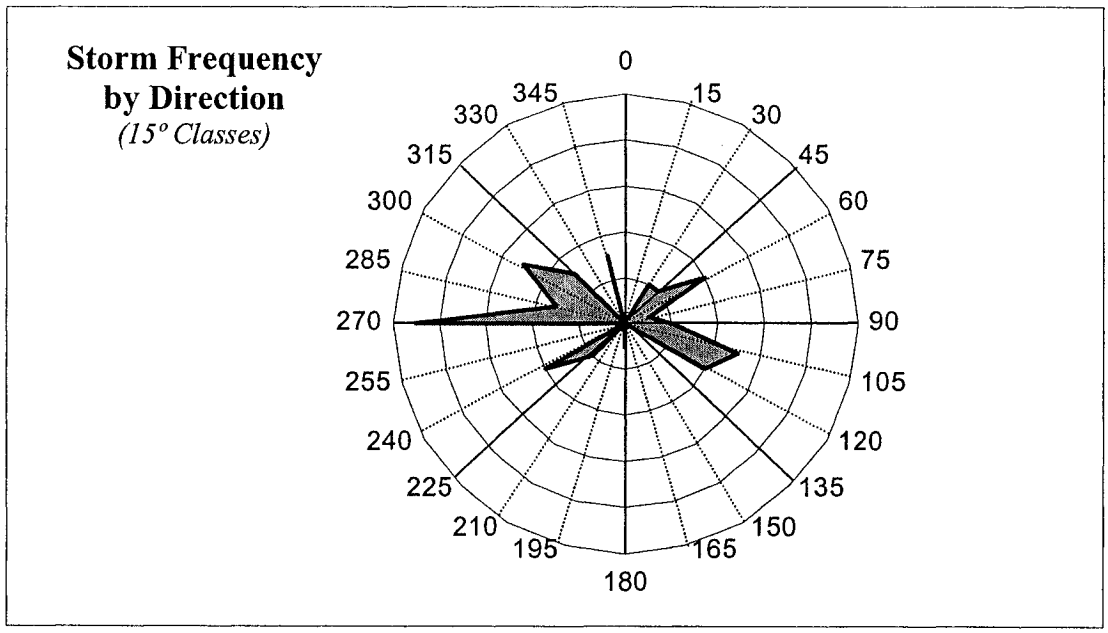

Figure 22: **Storm wind vector analysis for 15° classes. Directions were calculated as the average of the wind at the beginning and end of each storm event (Solomon *et al.* 1994).**

When the wind vector information is divided into 15° classes, the greatest number of storms originate at 270° (9 storms in total), however the predominant direction is

between 270° and 315° (20 storms in total). It is clear from the wind vector graph that the predominant storm direction is from the NW.

Data compiled and analyzed by Solomon *et al.* (1994) for Tuktoyaktuk shows similar trends to that of Eid and Cardone (1992). However, some differences must be noted. As stated previously, the wind data used in the Eid and Cardone report were taken primarily offshore, whereas wind data used in the Solomon *et al.* (1994) report was derived from the Tuktoyaktuk DEW-line station. Therefore, a difference of magnitude of 1.5 exists between the two reports. This difference is derived from the variation between the friction factor of the sea surface during a storm and of the land surface (Solomon *et al.* 1994).

The 50 events chosen by Eid and Cardone (1992) represented the storms of greatest significance in the period 1962-1988. Upon comparison of these 50 storms with the 211 storms reported in the 1994 report, there was only 60% congruence. Additionally, Eid and Cardone often grouped several storms into a single event, resulting in durations repeatedly in excess of 100 hours. This method would likely produce erroneous results, as dissipation of wave energy between several smaller events would significantly reduce the total cumulative wave energy intercepted by the coast (Solomon *et al.* 1994).

Storms were categorized in the Solomon *et al.* (1994) report based on sustained winds of ≥37 km/h for a minimum of 6 hours. Upon examining this data, it was apparent that several separate events were quite possibly one continuous 3-day event. This revised list of storms is available in Appendix A—2. To agglomerate the individual storms, the highest value for fetch was kept, as well as the maximum values for wave height and wind speed. The lowest value for minimum wind speed was kept, and the average for wind direction was obtained. Calculating total duration for the storm proved somewhat problematic, as it was not recorded at what time a storm interval began. It was decided that total duration would begin on the first recorded day, and would end after the duration of the last recorded storm day. For example, two distinct storms recorded as:

Date	Wind Direction (°)	Duration (hrs)
1960-09-17	320	7
1960-09-19	305	25

Would agglomerate into:

Date	Wind Direction (°)	Duration (hrs)
1960-09-17	312.5	73

This method of reduction brought the total number of storms from 211 to 186.

Data in the Solomon *et al.* (1994) report was analyzed. Basic statistical measures are presented in Table 4. Yearly storm frequency was calculated (Figure 23), and rose plots were created to demonstrate the storm wind vectors (Figure 24).

	EF km	Duration hours	Max Wind km/h	Mean Direction degrees	Hs metres
Mean	138.4	18.4	45.9	240.6	2.0
Median	367.8	13	44	195.2	2.3
Mode	71.4	7	37	290	2.2
Std Dev	81.170	19.912	7.842	99.485	0.577
Min	18.0	6.0	37.0	5.0	1.1
Max	367.8	109.0	72.0	365	4.1

Table 3: Storm database statistics (Solomon *et al.* 1994).

Of the 186 storms in the revised dataset, the average storm lasted 18.4 hours with a maximum wind velocity of 45.9 km/h, a wind direction of 240.6°, and an average wave height of 2.0 m. Variance analyses of key variables show that mean wind direction was the most varied, followed by high values for effective fetch and storm duration, with standard deviations of 99.5, 81.2 and 19.9, respectively. The maximum wave height (4.1 m) is associated with a large storm event on September 14, 1970. This storm was well documented as the largest recorded storm over the years of recorded data, although an unrecorded storm in 1944 may have had the same magnitude.

Storm frequency was extremely variable over the 40 years of available data from the Tuktoyaktuk DEW-line. 1963 represents a peak in storm activity, and was responsible for a major storm in late July that damaged the coastline as far west as Barrow, Alaska (Solomon and Hart 1999). 1973 represented the lowest number of storms per year. In the 1980's however, storm frequency again increased, and was relatively stable until the beginning of the 1990's, when the number of storms per thaw season again decreased.

When the wind direction information is divided into 15° classes, the greatest number of storms originate from 285° (33 storms in total), however the predominant direction is between 270° and 345° (117 storms in total). Results mirror those of Eid and Cardone (1992), as the predominant storm direction is NW.

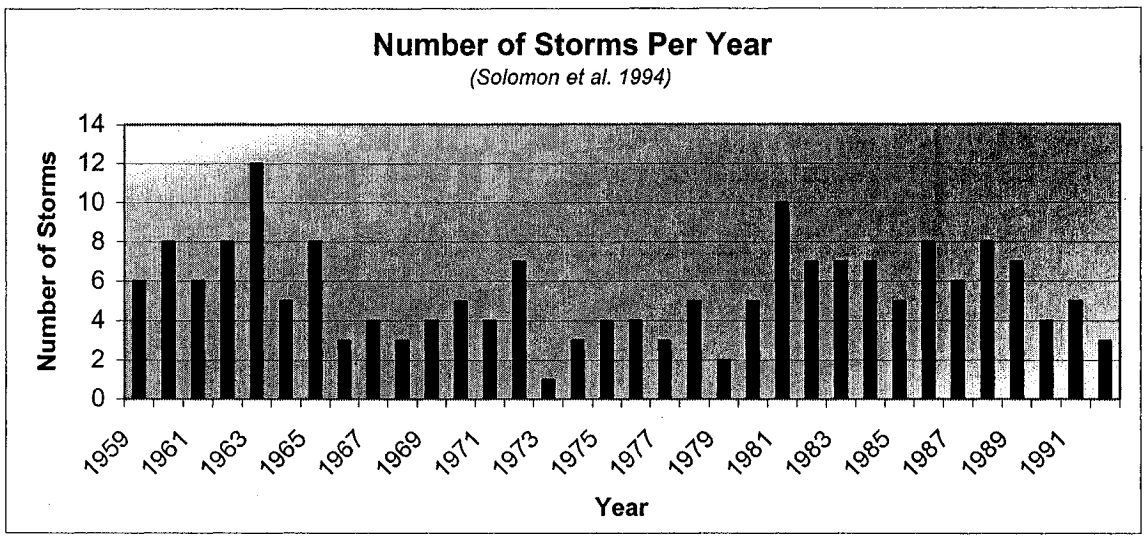

Figure 23: Storm frequency in the Canadian Beaufort Sea (1959-1992).

An original storm dataset was created from climate records obtained from the Environment Canada On-line Climate Data Archive for the period 1970-2000 (Appendix A—3). These data were obtained from the anemometer positioned at a height of 10 m at Tuktoyaktuk. Accuracy of the anemometer is within ± 1 m/s for winds below 15 m/s, and within 1.5 m/s for winds greater than 30 m/s (Murray and Maes 1986). These years were chosen as they coincide with available air photography for the same region. Using the criteria outlined above, 139 storms were identified in the region of Tuktoyaktuk NWT. Figure 25 demonstrates yearly storm values.

As demonstrated in both the Eid & Cardone (1992) and Solomon *et al.* (1994) datasets, there was relatively little storm activity in the 1970's. Peak activity occurred in the 1980's, which was then followed by a trough in the late 1980's and 1990's. Excluding the anomalously high storm activity of 1994, this trough has continued through recent years. Table 4 provides the associated statistical data.

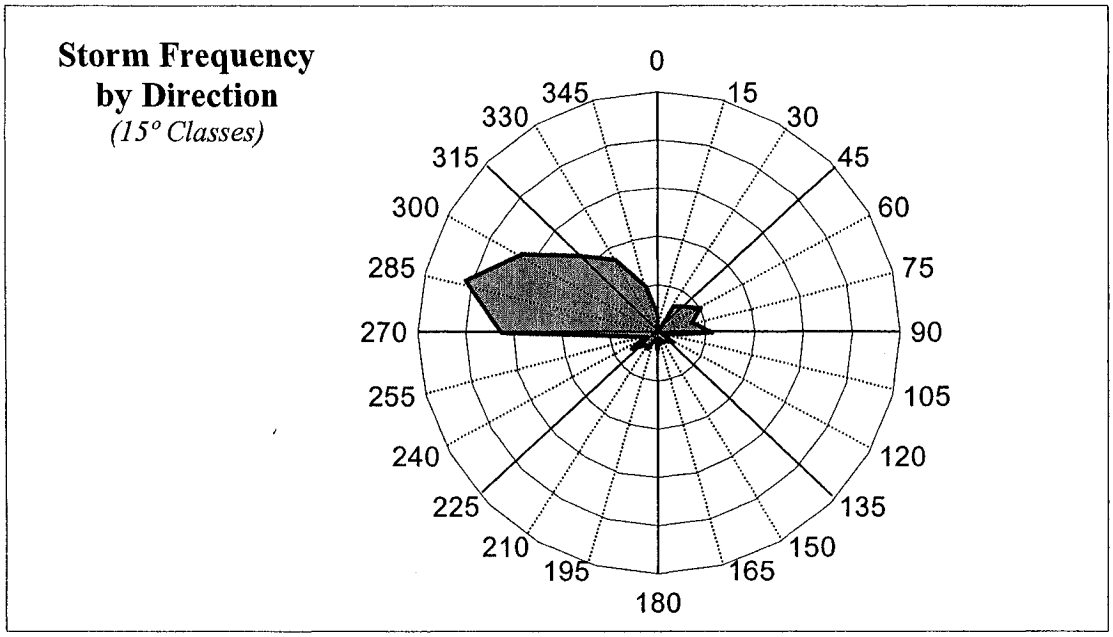

Figure 24: **Storm wind vector analysis for 15° classes. Directions were calculated as the average of the wind at the beginning and end of each storm event (Solomon *et al.* 1994).**

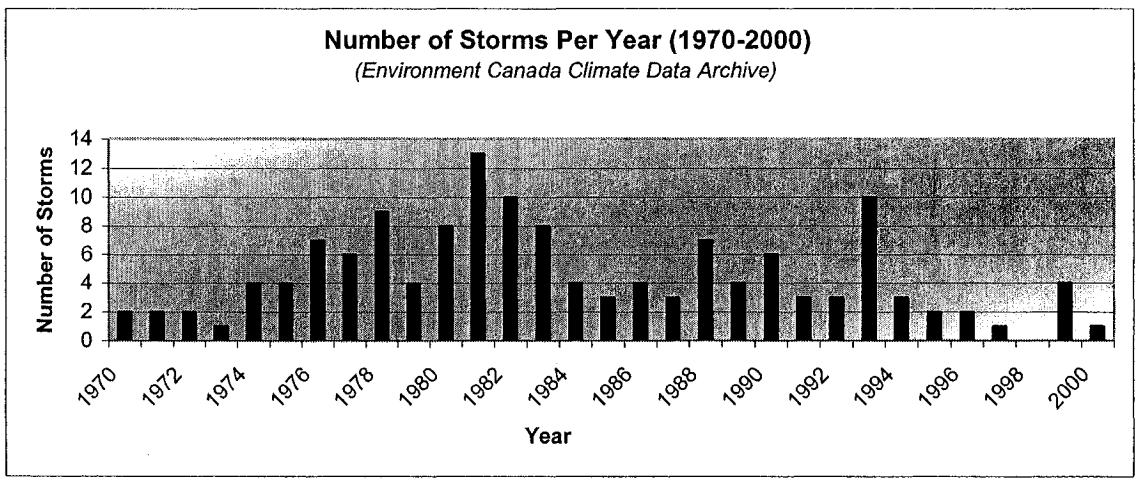

Figure 25: **Number of storms per year, 1970-2000. Original data obtained from the Environment Canada Climate Data Archive (on-line).**

Average storm duration and wind speed measured 16.4 hours and 42.3 km/h, respectively. Mean atmospheric pressure readings during storm activity were identified at 100.95 kPa, just below the average sea air pressure of 101.33 kPa. This corresponds to a general drop in air pressure as the storm front moves into the area. This drop in pressure is also responsible for a rise in sea level due to the reduced pressure on the ocean

surface. Generally, storm winds originated at 250° (predominantly from the west). Figure 27 demonstrates all of the calculated wind vector readings, grouped into 15° classes.

	Duration (hrs)	Mean Wind Direction (degrees)	Wind Deviation (degrees)	Avg Wind Speed (km/h)	Max Wind Speed (km/h)	Min Wind Speed (km/h)	Atmospheric Pressure (kPa)
Avg	16.4	249.2	20.6	42.3	50.7	35.7	100.95
Min	6.0	20.0	0.0	37.0	37.0	19.0	99.34
Max	74.0	340.0	70.0	58.5	87.0	44.0	102.60
Std Dev	11.7	88.8	13.9	3.9	8.9	3.2	0.64

Table 4: **Storm database statistics (1970-2000).**

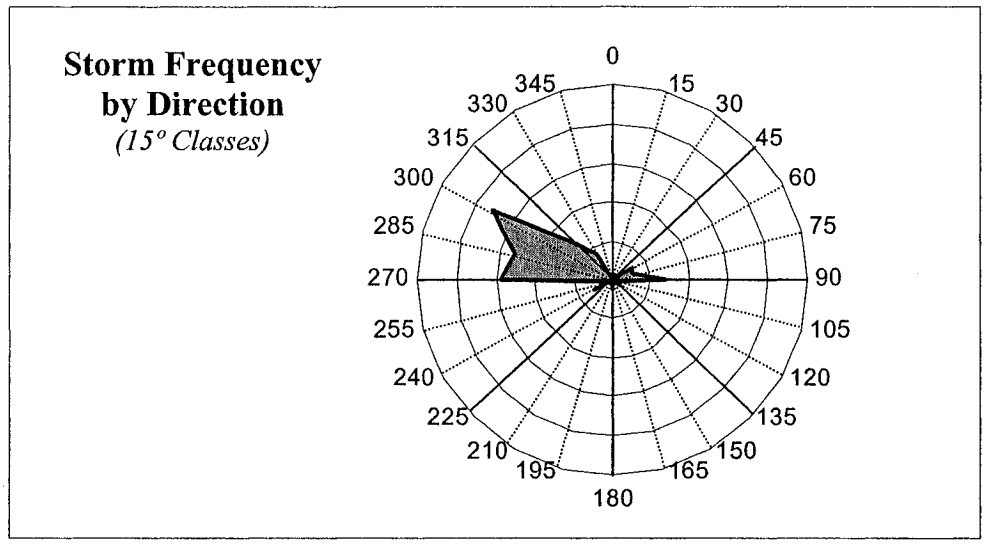

Figure 26: **Storm wind vector analysis for 15° classes. Directions were calculated as the average of the hourly readings throughout the storm period.**

3.5 Numerical Modeling

A numerical model was created based on Kobayashi *et al.* (1999) to predict the total horizontal retreat of a frozen cliff due to storm surge on the Beaufort Sea coast due to convective heat transfer to the frozen cliff sediments. Input variables include storm surge heights and duration, cliff height, seawater temperature and salinity, sediment characteristics, and wave conditions (Kobayashi *et al.* 1999).

In this model, it is assumed that seawater temperature and salinity remain constant for the duration of the storm. As well, alongshore uniformity and normally incident waves were assumed in the original model, in order to limit the analysis to the cross-shore direction (Kobayashi *et al.* 1999).

Several issues arise when attempting to model coastal processes based on environmental data. For instance, a specific wave pattern results from a unique set of conditions based on wind direction and coastal geometry; therefore, a different set of circumstances in the future will generate a different wave sequence, resulting in different morphological changes to the coastline. For example, a storm originating from the northeast with sustained winds of 40 km/h for 10 hours will produce waves of a certain height and period. These waves will be altered by the bathymetry in that region, and therefore will attack the coast in a very specific way, resulting in defined processes of coastal erosion. However, a storm originating from the northwest with sustained winds of 57 km/h for 30 hours will produce very different waves. These will also be influenced by the bathymetry of that aspect of the coast, and will thus affect the coastal sediments differently than the first storm. This problem is referred to as the *input chronology effect* (Dong and Chen 2001). This problem is more pronounced during shorter time intervals; it becomes increasingly insignificant over the period of several decades (Dong and Chen 2001). Also, as demonstrated in section 3.3.2, wind and/or wave data is often not exact, and may be inconsistent over the period of record. In the Canadian Beaufort Sea region, a consistent 30-year record is still lacking (Solomon *et al.* 1994; Solomon and Hart 1999).

The numerical model developed by Kobayashi *et al.* (1999) assumes that unfrozen sediment is transported away from the beach through wave action. The coarser sediment (sand and gravel) settles out of the water column in the nearshore zone, however the finer

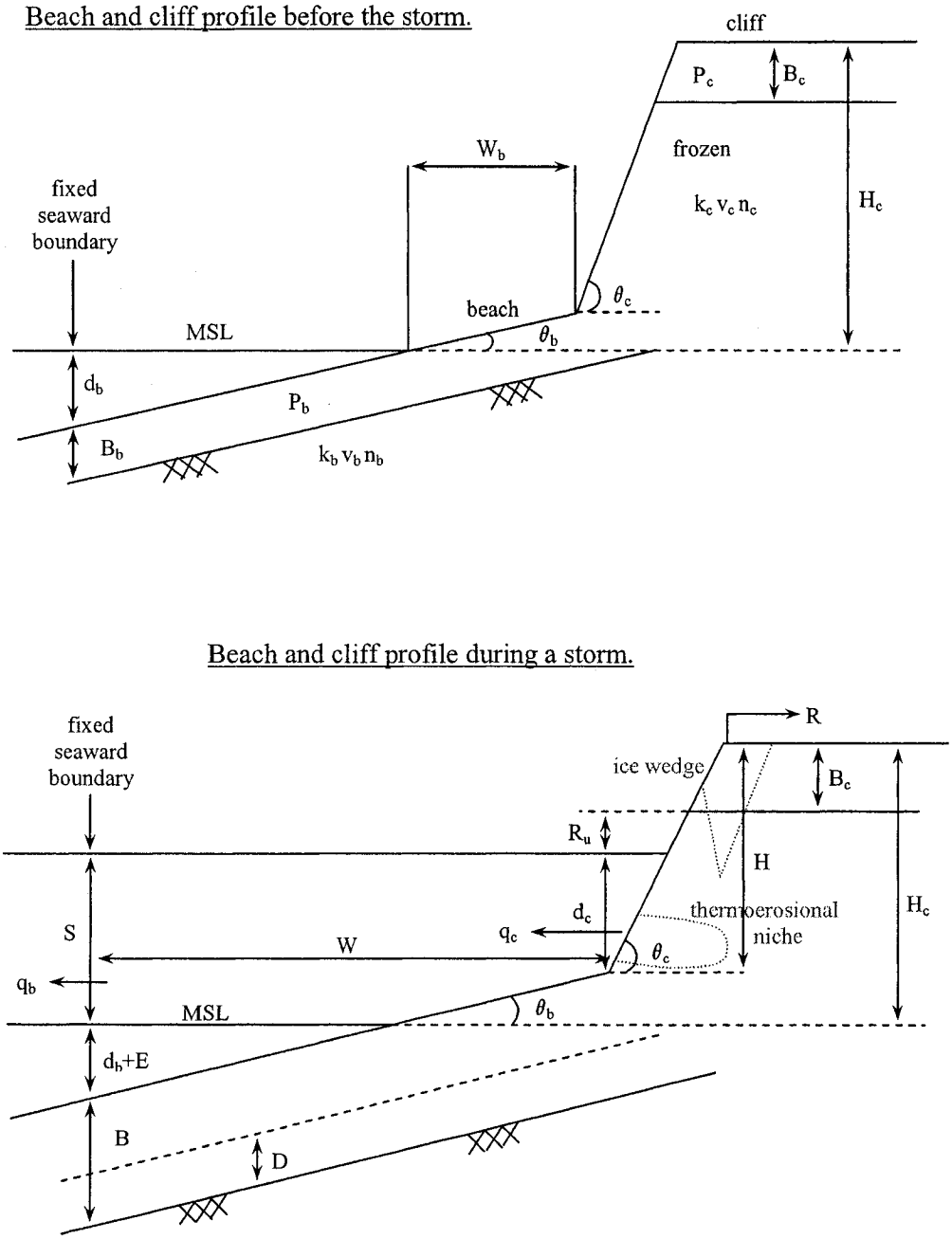

Figure 27: **Input and output variables associated with the numerical model (from Kobayashi *et al.* 1999).**

sediment (silt and clay) remains entrained within the water column and is transported into deep water. When the still water depth at the toe of the cliff (d_c) is ≤ 0 it is assumed that no cliff erosion is taking place, and that there is no offshore sediment transport. Therefore,

[2] $$\frac{dR}{dt} = 0 \ \ and \ \ q_c = 0 \ \ for \ \ d_c \leq 0$$

where R is the horizontal cliff retreat, and q_c is the offshore coarse sediment transport rate at the cliff toe. However during high magnitude events, $d_c > 0$ due to storm surge. Therefore, the inclined length of the frozen cliff sediment (ℓ_c) exposed to wave action is estimated as

[3] $$\ell_c = \frac{\min[(R_u + d_c),(H - B_c)]}{\sin\theta_c}$$

where *min* refers to the minimum values associated with the variables in the square brackets, R_u is the wave runup on the cliff face, H is the height of the cliff above its toe, B_c is the initial thickness of the unfrozen beach sediment, and θ_c is the seaward cliff slope angle. The latent heat of fusion into the frozen cliff sediment is considered the primary thermal force, resulting in a horizontal retreat rate equation of

[4] $$\frac{dR}{dt} = \frac{\ell_c h_c (T_w - T_m)}{L_c (H - B_c)} \ \ for \ d_c \rangle 0$$

where ℓ_c is the inclined length of the frozen cliff sediment, h_c is the convective heat transfer coefficient on the exposed frozen cliff sediment between the ambient seawater temperature (T_w) and the volumetric latent heat of fusion per unit volume of the frozen beach sediment (L_c), and T_m is the melting temperature of the ice embedded in the frozen beach and cliff sediment. The offshore coarse sediment transport (q_c) per unit width at the base of the cliff is assumed equivalent to the amount of sediment that is available to the beach zone. Therefore,

[5] $$q_c = [P_c B_c + v_c (H - B_c)] \frac{\ell_c h_c (T_w - T_m)}{L_c (H - B_c)} \ \ for \ d_c \rangle 0$$

where P_c is the coarse sediment volume per unit volume of the unfrozen cliff sediment and v_c is the coarse sediment volume per unit volume of the frozen cliff sediment. This model does not take into consideration accumulation of sediments at the cliff toe, as

predicting such an accretion rate would prove to be highly problematic (Kobayashi *et al.* 1999).

The volume balance of the unfrozen coarse sediment on the beach is expressed in Kobayashi *et al.* (1999) as

[6] $$\frac{dB}{dt} = \frac{q_c + q_{melt} - q_b}{P_b W}$$

where B is the thickness of the unfrozen beach sediment, q_{melt} is the coarse sediment supply rate due to the melting of the frozen beach sediment over the width (W), q_b is the offshore coarse sediment transport rate at the seaward boundary where water depth is given by ($S + E + d_b$) during the storm, and P_b is the coarse sediment volume per unit volume of the unfrozen beach sediment. S refers to the increase in water level above mean sea level during a storm, E is the total vertical eroded depth on the beach, and d_b is the fixed seaward boundary before the storm. Kobayashi and Vidrine (1995) showed in their report that the main controlling factor influencing the rate of erosion on the beach is not the heat conduction through the unfrozen sediment, but the heat conduction directly influencing the frozen sediments due to wave action and storm surge. Therefore $q_{melt} = 0$ when unfrozen sediment still remains on the beach ($B > 0$).

When the beach sediments are exposed to storm surge and wave action, the vertical melting depth (D) of the beach sediment is expressed as

[7] $$\frac{dD}{dt} = \frac{h_b(T_w - T_m)}{L_b} \quad for \quad B = 0$$

where h_b is the convective heat transfer coefficient on the exposed frozen beach sediment, L_b is the volumetric latent heat of fusion per unit volume of the frozen beach sediment, and B is the thickness of the unfrozen beach sediment. Therefore the coarse sediment volume released into the nearshore zone (expressed as a rate) per unit volume of melted sediment is defined as

[8] $$q_{melt} = v_b W \frac{h_b(T_w - T_m)}{L_b} \quad for \quad B = 0$$

where v_b is the coarse sediment volume per unit volume of the frozen beach sediment. The amount of coarse sediment available to be transported into the nearshore zone is dependent upon the duration of the storm event. Wave energy in the vicinity of Herschel

Island is attenuated due to the shallow nearshore water conditions and the gentle gradient of the continental slope. The upper limit of the coarse sediment transport rate is therefore expressed as

[9] $$q_p = \alpha P_b \left(\sqrt{S + E + d_b} \tan\theta_b - \frac{2}{3} A^{3/2} \right)$$

where α is an empirical parameter (0.01 $m^{1.5}/s$ for ice-free sand beaches), θ_b is the beach slope angle, and A is a parameter related to equilibrium beach profiles (approximately 0.1 $m^{1/3}$ for sand). The parameter α in equation [8] was designed by Kobayashi *et al.* (1999) specifically for arctic beaches backed by cliffs, as is the case on Herschel Island. For this equation to function properly, the fixed seaward boundary before the storm (d_b) is equal to $d_b = (4A^3/9)/(\tan^2\theta_b)$ to ensure that $q_p = 0$ when $(S + E) = 0$ before the storm begins (Kobayashi *et al.* 1999). The typical beach slope was measured at $\tan\theta_b = 0.1$.

Upon examining equations [1] through [8], it is apparent that once storm surge and wave action have removed the initial layer of unfrozen sediment (B_b and B_c) from the base of the cliff, the potential coarse sediment supply rate (q_p) is dependent upon the ability of the water column to entrain and transport the melted sediment into the nearshore zone, where it may then be carried away by longshore currents.

The convective heat transfer coefficients (h_b and h_c) may be expressed as

[10] $$h_c = \frac{a f_w C_w U_b}{1 + F\sqrt{0.5 f_w}}$$

where a is the empirical parameter for wave-induced melting, f_w is the wave friction factor at the melting surface, C_w is the volumetric heat capacity of the seawater, U_b is the representative fluid velocity immediately outside the boundary later, and F is the parameter depending on whether the turbulent boundary layer flow is hydraulically smooth or fully rough. The use of heat coefficients in equations [3, 4, 6, 7 & 9] is imprecise due to the lack of data on the wave-induced melting of frozen sediment (Kobayashi *et al.* 1999).

Even though U_b was developed for use in deep water, it is also applicable inside the surf zone (Cox *et al.* 1996 *in* Kobayashi *et al.* 1999), providing the equation

[11] $$U_b = \frac{\pi H_r}{T_r \sin \cdot h(k_r d_r)}$$

where the wave depth (d_r) is calculated as being equivalent to d_c (with h_c also holding true on the cliff), and the average beach depth $(d_c + S + E + d_b)/2$ for h_b on the beach (Kobayashi *et al.* 1999). T_r is the wave period, and k_r is the linear wave number based on T_r and the wave depth, d_r. The wave data used as input to this model was obtained using the base wind data listed in Appendix A—3. An inherent problem with the base data lies in the definition of storm surge height. As no observed data was available, an equation to predict storm surge based on fetch length, wind speed, and average water depth was obtained from the Army Corps of Coastal Engineering Manual (1986),

[12] $$\frac{U^2 F^{\wedge}}{1400d}$$

where U is the average wind speed (miles/hour), $F^{\wedge}$ is the fetch distance (miles), and d is the average water depth (feet). An average fetch distance of 124.27 miles (200 km) was used to represent average maximum fetch during late summer in the southern Beaufort Sea (Hudak and Young 2002), and an average depth of 98.4 feet (30 m) was used to characterize the southern Beaufort Shelf (McGladrey 1984). However, this equation only provides a single value for storm surge, not how the surge heights vary at different points during the storm. Therefore, the model assumes a sinusoidal surge linked to the time steps of the model (Kobayashi *et al.* 1999).

Erosion of the coastal sediments was thus numerically modeled using values obtained for Herschel Island. The island was divided into three distinct zones based on the predominant wind orientation (W/NW/N, NE/E/SE, S/SW) and existing coastal morphologies, such as cliff height, cliff slope, and beach width (Table 5, Figure 38). The results of the simulations were then compared with known rates of retreat obtained using remote sensing techniques over the same 30-year period (Lantuit 2002, 2004) in order to validate the results.

Erosion of frozen cliff sediments in the model described above oftentimes results in the formation of a thermoerosional niche. The mechanics of this physical development, as well as results from the numerical model will be discussed in Chapter 4. When the development of the niche reaches a critical point, the overburden pressure exceeds the tensile strength of the sediments, resulting in a block failure. These results are also examined in Chapter 4.

CHAPTER 4 – COASTAL RETREAT & NICHE DEVELOPMENT

4.1 Introduction

As previously discussed, erosion of the coastal sediments in the Canadian Beaufort Sea is due primarily to wave action and storm surge during low frequency, high magnitude events. However, these factors cannot fully explain the high rates of coastal erosion in this region (Héquette and Barnes 1990). The interaction of sea ice with the nearshore zone creates an unstable profile that may cause increased rates of erosion as the beach regains equilibrium (Héquette and Barnes 1990). Once the fine- to medium-grained sediments are deposited in the nearshore zone, they are carried away from the beach by longshore and offshore currents. Storm surge elevations in this region are due to wind stress and wind direction, unlike in other regions where the surge is a function of atmospheric pressure and water depth (Solomon *et al.* 1994). The temperature of both air and seawater plays a crucial role in the stability of coastal sediments. Therefore, it is important to consider both the thermal and mechanical aspects that cause erosion (Aré 1988; Nairn *et al.* 1988; Wolfe *et al.* 1998; Kobayashi *et al.* 1999).

The development of wave heights in the Beaufort Sea are based primarily on wind direction, wind speed, and wind duration – available fetch plays only a minor role (Murray and Maes 1986). Winds generated over open waters may produce wave heights of 4 m or more, with peak periods up to 10 s (Pinchin *et al.* 1985; Hill and Nadeau 1989). Eid and Cardone (1992) predicted a 100-year storm design wave of 6.2 m in height for the same region.

During storm events, a thermoerosional niche may form at the base of the cliff due to the effect of increased water levels and wave heights. As the cold, saline waters of the Beaufort Sea interact with the coastal sediments, thermal conduction melts the intrasedimental ice, leading to increased rates of erosion of the coastal sediments. If massive ice is present in the coastal segment, substantial backwasting may occur in a relatively short period. Once the thermoerosional niche extends beneath the cliff to a certain point, the overlying block may become unstable. The presence of a failure plane associated with an ice wedge or other weakened zone allows the entire segment to detach from the cliff along a shear plane. This block then falls into the water at the base of the

cliff, essentially protecting that segment from further erosion until all the sediments are removed into the nearshore and offshore zones.

4.2 Geomorphic Principles

The sediments of the Arctic coastline consist of unconsolidated gravel, sand, silt, and clay, cemented together by icy permafrost. The presence of permafrost provides increased strength and cohesion, allowing coasts to form steeply angled bluffs (Davidson-Arnott 1986; Héquette and Barnes 1990). The grain-size of the sediment does not control coastal retreat, however the rheological properties such as plasticity, porosity, consolidation pressure, water content and ice content do (Héquette and Barnes 1990). Other critical factors influencing bluff retreat are the presence, size, orientation, and spacing of ice wedges, as well as the thermal energy transferred to the coast through wave action and solar radiation (Walker 1988).

Wave height and wave energy are extremely influential controls on the amount of coastal recession that occurs in that they govern the amount of sediment that is transported away from the beach zone. The Beaufort Sea has been characterized as a low-energy environment due to the wide and shallow continental shelf, and the presence of a permanent ice pack that limits wave growth (Héquette and Barnes 1990; Ruz *et al.* 1992). Because of these restrictions, Harper and Penland (1982) found that nearly 80% of deepwater waves in the Beaufort Sea are less than 1 m in height. This figure must refer to wave height during normal conditions, as wave heights during storm conditions are often in excess of 3.0 m. The 25- and 100-year return period for deep-water wave height has also been calculated at 6.2 and 7.7 m, respectively (Pinchin *et al.* 1985; Murray and Maes 1986; Eid and Cardone 1992; Solomon *et al.* 1994). Wave heights are often coupled with both tidal variations (0.3 - 0.5 m in the Beaufort Sea), and storm surges that form due to wind push and decreased air pressure. These surges have been recorded at 2.4 m above sea level at Tuktoyaktuk, which may represent a maximum for the past 100 years (Harper *et al.* 1988; Ruz *et al.* 1992; Solomon *et al.* 1994). However, this maximum height is likely due to a combination of storm surge, swash effect, tides,

and run-up on slopes rather than exclusively by a mean sea level rise (Mackay 1986; Walker 1988).

Physical processes associated with bluff erosion were described in Chapter 2, and include retrogressive thaw slumps, active layer detachment failures, the development and breaching of thermokarst lakes, and block failure associated with thermoerosional niche development. These processes are often wave-induced and dependent upon the amount and type of ground ice present in the coastal segment and the composition of the bluff sediments (Mackay 1986; Dallimore 1988; Héquette and Barnes 1990, Ruz *et al.* 1992). Thermokarst processes such as retrogressive thaw slumps often follow distinct cyclical patterns, characterized by an active phase followed by an interval of stability (Rampton and Bouchard 1975; Harry 1985; Mackay 1986). As material is eroded from the headwall during periods of activation, some of the material collects at the base of the slump, protecting it from both the direct influences of wave energy and further thermal degradation, thus allowing it to stabilize. During periods of increased wave activity, this material is quickly eroded from the base of the cliff creating a state of disequilibrium, thus reactivating the slumping process. This cycle of dormancy and activation has been identified as one of the critical processes affecting coastal erosion in the Beaufort Sea region (Mackay 1960, 1966, 1986; MacDonald and Lewis 1973; Harper 1978; Harry 1982; Forbes and Frobel 1985; Harry 1985; Héquette and Barnes 1990). Thus regional retreat is also related to the amount of sediment that may be eroded through wave action and transported away from the coastal zone by nearshore and longshore currents (Harper and Penland 1982; Héquette and Barnes 1990; Ruz *et al.* 1992).

While thermokarst processes make significant amounts of sediment available for erosion through waves and currents, they are not responsible for all the erosion that occurs. Other factors must also then be responsible for the rapid rates of erosion demonstrated in this environment (Héquette and Barnes 1990). Ice processes in the nearshore zone have been found to dislodge significant amounts of sediment from the seafloor through ice gouging, ice pile-up, and ice-enhanced current scour (Héquette and Barnes 1990; Hill 1990). Therefore it is the combination of physical and thermal processes, including those associated with sea ice in the nearshore zone, which are responsible for the large availability of sediment in this region.

The amount of coastal erosion that may occur during a storm is dependent upon the interaction of various factors throughout the thaw season. Beginning in May, landfast ice begins to break-up and move away from the shore zone, carrying with it entrained sediment. As this sediment is removed, the bathymetric profile loses its equilibrium. At the same time, the outer layers of coastal sediments begin to thaw (*a*). In June and July, the melting front has penetrated into the coastal sediments, resulting in thermokarst processes such as retrogressive thaw slumps and active layer detachment slides. Viscous sediment associated with these processes moves into the nearshore zone and aids in bringing the bathymetric profile back into equilibrium. Storms during this time may exacerbate this process (*b*). By August and September, thermokarst processes have reached their maximum, and large storms may result in extensive backwasting of the coastal sediments.

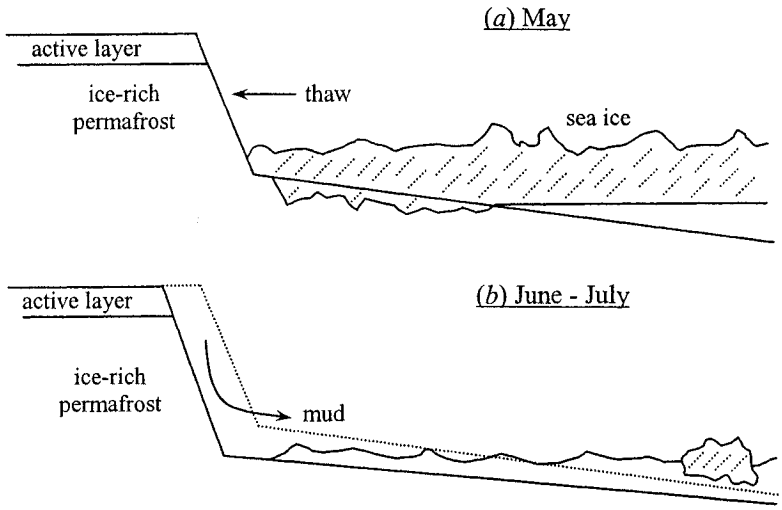

Stages of storm erosion during this time include (1) the initial stripping of thawed sediments by wave action which serve to protect the underlying frozen cliff sediments, (2) the development of a thermoerosional niche at the base of the cliff due to the effect of wave action melting the interstitial ice and transporting the unconsolidated sediment away from the beach zone, and (3) the mechanical failure of the sediments overlying the niche due to overburden pressure along a shear plane, usually associated with the presence of an ice wedge oriented shore-parallel (Harry 1982; Dallimore *et al.* 1996).

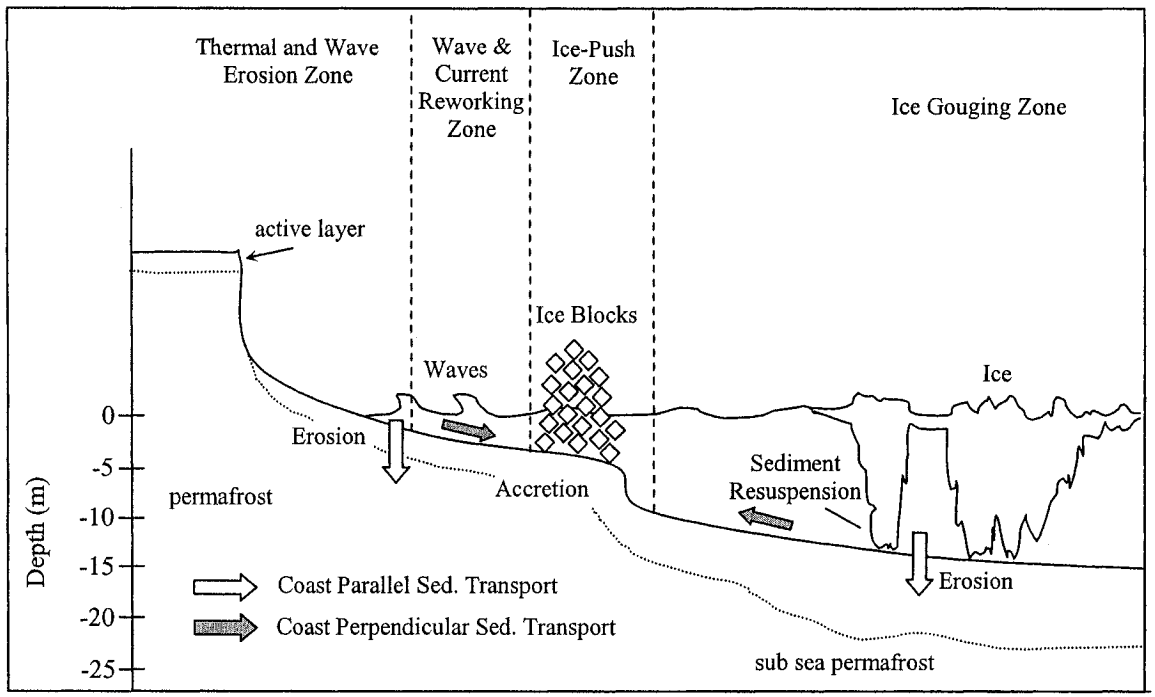

Figure 28: Mechanical interactions with the coastal zone (Héquette and Barnes 1990).

One of the most critical forms of bluff retreat is through block failure associated with thermoerosional niche development. As wave heights increase, the coastal sediments come into direct contact with wave energy. This process is expedited by the magnitude of surge associated with the storm (Walker 1988). The growth of the niche will continue as long as there is enough wave energy to transport the sediment away from the beach zone. When the niche is sufficiently deep, the overlying sediments may fail, generally along a line of weakness (often associated with ice-wedge terrain). This block then protects the cliff face until all the sediment has been carried away to the nearshore and offshore zones (Harry 1982; Walker 1988).

The stability of a slope depends on the ratio between shear strength (resistance) and shear stress. The shear stress of a slope is expressed as

[13]

$$\tau = \gamma.z.\sin\theta.\cos\theta$$

where γ is the weight of the soil, z is the depth of the failure plane, and θ is the angle of slope. Instability of soil associated with block failure occurs largely in clay soils due to the decreased angle of internal friction between the grains of clay (Figure 29). As shear stress increases with depth, the removal of the underlying support through niche

formation acts as a catalyst for block failure (Carson and Kirkby 1972). However, due to the presence of permafrost and ice-bonded sediments, shear stresses associated with the slope profile may resemble those of rock mechanics instead of soil mechanics. In this case, the cohesion from ice cementing far exceeds the strength from internal friction. However, once the depth of the crack exceeds H'_c, failure of the slab will occur (Carson and Kirkby 1972).

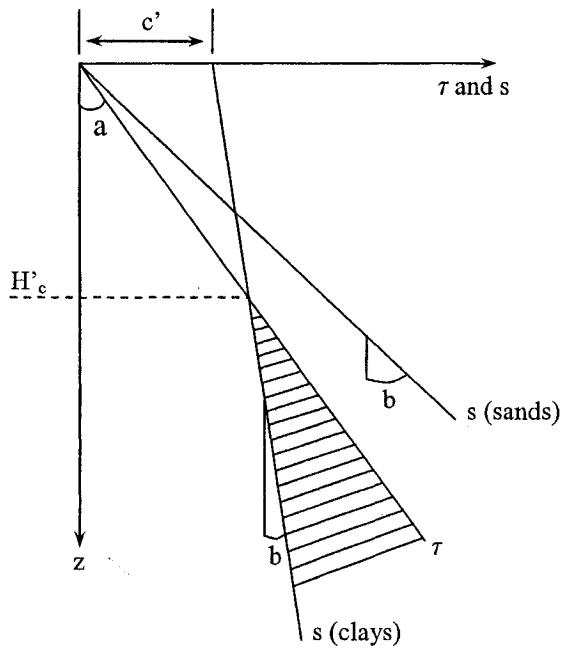

Figure 29: **Change in shear stress (τ) and shear strength (s) with depth on an infinite slope. H'_c is the critical depth for deep slips, z is depth below the surface (Carson and Kirkby 1972).**

4.3 Numerical Analysis

The model used in this research was developed by Kobayashi *et al.* (1999) to predict niche formation and horizontal retreat of a coastal bluff in permafrost environments. The first version of the model developed by Kobayashi and Vidrine (1995) was for use in permafrost environments on gently angled slopes. The second version (1999) was altered for steeply angled cliffs; therefore, the second version of the model was used for this analysis.

Before modeling began, several assumptions were made. To begin with, alongshore uniformity was assumed in order to simplify the modeling process (Kobayashi and Vidrine 1995). Temperature and salinity of the seawater were assumed to be constant, although in reality they would both change based on freshwater input from melting ice within the coastal sediments and from Mackenzie River input variations (Kobayashi and Vidrine 1995). Although each individual storm produces an associated value of horizontal retreat, it is the sum of these values, taken as a first approximation, which is used to calculate total erosion over the period 1970-2000. Also, the depth of niche formation increases with time, however it is not known how the height of the niche changes with time. It will therefore be assumed that the height of the thermoerosional niche is equal to the combined height of the storm surge (which includes tidal variation and pressure decrease) as added to the average storm wave height (Kobayashi and Vidrine 1995). In order to calculate the amount of sea level rise associated with a drop in atmospheric pressure, the local records (measured in kPa) were converted into mb (1 kPa = 10 mb). The average pressure was obtained for each individual storm, and then subtracted from the average sea level pressure of 101.3 kPa (1013 mb). A 1 mb drop in air pressure is equivalent to a 1 cm rise in sea level (WMO 1978).

The model used in this analysis (Kobayashi *et al.* 1999) can predict both the creation of a thermoerosional niche as well as the horizontal retreat of the cliff (Kobayashi and Vidrine 1995). Due to the difficulty in modeling block failure associated with niche development, this aspect was not included in the analysis. The model was used to simply calculate the overall horizontal retreat of a frozen cliff. The development of the niche is dependent upon the availability of wave power to remove the sediments into the nearshore and offshore zones. Once the unfrozen sediment has been removed

from both the beach and cliff face, latent heat transfer becomes unimportant to the development process, and the amount of horizontal retreat is primarily due to the convective heat transfer from the seawater to the frozen sediments (Kobayashi and Vidrine 1995). Therefore the rate at which the niche forms is dependent upon the initial thickness of unfrozen sediment insulating the frozen cliff, the amount of power generated through wave action, the ability of the waves and currents to transport the coarse sediment into the nearshore and offshore zones, and by the duration of the storm.

4.3.1 Model Results

A sensitivity analysis was conducted to determine which variables were important when modeling overall horizontal retreat of the cliff sediments. Variables that caused a large change in total retreat (R) were deemed sensitive. Variables that did not cause a substantial increase or decrease in total erosion were considered insensitive. In their study, Kobayashi and Vidrine (1995) found that the rate of melt of exposed frozen sediment (C_f) due to wave action and heat conduction is one of the most sensitive variables controlling horizontal retreat. The amount of frozen sediment removed during a storm event is dependent upon the initial thickness of unfrozen sediment (B*), therefore this also represents a crucial variable (Kobayashi and Vidrine 1995). Gradual melting of frozen cliff sediments beneath this insulating layer (C_u) is not important during the storm, due to the more direct influences of wave action and thermal conduction. However it plays a large role in determining the rate of thaw both before and after the storm (Kobayashi and Vidrine 1995).

Using the original dataset compiled from the Environment Canada On-line Data Archive (Appendix A—3), modeling of 139 storm events between 1970 and 2000 showed that the two most important elements affecting horizontal retreat of the cliff face are (1) wave energy, and (2) storm duration. This was also demonstrated by Solomon *et al.* (1994) during their research of coastal recession at both Tuktoyaktuk and Kay Point.

Figure 30 demonstrates predicted sensitivity of horizontal cliff recession due to storm duration. The model suggests that horizontal retreat is minimal for storms of 18 hours or less, but retreat increases rapidly with storms exceeding 24 hours. This is in

agreement with observed rates of retreat (Eid and Cardone 1992; Solomon *et al.* 1994). Susceptibility increases with storm duration and increased thermal conduction to the coastal sediments.

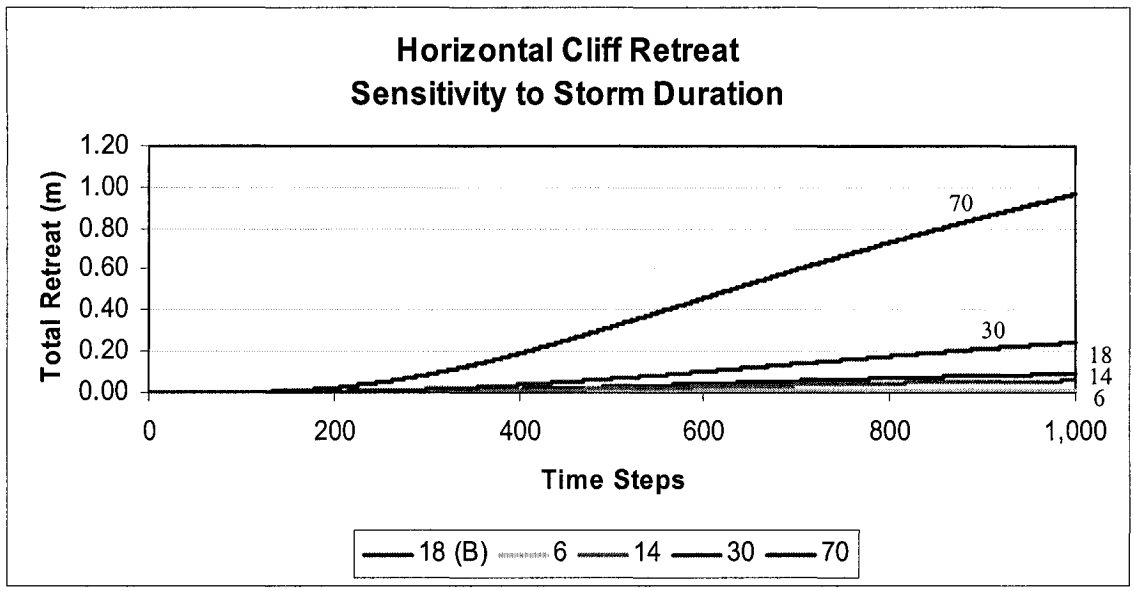

Figure 30: **A plot of the horizontal cliff retreat (R) sensitivity to storm duration. Storms ranged from 18 hours (base run) to 70 hours. Retreat rates remained fairly constant throughout the medium-length storms, however increased significantly when subjected to a severe storm.**

Water temperature was also found to be an important factor governing retreat rates (Kobayashi and Vidrine 1995). As mentioned earlier, it is extremely difficult to measure water temperature in this area. Therefore, although this variable has been shown to theoretically influence the stability of coastal bluffs, there is very little physical data to confirm this. Therefore, sensitivity to water temperature was run through the model in order to validate this claim (Figure 31). An original water temperature value of 5°C was used in the model, in order to resemble approximate water temperatures of the Beaufort Sea during mid- to late summer. Total horizontal cliff retreat using this value measured roughly 0.95 m. Keeping all other variables the same, the model was again run using a value of 0°C for water temperature. Results showed a marked decrease in the amount of cliff retreat, only 0.17 m. A third run was conducted using a water temperature of 10°C. Again, total cliff retreat increased by 0.04 m to 0.13 m. By running these values through

the model, it was shown that water temperature is an important factor governing the rates of coastal erosion.

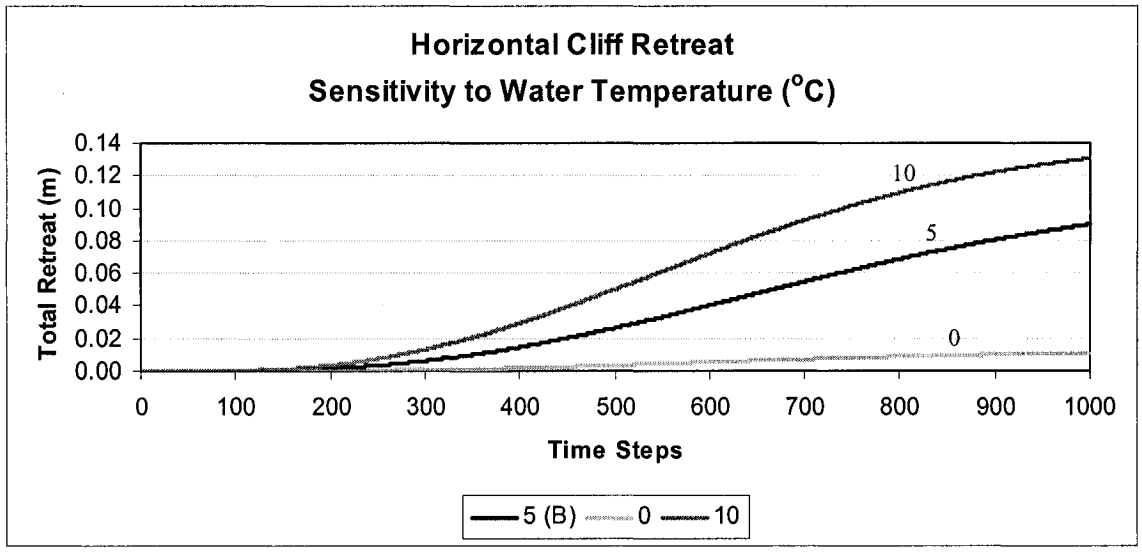

Figure 31: **A plot of the horizontal cliff retreat (R) sensitivity to water temperature (°C). A base run of 5°C was compared with model results for water temperatures of 0°C and 10°C to determine the effects on total horizontal cliff retreat. Differences in water temperature have a large effect on the amount of coastal retreat.**

Considering the susceptibility of ground ice to thawing, especially in a region where the salinity of the water depresses the freezing temperature below 0°C, it would be expected that horizontal retreat might increase depending on the variation in water temperature between 0°C and 10°C. This sensitivity analysis further validates this claim. One might also expect a correlation between water temperature, ground ice content, and the amount of horizontal retreat during a storm.

The sensitivity of cliff retreat to ground ice content (measured as a total percentage of possible sediment volume) was also modeled. Figure 32 shows that there does not seem to be much difference in the amount of coastal erosion observed, regardless of the amount of ground ice in the coastal sediments. However, Kobayashi *et al.* (1999) state that cliff retreat *is* sensitive to the volume of ice in the coastal sediments. Results of this study indicate that there appears to be *more* coastal erosion occurring when there is *less* ground ice. While it is expected that coastal sediments with a higher percentage of ground ice would be more susceptible to erosion, the model demonstrates

little sensitivity to this variable, and even an inverse relationship to what is theoretically expected. A possible explanation for this could be that the cliff sediments become more resistant to erosion with increasing amounts of ground ice, thus requiring a greater input of wave energy to initiate thawing.

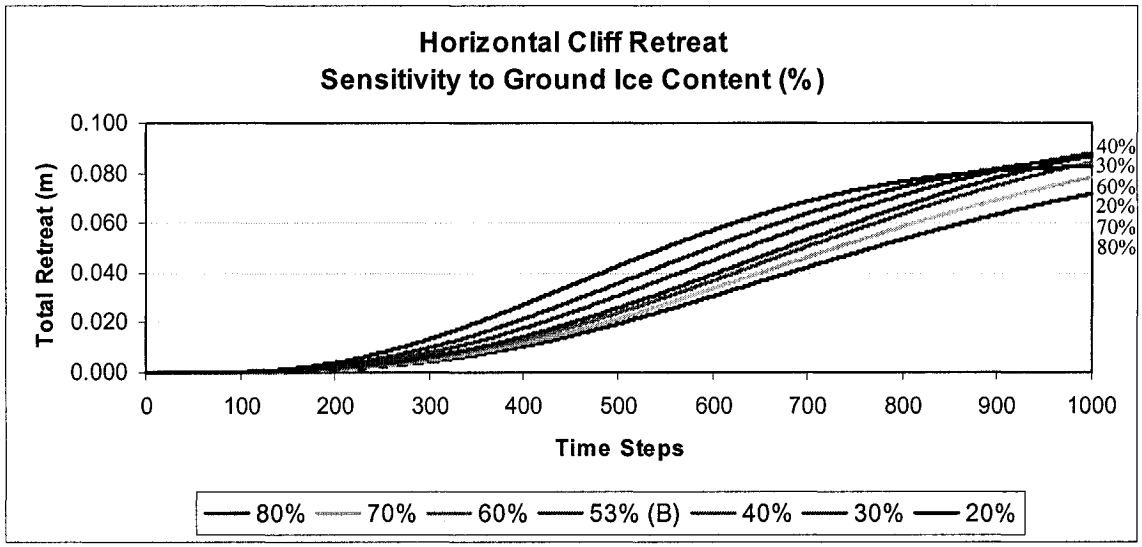

Figure 32: **A plot of horizontal cliff retreat (R) sensitivity to ground ice content (%). A base run of 53% ground ice volume was compared with six other values between 20% and 80%. In this model, coastal retreat rates do not seem to be sensitive to the amount of ice contained in the coastal sediments.**

Other sensitivity runs were conducted on variables thought to play a significant role to coastal erosion in the Beaufort Sea. These included the sensitivity of horizontal cliff retreat to beach width (metres), cliff slope (degrees), cliff height (metres), wave height (metres), and storm surge height (metres).

The width of the beach is an important variable in the model (Figure 33), as would be expected. The narrower the beach, the higher the probability that waves and storm surge will interact directly with the cliff sediments. Also, the greater the width of the beach, the larger the area of distribution for wave energy. Therefore, when a beach width of 2 m was compared with a width of 0 m, total erosion increased over 100%. However, other variables associated with the cliff and beach sediments do not seem to be as important to the amount of horizontal cliff retreat (Figures 34 and 35). Above a certain height, it is expected that the total height of the cliff would not play a large role in the amount of coastal erosion, as waves only interact with those sediments at the base of

the cliff. This variable may have more of an impact when considering the role of block failure to cliff armouring, but those processes are not dealt with here. Cliff slope plays a larger role in coastal sensitivity, with lesser slopes resulting in higher rates of erosion, due to the increased ability of waves and surge to influence the coastal sediments.

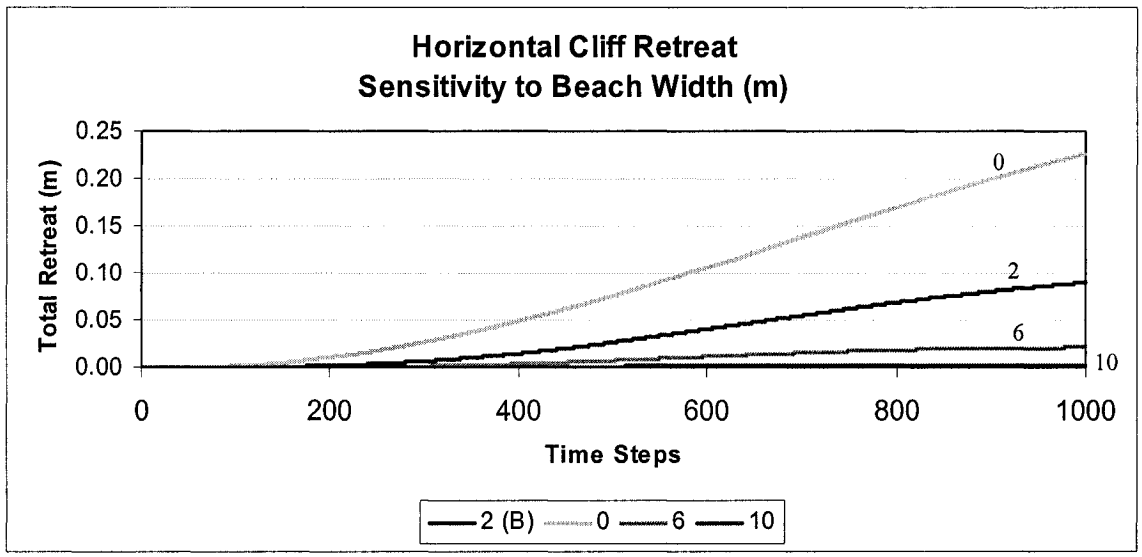

Figure 33: **A plot of the horizontal cliff retreat (R) sensitivity to beach width (m). The base model was run with a beach width of 2 m. Three other runs were conducted with beach widths of 0 m, 6 m, and 10 m. The amount of coastal erosion is dependent upon the width of the beach, which also controls the degree of wave (energy) dispersion.**

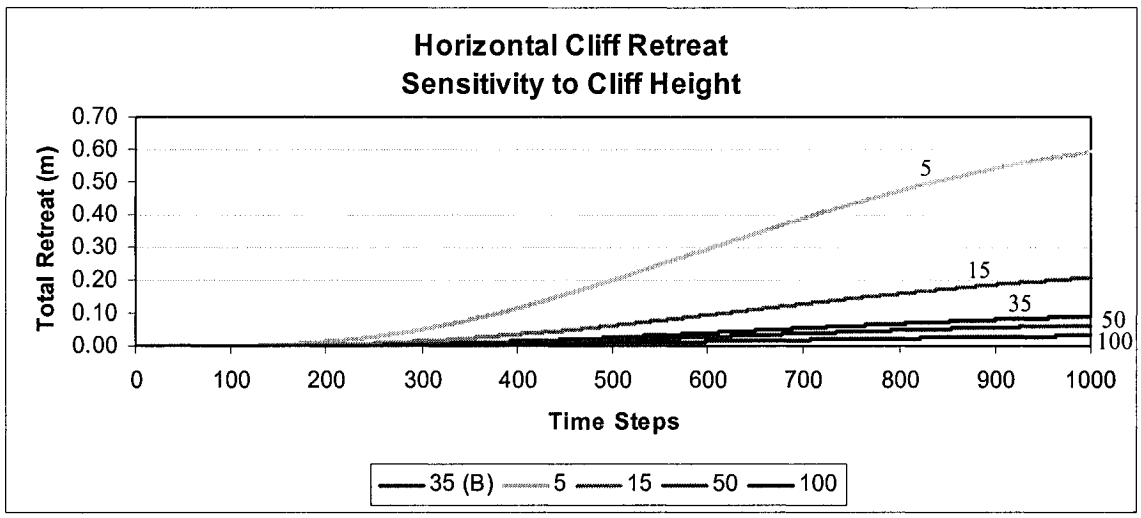

Figure 34: **Horizontal cliff retreat (R) sensitivity to cliff height (m). In the original model, cliff height was 35 m. Four other models were run with cliff heights ranging from 5 m to 100 m. Model runs demonstrate higher rates of erosion in areas with lower cliff heights.**

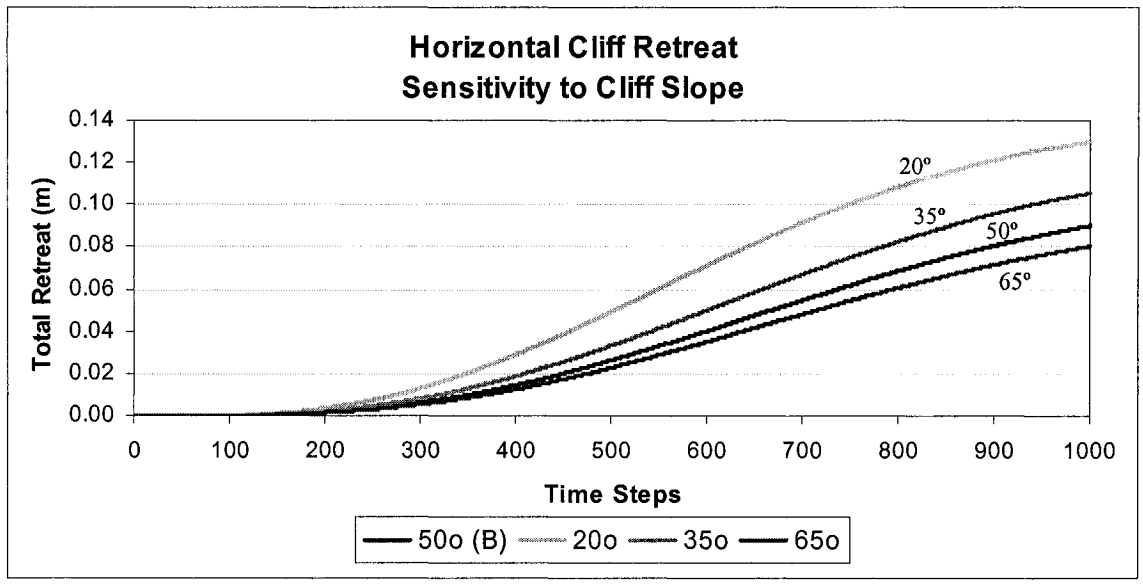

Figure 35: **A plot of the horizontal cliff retreat (R) sensitivity to cliff slope (°). The base slope was 50°, indicating a steeply angled cliff. Other runs contained slopes of 20°, 35°, and 65°. The model demonstrated only mild sensitivity to cliff slope, producing values that ranged from 0.08 metres of erosion associated with a 65° slope to 0.13 metres of erosion associated with a slope of only 20°.**

While it has been proven that cliff erosion is susceptible to total wave height, the analysis demonstrates minimal sensitivity to this variable, highlighting a flaw in the model outputs (Figure 36). Kobayashi *et al.* (1999) suggest that this lack of sensitivity to wave height will remain constant as long as waves continue to break in the nearshore zone, as opposed to directly in front of the coastal sediments. However, wave height is an important variable in the wave energy calculation (Equation 1). Clearly, this model is not able to accurately demonstrate the importance of this variable, thus highlighting a major flaw.

Alternatively, it is the storm surge height that plays a dominant role in the total amount of coastal erosion (Figure 37). Clearly, *R* increases with increasing storm surge levels. This indicates that coastal sediments are highly susceptible to a constant exposure to seawater (Kobayashi *et al.* 1999). An increase in storm surge heights also increased the amount of total vertical beach erosion depth (*E*) (Kobayashi *et al.* 1999). Therefore, not only are the exposed coastal sediments influenced by direct contact with the seawater, but as vertical beach erosion progresses, total cliff height increases relative to a fixed position on the beach.

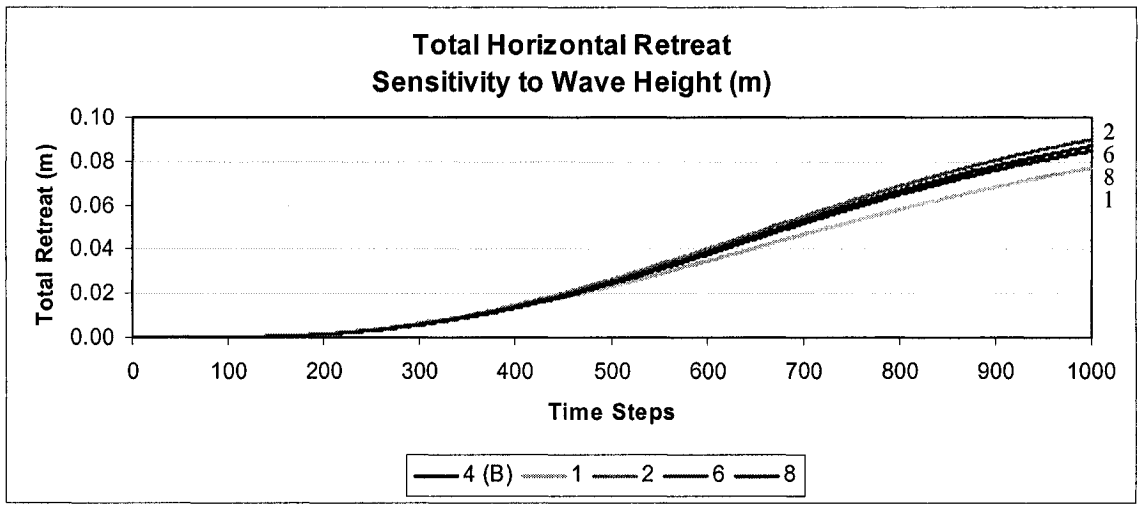

Figure 36: **A plot of the horizontal cliff retreat (R) sensitivity to wave height (m). Average wave height calculated during the 139 storms used in this study was 4 m, therefore this value was used as the base run. Other heights between 1 – 8 m were also run through the model, showing minimal sensitivity to this variable.**

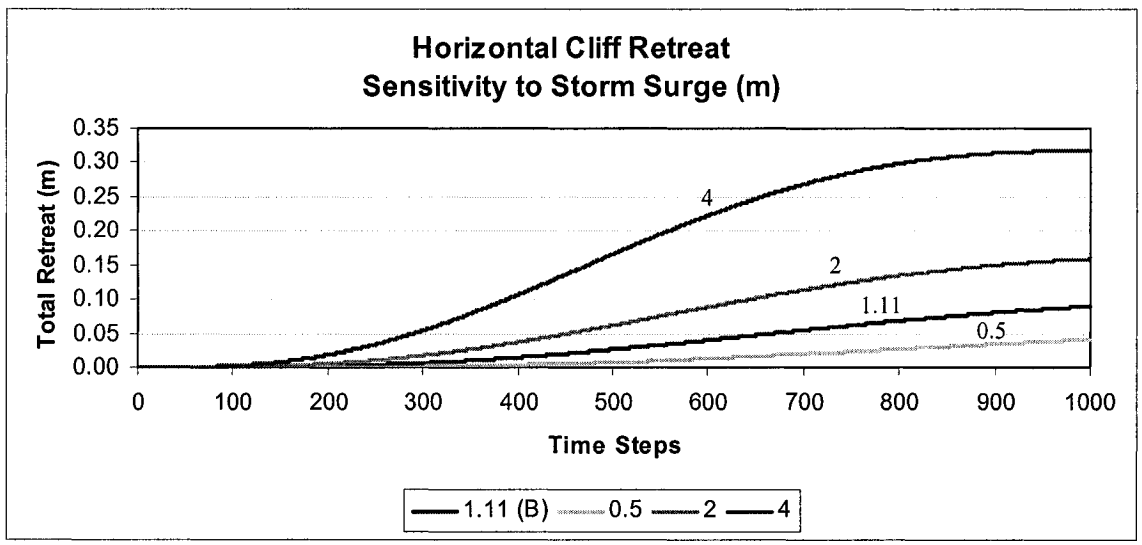

Figure 37: **A plot of the horizontal cliff retreat (R) sensitivity to storm surge height (m). The average storm surge height recorded during all 139 storms was 1.11 m, therefore this value was used in the base run. Other storm surge heights used to evaluate sensitivity were 0.5 m, 2 m, and 4 m. Cliff retreat increases markedly when modeled using durations associated with the most severe storms in this region of the Beaufort Sea.**

Other sensitivity analyses have been run while wave hindcasting and modeling coastal erosion in the Canadian Beaufort Sea. In their study, Murray and Maes (1986) found that for winds greater than 30 km/h, the recorded onshore winds could be as much as 20% higher than those recorded offshore, due to a greater friction factor during storm periods at sea. However, later in their report the authors state that the onshore winds *underestimate* the offshore winds by 20%. Considering the importance of this variable to the growth of wave height, such inaccuracies make the validation of a numerical model quite difficult. Other authors have reported a difference of 1.5 between onshore and offshore winds in this region (Eid and Cardone 1992, Solomon *et al* 1994), therefore this value was taken into consideration during the current modeling process.

Tabulated storm data (contained in Appendix A—3) were categorized using the direction of origin of the storm winds. Referring to a map previously created by McDonald and Lewis (1973), Herschel Island was subdivided into 3 main sectors based on orientation and physiography (Figure 38). The characteristics of each group are specified in Table 5.

	Wind Direction	**Cliff Height**	**Cliff Slope**	**Beach Width**
Group A	250° - 50°	35 m	50°	2 m
Group B	60° - 160°	20 m	25°	4 m
Group C	170° - 240°	5 m	10°	6 m

Table 5: Characteristics of Herschel Island subdivisions.

An average ice content of 53% and a beach slope of 10° were utilized in the modeling process, as these were the values originally used by Kobayashi *et al.* (1999) in their modeling investigations of North Head and Tuktoyaktuk, NWT.

Group A contained 113 individual storms, Group B contained 23 storms, and Group C contained 3 storms. The model parameters were altered to reflect the coastal conditions of each category, and then all individual storms were run. Output parameters (measured in metres) included *Still Water Depth at Cliff Toe (dc)*, *Horizontal Cliff Retreat (R)*, and *Total Beach Erosion Depth (E)*. The final values of *R* for each storm were then summed to obtain a total horizontal retreat value for each year. These values were compiled over the period of 1970-2000 to obtain the total cliff erosion. Case A showed the highest amount of erosion, 13.2 m. This value corresponds well with

observed data obtained from air photography and satellite imagery (Lantuit, personal communication). Case B showed only 1.5 m of erosion over the same 30-year period, which is much lower than observed rates over the same period of time (Lantuit, personal communication). Case C showed only 0.1 m of erosion, which does correspond well with observed data.

The low erosion rates predicted by this model for Case B are quite interesting. The model used in this study is predominantly driven by wave energy during storm events in the Beaufort Sea. As previously discussed, the largest storms with the highest frequency occur from the W/NW. Therefore, it may be assumed that in such a model the eastern side of Herschel Island should not experience as much erosion as the west and northwestern sides. However, satellite imagery and aerial photography show a much larger erosion rate from this side of the island, in excess of 10 m (Lantuit, personal communication). Clearly, other factors must then be responsible.

There are several main differences between the western and eastern coastlines of Herschel Island (Figure 39). These include beach width, cliff height, cliff slope (Table 5), ground ice content, and exposure to solar insolation. As wave action is clearly not responsible for the high magnitude of coastal erosion in this region, these other factors must then be responsible. As the eastern coastline of the island receives more solar insolation, it is assumed that this is the most important factor affecting erosion, and one of the factors responsible for the higher number of retrogressive thaw slumps. Other influencing factors are beach width, cliff height and cliff slope (de Krom 1990). An analysis of air photographs taken of the east and southeast parts of the island show a greater concentration of retrogressive thaw slumps and active layer detachment failures than the west and northwest sides, further validating the assumption that thermokarst processes are more influential to the east and southeast aspects of the island.

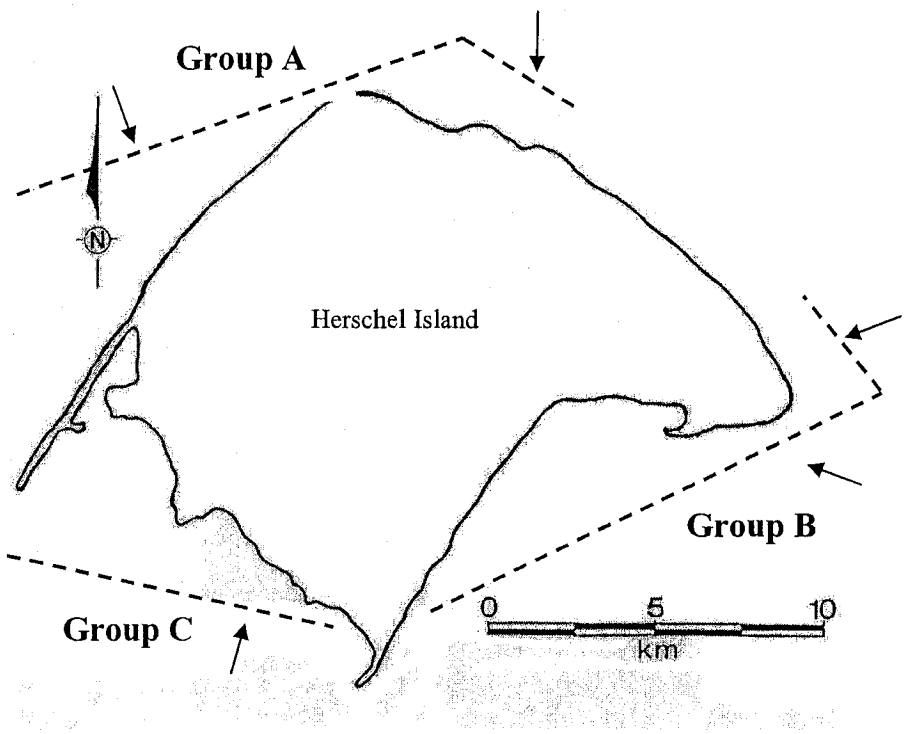

Figure 38: **Classification of Herschel Island (after McDonald and Lewis, 1973). Arrows show the wind direction.**

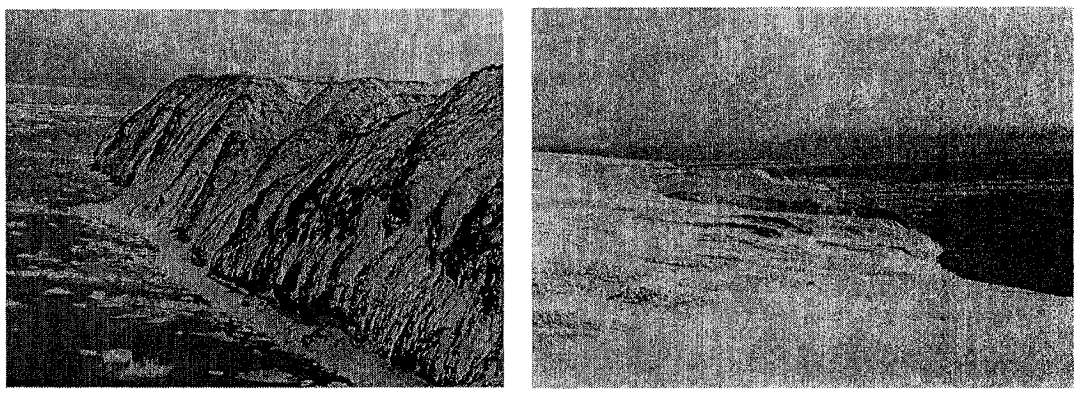

Figure 39: **Northwestern coastline of Herschel Island (left) and eastern coastline – Thetis Bay (right). September 2003.**

Two storms during the modeling process stood out from the rest based on the total amount of horizontal retreat that ensued. The first storm occurred on August 29, 1981 and lasted for 74 hours. The second storm took place on September 21, 1993 and lasted for 38 hours. As the latter storm has been extensively studied by Solomon and Covill (1995), only the 1981 storm will be examined here.

Figure 40 shows the variation in wind speed during the storm, as well as the storm surge height variation (*St*), water depth at the cliff toe (*dc*), the total horizontal cliff retreat (*R*), and the total beach erosion depth (*E*). Average wind speed was 42.7 km/h with a peak speed reaching 63 km/h approximately 48 hours into the storm. Average wind direction originated from the NW (310°) and deviated 40° during the storm. Total surge height reached 1.11 m at hour 37, however the total water depth at the cliff toe (*dc*) reached a maximum value of 3.10 m at hour 42, resulting in a lag of 5 hours between storm surge height and total water depth. Total water depth is a combination of storm surge height, wave height, and total vertical beach erosion (*E*).

Both total horizontal cliff retreat (*R*) and total beach erosion depth (*E*) showed signs of increasing, even after the storm was officially over (defined as wind speed less than 37 km/h for more than 6 hours). Total cliff retreat for this storm measured 0.95 m and total vertical beach erosion measured 3.00 m. Clearly, when discussing coastal erosion in permafrost environments, attention must be paid not only to total *horizontal* retreat of the cliff face, but also to total *vertical* erosion of the beach. This detail is lacking in the main body of literature.

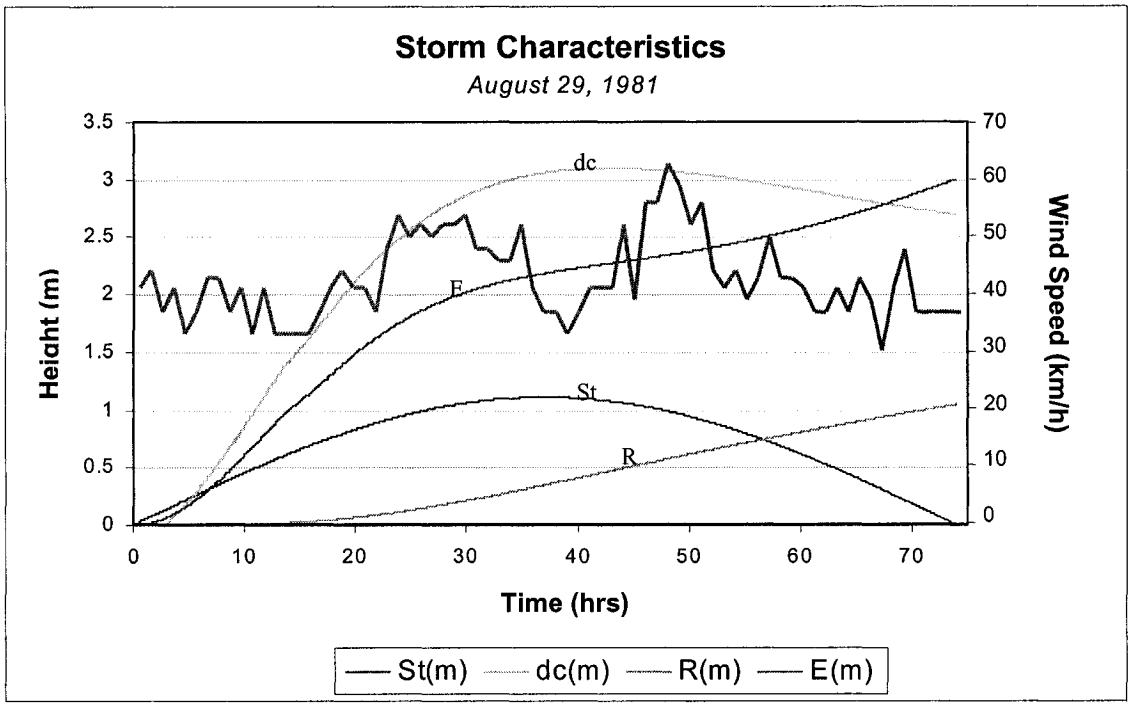

Figure 40: **A plot of the August 29, 1981 storm statistics, including the variables storm surge height (*St*), still water depth at the cliff toe (*dc*), total horizontal cliff retreat (*R*), and total vertical beach erosion (*E*). Each of these parameters are measured in metres on the y-axis. The graph shows that total vertical beach erosion and total horizontal cliff retreat continue to increase even after the storm has terminated. This increase will likely continue until the beach and nearshore zones have again reached a state of equilibrium. It also highlights the fact that erosion may continue even after the "official" storm has concluded.**

4.4 Climate Change

Climate change predictions suggest that over the next 50 to 100 years the rate of global sea level rise may double, from approximately 3 mm/yr to 6 mm/yr. This, coupled with increased fetch due to a decrease in the extent of the Arctic pack ice, would result in greater wave action – and erosion – on shorelines in the Beaufort Sea (Solomon *et al.* 1994). The International Panel on Climate Change (IPCC) has suggested a 1-4°C increase in temperature would occur in the same amount of time (Smith, M.W. 1988; McGillivray *et al.* 1993; IPCC 2001). This increase in temperature would have a noticeable effect in the Arctic due to the increased sensitivity of snow and ice to changes in temperature (McGillivray *et al.* 1993).

It has been argued, however, that mean annual temperature should not be the sole factor taken into account when modeling climate change in the Arctic. While average yearly temperatures may increase between 1-4°C, winter temperatures may increase by 11°C in contrast to a summer temperature increase of 2-3°C (Smith 1988). In addition to this marked difference in temperature, precipitation would also increase by 10-50% in summer and up to 60% in winter. This would create a thicker snow cover, insulating the permafrost beneath from the cold air temperatures that would normally maintain the ground temperature profile in equilibrium (Smith 1988). Figure 41 outlines the interactions between these variables. Even though it is known that changes in both summer and winter precipitation rates would alter the ground thermal regime, this aspect was not included in the present modeling exercise.

As the inner shelf of the Beaufort Sea is storm-wave dominated, knowledge of the potential impacts of climate change is quite valuable, especially considering the expanding oil and gas industry in the area (Hill and Nadeau 1989). A 20% increase in fetch would likely only produce a 3% increase in wave height (Murray and Maes 1986), further emphasizing that this is not a controlling factor to coastal erosion. Sensitivity of wave height to climate change was also investigated through the diminishment of sea ice and resultant increase in fetch in the Arctic zone by McGillivray *et al.* (1993). This investigation took into account only changes in fetch, ignoring such variables as the effects of a projected warming on sea level, shoreline erosion, seiche, and the effects of

altered fresh water discharge from major sources such as the Mackenzie River (McGillivray *et al.* 1993). Model results are shown in Table 6.

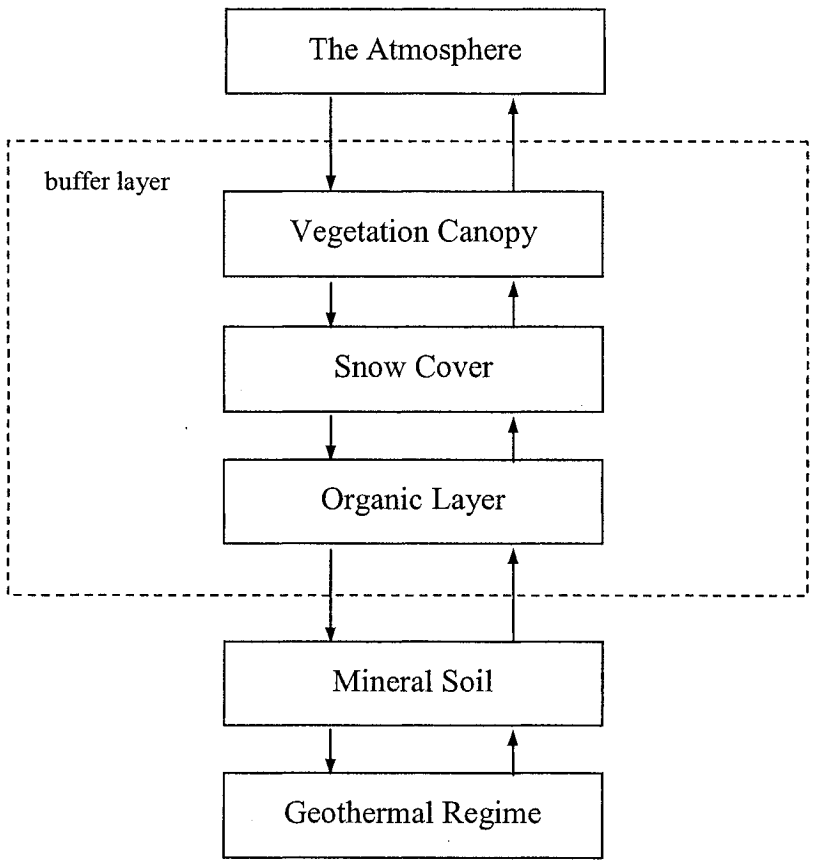

Figure 41: Interactions affecting the ground thermal regime (after Smith 1988).

Model Name	Fetch (nautical miles)	% Increase in Wave Height
Base Model	200	--
1989	330	16
CCC	360	22
GISS	600	39

Table 6: **Increase in available fetch and resultant wave height increases based on several model scenarios. The 1989 model refers to the instrumental record for the region, selected because 1989 was an exceptionally warm year. CCC refers to parameters created for a climate change model run by the Canadian Climate Centre in 1990, and GISS refers to a model run parameterized by the Goddard Institute for Space Science in 1984 (McGillivray *et al.* 1993).**

There are obvious differences in the projected wave height increase between the three models used in the McGillivray *et al.* (1993) study. Due to the increases in wave height produced by the CCC and GISS models, a value for the present study was chosen closer to the 1989 model results, as this percentage also falls within climate change values estimated in other reports (Lachenbruch 1988, 1994; Solomon *et al.* 1994; Burn 1994, 1998; Cohen 1997, IPCC 2001). Therefore a 15% increase in wind speed (m/s) was introduced to the model, which in turn affected both wave height (m), wave period (s), and storm surge height (m).

Other variables were altered to create a more realistic climate change scenario. The beach width was decreased by 0.5 m to take into account rising sea levels (IPCC 2001), the water salinity was decreased from 15% to 12% to reflect decreasing salinity due to increased fresh-water input from melting pack ice, and the seawater temperature was increased from 5°C to 7°C. The IPCC predicts a global sea level rise of 507-735 mm over the coming 100 years; therefore a value of 0.5 m corresponds well with this. It is logical that the thickness of the unfrozen cliff sediment would increase with increasing air temperature and precipitation, however it is not known by how much. Also, with an increase in both the intensity and frequency of storms in the Beaufort Sea (Solomon *et al.* 1994), it is possible that a few centimetres of unfrozen sediment would be removed from the cliff face at a higher rate. Therefore it was decided not to alter this variable.

An increase in storm frequency was calculated proportional to the increasing length of the open water season. Over the period 1970-2000, there was an average of 5 storms per open water season, which lasted from mid-June until mid-October (4 months). Extending the open water season by one month results in a storm frequency of:

[14]
$$\frac{5\ storms}{4\ months} = \frac{x\ storms}{5\ months}$$
$$4x = 25$$
$$x = 6.25$$

There is a difference of 1.25 storms between an open water season of 4 months and an open water season of 5 months, which corresponds to a 25% increase in storm frequency. Therefore, the total amount of horizontal cliff retreat obtained from the climate change scenario was multiplied by 25% to obtain an erosion value that includes storm frequency.

4.4.1 Climate Change Modeling Results & Discussion

The climate change parameters listed in the above section were applied to Group A, Group B, and Group C independently. Sites in category A showed the largest increase in erosion, as this is the side of the island most vulnerable to wave attack. Model results from the original database showed 13.2 m of erosion over the previous 30 years. When these storms were run with the climate change adjustments, there was an appreciable increase in erosion rates totalling 3.4 m. Therefore the model predicted coastal erosion rates of 16.6 m over the coming 30 years. When coupling this figure with a 25% increase in storm frequency, the value increases to 20.75 m. Figure 42 shows the difference between total horizontal cliff retreat values (R) per storm in Group A.

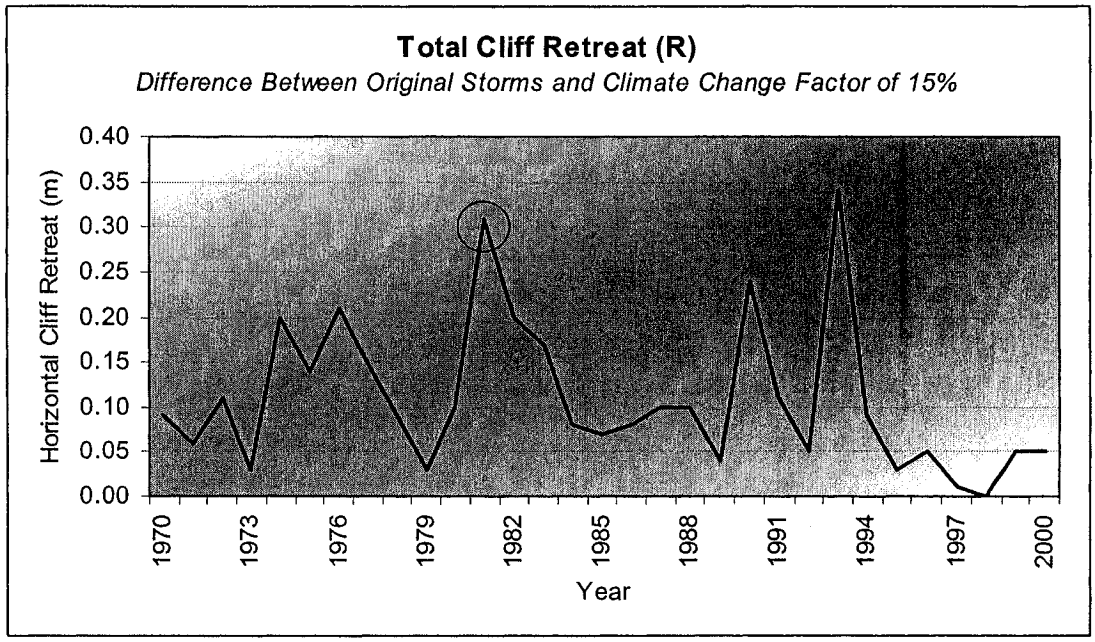

Figure 42: **Horizontal cliff retreat (R) comparison between 113 original storms (1970-2000) and storms influenced by a climate change factor of 15%. The circle highlights the large storm of 1981.**

The average difference between the individual retreat rates is 0.03 m with a standard deviation of 0.02 m. As seen in Figure 41, certain storms display a larger difference in their total retreat rates than others. In most cases, this is due to storms which have a longer duration.

Total horizontal cliff retreat in Group B increased from 1.46 m to 1.53 m. When coupled with an increase in storm frequency of 25%, this value increases to 1.91 m. Group C showed the least amount of coastal erosion during the period 1970-2000, 0.09 m. With the climate change factor, this value increases to 0.14 m, including the 25% increase for storm frequency.

The largest recorded storm event that occurred on August 29, 1981 is circled in Figure 42. The other large peak corresponds to the large storm event of September 21, 1993. Figures 43 and 44 show both the Total Horizontal Cliff Retreat (R) and the Total Vertical Beach Erosion Depth (E) associated with the 1981 storm. Final R values for both the original storm and the storm in the climate change scenario were 0.95 m and 0.97 m, respectively. It was expected that there would be a greater difference between these two values, considering the magnitude of this storm. These results demonstrate that

storm intensity may not be a factor which heavily influences coastal erosion, as variables such as the creation of a thermoerosional niche and subsequent block failure, or saturation of the water column with suspended sediment may prevent further erosion of the cliff segment.

The results of Total Vertical Beach Erosion in Figure 44 are quite interesting. As with *R*, it is expected that there would be a greater amount of beach erosion in the climate change scenario than in the original storm scenario. However, the climate change scenario shows 0.78 m less erosion after 72 hours. As with *R*, it is unknown why the results are not showing what is expected. It seems that beach erosion in the climate change scenario peaks earlier than in the original storm. This may cause the unfrozen beach sediment to erode so quickly that there is not enough time for the latent heat from the wave power to begin the melting process on the underlying frozen sediments. Therefore, even though the curves are similar, there would be less erosion overall. A second scenario, similar to that for *R*, is that the water column becomes saturated at an early point in the erosion process, and is unable to remove further sediment in suspension from the beach zone.

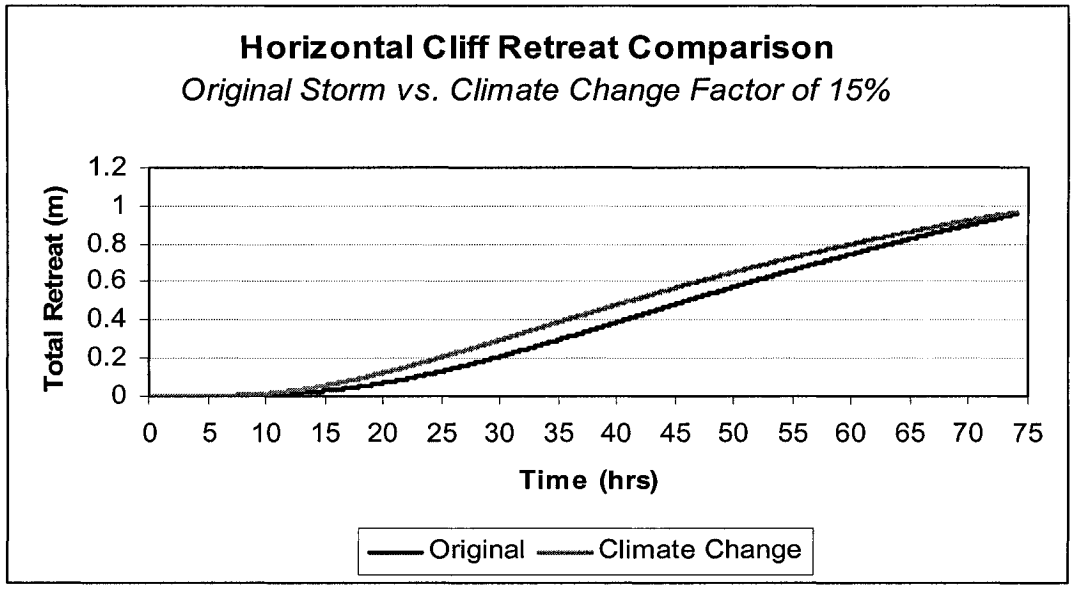

Figure 43: **A plot of the August 29, 1981 comparison of horizontal cliff retreat (R) between the original storm and the same storm influenced by a climate change scenario. In the climate change scenario, coastal erosion occurs slightly earlier and at a greater rate. However, rates of erosion between the two scenarios equalize as the end of the storm approaches.**

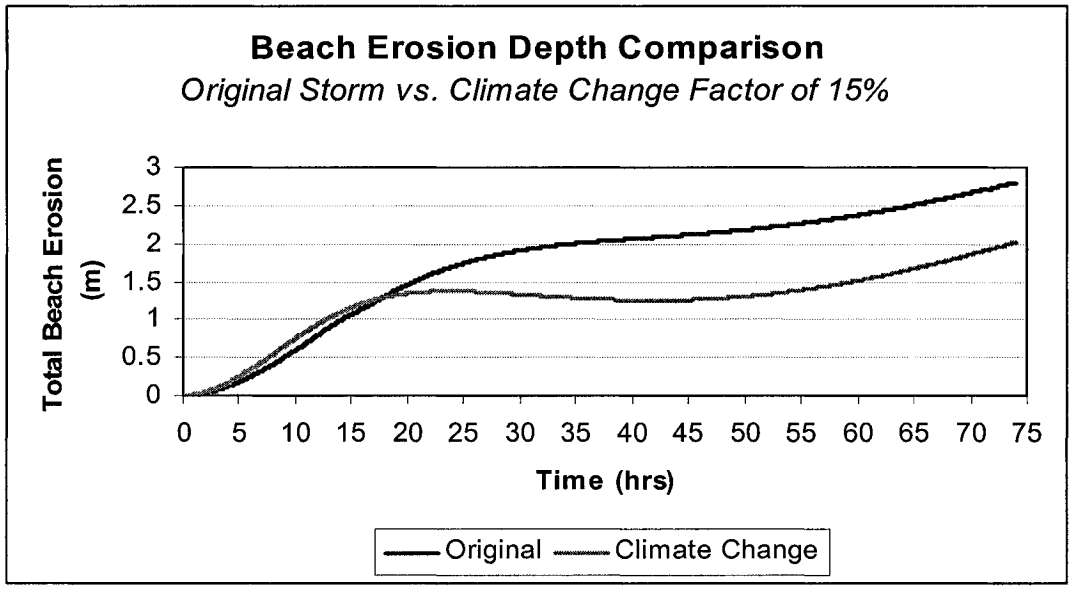

Figure 44: **A plot of the August 29, 1981 comparison of total beach erosion (E) between the original storm and the same storm influenced by a climate change scenario. In the climate change scenario, erosion begins slightly sooner, but at a much greater rate than with the original storm. However, this rate of erosion quickly stabilizes, resulting in *less* total beach erosion for the same storm.**

CHAPTER 5 – CONCLUSIONS

5.1 Introduction

Even though Canadian Arctic studies have been ongoing for over 100 years, there is still much to be understood about the climatic and geomorphic factors and interactions in this sensitive environment. While many studies have been conducted on the geomorphic and thermal properties of permafrost, little has been undertaken which examines the coastal profile in detail. In the late 1960's and early 1970's, this gap was first addressed due to the interest of oil and gas companies in drilling the southern Beaufort Sea. However, once the land claim settlement process began in earnest in the mid 1970's and early 1980's, a moratorium was placed on new ventures in this area. In recent years, interest has again been kindled and environmental impact assessments have begun in order to exploit the reserves of oil and natural gas that lie beneath the Beaufort Sea. Due to the increased need for geologic, geomorphologic, sedimentologic, and oceanographic information on this environment, research has again begun to fill-in the existing gaps.

Due to the difficult nature of collecting data in this remote and harsh environment, computer models and simulations are being used with increasing frequency in order to predict changes in this area (Pinchin *et al.* 1985; Eid and Cardone, 1992; Solomon *et al.* 1994; Kobayashi *et al.* 1999). Often, coastal erosion and sediment transport studies have used over-water wind data to hindcast deep water wave heights and wave periods. From this information, wave power and longshore current direction and speed can be calculated. This data is then used to predict the amount of coastal erosion that may occur at a specific site over a defined period of time.

Changes in Earth's climate will have an effect on these processes, although it is difficult to predict what effect that will be. An average temperature increase of 1-4°C and an increase in average precipitation of 30-60% within the next 30-50 years could drastically change the ground temperature profile in the long-term. Therefore, it is the purpose of this study to attempt to predict how climate change will affect coastal retreat rates on Herschel Island, Yukon Territory, in the coming 30 years.

5.2 Summary of Results

The goals of this study are to (1) to accurately hindcast the wave climate of the southern Beaufort Sea in the vicinity of Herschel Island in order to predict the increase in erosion rates based on a defined climate change scenario, and (2) to anticipate how changes in both mechanical and thermal erosion rates will affect the backwasting of ice-rich coasts. Other minor conclusions include the identification of coastal erosion processes on Herschel Island, the improved understanding of thermoerosional niche processes, and improved understanding of both the benefits and drawbacks of the numerical model developed by Kobayashi *et al.* (1999).

The main conclusions of this study are:

1. Assuming that the frequency and intensity of storm related wave and surge activity continues at current rates (or greater), ice-rich coasts will experience approximately a 25% increase in erosion rates.

2. Mechanical erosion will increase in a predictable fashion that is directly proportional to the increase in total wave energy and increased storm frequency.

3. Increases associated with thermal erosion increase are more difficult to predict because of potential negative feedbacks linked to the armouring of coasts.

A series of minor conclusions are also linked to this study, and include:

i. The main erosional processes on Herschel Island include retrogressive thaw slumping, active layer detachment failures, thermoerosional niche formations, block failures, and the breaching of thaw lakes. These processes are predominantly affected by coastal orientation.

ii. The importance of thermoerosional niche development as it affects erosion in ice-rich coastal sediments has not been extensively studied in the literature. This

study both confirms existing states of knowledge and advances the importance of this mechanism to high rates of erosion in this sensitive environment.

iii. The numerical model created by Kobayashi *et al.* (1999) predicted fairly accurate coastal retreat values for Herschel Island of between 0.01-2.95 m per year, which is supported by rates reported in Solomon and Gareau (2003) of 0.0-1.0 m per year, and Hill and Solomon (1999) of 0.40-1.45 m per year. The model was sensitive to storm duration, water temperature, beach width, cliff slope and storm surge height. These results were expected. However, the model was *not* sensitive to ground ice content, wave height, or cliff height, nor could it demonstrate why these variables were not being affected in the way that they theoretically should. Specifically, the insensitivity to wave height pinpoints a major flaw in the model, which could not be addressed in the scope of this project. Due to a lack of field data, regression and correlation analyses could not be completed to sensitize the model to real-world conditions.

iv.

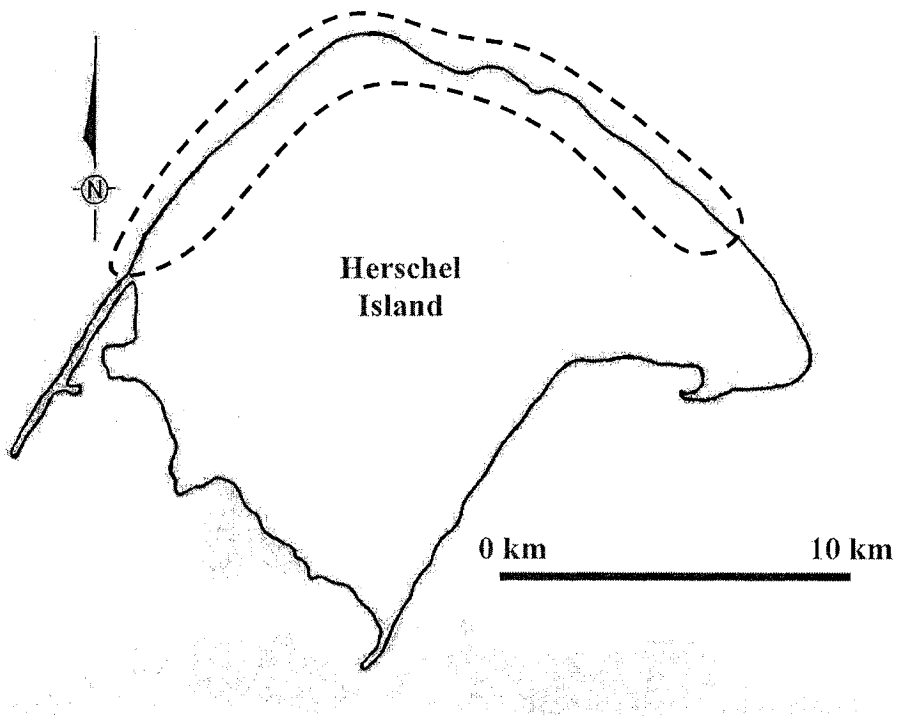

The greatest amount of coastal erosion occurs on the west, northwest and northern costs of Herschel Island (area enclosed by the dashed line). Over the past 30 years, erosion in this area has amounted to approximately 13.2 m. Using the climate change scenario developed in this thesis, retreat rates increased by 3.4 m totalling 16.6 m. While satellite imagery and remote sensing techniques have shown that coastal retreat is actually occurring at a greater rate on the east and southeast coast of the island (Lantuit, personal communication), this is due to factors other than wave-induced erosion.

5.3 Conclusions & Suggestions for Further Research

There are a number of ways this model could be improved. The collection of field data on storm surge heights and wind speeds at various locations along the southern coast of the Beaufort Sea would enable a sensitivity analysis to be run on the model, as well as regression and correlation analyses (Kobayashi *et al.* 1999). The collection and recording of all data should be done in a manner that allows for easy addition or comparison with existing datasets. As well, a detailed GPS survey of the coastline every few years would allow for accurate coastal erosion readings. At specific locations of interest, a detailed ground ice database, including the distribution and size of ice wedges, as well as an investigation of massive icy beds would be of use in the prediction of erosion and/or subsidence in the area.

Programs for modeling both climate and other physical systems are constantly being improved upon, and perhaps in a few years there will be a model which will incorporate with greater accuracy the large number of variables and interactions present in a study such as this one. Of great use would be a two-part model, focusing on both the expected changes to the ground thermal regime, as well as the coastal erosion aspects included herein.

BIBLIOGRAPHY

ACGR (Associate Committee on Geotechnical Research). 1998. Glossary of permafrost and related ground ice terms. *Permafrost Subcommittee*, National Research Council of Canada, Technical Memorandum **142**. 156 pp.

Andersland, O.B. and Anderson, D.M. Geotechnical Engineering for Cold Regions. New York: McGraw Hill, 1978. 566 pp.

Andersson, J.G. 1906. Solifluction; a component of subaerial denudation. *Journal of Geology*. **14**: 91-112.

Arctec Newfoundland Limited. 1987. Effect of sea ice on Beaufort Sea coastal processes. *Geological Survey of Canada*, Open-File Report No. **1688**.

Aré, F.E. 1983. Thermal abrasion of coasts. *In* 4th International Permafrost Conference, Fairbanks, Alaska, pp. 24-27.

Aré, F. 1988. Thermal abrasion of sea coasts. *Polar Geography and Geology*. **12**: 1-157.

Barry, R.G. 1988. Permafrost data and information: status and needs. *In* 5th International Permafrost Conference, Trondheim, Norway, pp. 119-122.

Bouchard, M. 1974. Géologie des dépots meubles de l'ile Herschel, Territoire du Yukon. M.Sc. Thesis, Department of Geography, Montreal, Université de Montréal. 70 pp.

Brown, R.J.E. 1963. The relation between mean annual air and ground temperatures in the permafrost region of Canada. *International Conference on Permafrost*, Purdue University, National Research Council Canada. Session 5. 30 pp.

Brown, J., Jorgenson, M.T., Smith, O.P. and Lee, W. 2003. Long-term rates of coastal erosion and carbon input, Elson Lagoon, Barrow, Alaska. *In* 8th International Permafrost Conference, Zurich, Switzerland, pp. 101-106.

Burn, C.R. 1994. Permafrost, tectonics, and past and future regional climate change, Yukon and adjacent Northwest Territories. *Canadian Journal of Earth Science*. **31**: 182-191.

Burn, C.R. 1998. Field investigations of permafrost and climatic change in northwest North America. *In* 7th International Permafrost Conference, Yellowknife, N.W.T., Canada, pp. 107-120.

Carson, M.A. and Kirkby, M.J. Hillslope Form and Process. London: Cambridge University Press, 1972. 475 pp.

Cohen, S. J. 1997. What if and so what in northwest Canada: could climate change make a difference to the future of the Mackenzie Basin? *Arctic.* **50**(4): 293-307.

Couture, N. & Pollard, W. 1998. An assessment of ground ice volume near Eureka Northwest Territories. *In* 7th International Permafrost Conference, Yellowknife, Canada, Université Laval, Centre d'études nordiques, Collection Nordicana, No 57, pp. 195-200.

Couture, N.J. 2000. Sensitivity of permafrost terrain in a high arctic polar desert: an evaluation of response to disturbance near Eureka, Ellesmere Island, Nunavut. M.Sc. Thesis, Department of Geography. Montreal, McGill University. 102 pp.

Dallimore, S.R., Kurfurst, J.J. and Hunter, J.A.M. 1988. Geotechnical and geothermal conditions of near-shore sediments, southern Beaufort Sea, Northwest Territories, Canada. *In* 5th International Permafrost Conference, Trondheim, Norway, pp. 127-131.

Dallimore, S.R., Wolfe, S.A. and Solomon, S. 1996. Influence of ground ice and permafrost on coastal evolution, Richards Island, Beaufort Sea coast, N.W.T. *Canadian Journal of Earth Sciences.* **33**: 664-675.

Davidson-Arnott, R.G.D. and Pollard, W.H. 1980. Wave climate and potential longshore sediment transport patterns, Nottawasaga Bay, Ontario. *Journal of Great Lakes Research.* **6**(1): 54-67.

de Krom, V. 1990. Retrogressive thaw slumps and active layer slides on Herschel Island, Yukon. M.Sc. Thesis. Department of Geography. Montreal, McGill University, 157 pp.

Dyke, L.D. 1991. Temperature changes and thaw of permafrost adjacent to Richards Island, Mackenzie Delta, N.W.T. *Canadian Journal of Earth Sciences.* **28**: 1834-1842.

Eid, B.M. and Cardone, V.J. 1992. Beaufort Sea extreme waves study. *Environmental Studies Research Funds*, Calgary, Alberta. Report Series No. **114**. 143 pp. + appendices.

French, H.M. 1994. Living on Ice: problems of urban development in Canada's north. *Geoscience Canada.* **21**(4): 163-175.

French, H.M. The Periglacial Environment. 2nd ed. England: Addison Wesley Longman Limited, 1996. 341 pp.

Fulton, R.J. 1989. Quaternary geology of the Canadian Interior Plains; Chapter 2. *In* Quaternary Geology of Canada and Greenland. R.J. Fulton (ed.). Geological Survey of Canada, Geology of Canada, no. 1.

Gold, L.W., Johnston, G.H., Slusarchuk, W.A. and Goodrich, L.E. 1972. Thermal effects in permafrost. *Proceedings of Canadian Northern Pipeline Research Conference*, Ottawa, NRC, pp. 25-45.

Grechishchev, S. 2003. Ice segregation and slope stability in permafrost areas. *In* 8th International Permafrost Conference, Zurich, Switzerland, pp.313-317.

Harper, J. R., Owens, E.H. and Wiseman, W.J. Jr. 1978. Arctic beach processes and the thaw of ice-bonded sediments in the littoral zone. *In* 3rd International Permafrost Conference, Edmonton, AB, Canada, pp. 195-199.

Harper, J.R. and Penland, S. 1982. Beaufort Sea sediment dynamics. Victoria, B.C., Geological Survey of Canada, Report. 125 pp.

Harper, J.R., Falconer, H. and Stewart, G.G. 1988. Maximum storm surge elevations in the Tuktoyaktuk region of the Canadian Beaufort Sea. *Arctic.* **47**(1): 48-52.

Harper, J.R. 1990. Morphology of the Canadian Beaufort Sea Coast. *Marine Geology.* **91**: 75-91.

Harper, J.R., Reimer, P.D. and Collins, A.D. 1985. Beaufort Sea physical shore-zone analysis. *Geological Survey of Canada.* Open-File Report No. **1689**. 105 pp.

Harris, C. and Lewkowicz, A.G. 1993. Form and internal structure of active-layer detachment slides, Fosheim Peninsula, Ellesmere Island, Northwest Territories, Canada. *Canadian Journal of Earth Sciences.* **30**(8): 1708-1714.

Harris, C. and Lewkowicz, A.G. 2000. An analysis of the stability of thawing slopes, Ellesmere Island, Nunavut, Canada. *Canadian Geotechnical Journal.* **37**(2): 449-462.

Harry, D.G. 1982. Aspects of the permafrost geomorphology of southwest Banks Island western Canadian arctic. Ph.D. Thesis, University of Ottawa. 230 pp.

Harry, D.G., French, H.M. and Pollard, W.H. 1985. Ice wedges and permafrost conditions near King Point, Beaufort Sea coast, Yukon Territory. Geological Survey of Canada Current Research, Part A, Rep. **85-1A**, pp. 111-116.

Harry, D.G. 1988. Ground Ice and Permafrost. *In*: Advances in Periglacial Geomorphology. M.J. Clark (ed.). John Wiley & Sons, Ltd., 113-149.

Harry, D.G., French, H.M. and Pollard, W.H. 1988. Massive ground ice and ice-cored terrain near Sabine Point, Yukon Coastal Plain. *Canadian Journal of Earth Sciences.* **25**(11): 1846-1856.

Hebert, P.D.N. (ed). 2002. *Canada's Aquatic Environments* [Internet]. CyberNatural Software, University of Guelph. http://www.aquatic.uoguelph.ca.

Heemink, A.W. 1986. Storm surge prediction using kalman filtering. *Rijkswaterstaat Communications*. No. **46**. 194 pp.

Héquette, A. and Barnes, P.W. 1990. Coastal retreat and shoreface profile variations in the Canadian Beaufort Sea. *Marine Geology.* **91**: 113-132.

Héquette, A. and Hill, P.R. 1993. Storm-generated currents and offshore sediment transport on a sandy shoreface, Tibjak Beach, Canadian Beaufort Sea. *Marine Geology*, **113**: 283-304.

Héquette, A., Desrosiers, M. and Barnes, P.W. 1995. Sea ice scouring on the inner shelf of the southeastern Canadian Beaufort Sea. *Marine Geology.* **128**: 201-219.

Héquette, A., Desrosiers, M., Hill, P.R. and Forbes, D.L. 2001. The influence of coastal morphology on shoreface sediment transport under storm-combined flows, Canadian Beaufort Sea. *Journal of Coastal Research.* **17**(3): 507-516.

Hill, P.R., Mudie, P.J., Moran, K. and Blasco, S.M. 1985. A sea-level curve for the Canadian Beaufort Shelf. *Canadian Journal of Earth Science.* **22**: 1383-1393.

Hill, P.R. 1990. Coastal geology of the King Point Area, Yukon Territory, Canada. *Marine Geology.* **91**: 93-111.

Hill, P.R., Blasco, S.M., Harper, J.R. and Fissel, D.B. 1991. Sedimentation on the Canadian Beaufort Shelf. *Continental Shelf Research.* **11**(10): 821-842.

Hill, P.R., Héquette, A. and Ruz, H.-H. 1993. Holocene sea-level history of the Canadian Beaufort Shelf. *Canadian Journal of Earth Sciences.* **30**: 103-108.

Hill, P.R. and Solomon, S. 1999. Geomorphologic and sedimentary evolution of a transgressive thermokarst coast, Mackenzie Delta region, Canadian Beaufort Sea. *Journal of Coastal Research*, **15**(4): 1011-1029.

Hudak, D.R. and Young, J.M.C. 2002. Storm climatology of the southern Beaufort Sea. *Atmosphere-Ocean.* **40**(2): 145-158.

International Permafrost Association. 1998. Multi-Language Glossary of Permafrost and Related Ground-Ice Terms. R.O. Everdingen (ed). Calgary: The Arctic Institute of North America, University of Calgary, Canada.

IPCC, 2001. *Climate Change 2001: The Scientific Basis. Contribution of Working Group I to the Third Assessment Report of the Intergovernmental Panel on Climate Change.* [Houghton, J.T., Y. Ding, D.J. Griggs, M. Noguer, P.J. van der

Linden, X. Dai, K. Maskell, and C.A. Johnson (eds.)]. Cambridge University Press, Cambridge, United Kingdom and New York, NY, USA, 881 pp.

Isozaki, I. 1968. An investigation on the variations of sea level due to meteorological disturbances on the coast of Japanese islands (II): Storm surges on the coast of the Japan Sea. *Journal of the Oceanographical Society of Japan*. **24**(4): 178-190.

Isozaki, I. 1970. An investigation on the variations of sea level due to meteorological disturbances on the coast of Japanese islands (VI): Storm surges on the coasts of the Inland Sea and Osaka Bay. *Papers in Meteorology and Geophysics*. **21**(3): 291-321.

Johnson, K., Solomon, S., Berry, D. and Graham, P. 2003. Erosion progression and adaptation strategy in a northern coastal community. *In* 8th International Permafrost Conference, Zurich, Switzerland, pp. 489-494.

Kelley, D. 2003. Storm surges: is that an ocean in my basement? *Association of Science Teachers Journal*. **4**(1): 9 pp.

Kobayashi, N. 1985. Formation of thermoerosional niches into frozen bluffs due to storm surges on the Beaufort Sea coast. *Journal of Geophysical Research*. **90**(C6): 11983-11988.

Kobayashi, N. and Aktan, D. 1986. Thermoerosion of frozen sediment under wave action. *Journal of Waterway, Port, Coastal and Ocean Engineering*. **112**(1): 140-158.

Kobayashi, N. and Reimnitz, E. 1988. Thermal and mechanical erosion of slopes and beaches. *Arctic Coastal Processes and Slope Protection Design*. Chen, A.T. and Leidersdorf, D.B. (eds.). ASCE, pp.46-62.

Kobayashi, N. and Vidrine, J.C. 1995. Combined thermal-mechanical erosion processes model. *Center for Applied Coastal Research*, Research Report No. **CACR-95-12**. 75 pp.

Kobayashi, N., Vidrine, J.C., Nairn, R.B. and Solomon, S.M. 1999. Erosion of frozen cliffs due to storm surge on Beaufort Sea coast. *Journal of Coastal Research*. **15**(2): 332-344.

Komar, P. Beach Processes and Sedimentation. (2nd ed.) New Jersey: Prentice-Hall, Inc., 1998. 544 pp.

Lachenbruch, A.H., Cladouhos, T.T. and Saltus, R.W. 1988. Permafrost temperature and changing climate. *In* 5th International Permafrost Conference, Trondheim, Norway. Volume 3, pp. 9-17.

Lachenbruch, A.H. 1994. Permafrost, the active layer, and changing climate. *U.S. Geological Survey*, Open-File Report No. **94-694**, 43 pp.

Lantuit, H. 2002. Remotely sensed approach to coastal evolution on Herschel Island, Yukon Territory. Unpublished maîtrise thesis, Université Paris, Paris, France. 102 pp.

Lewis, C.P. and Forbes, D.L. 1974. Sediments and sedimentary processes, Yukon Beaufort Sea Coast. Ottawa: Department of Indian Affairs and Northern Development. Environmental-Social Committee, Northern Pipelines, Task Force on Northern Oil Development Rep. 74-29. 40 pp.

Lewkowicz, A.G. 1992. Factors influencing the distribution and initiation of active-layer detachment slides on Ellesmere Island, arctic Canada. *In* Periglacial Geomorphology. Edited by J.C. Dixon and A.D. Abrahams. Toronto: John Wiley and Sons, Ltd.

Mackay, J.R. 1959. Glacier ice-thrust features of the Yukon coast. *Geographical Bulletin.* **13**: 5-21.

Mackay, J.R. 1963. Notes on the shoreline recession along the coast of the Yukon Territory. *Arctic.* **16**: 195-197.

Mackay, J.R. 1966. Segregated epigenetic ice and slumps in permafrost. *Geographical Bulletin.* **8**: 59-80.

Mackay, J.R. 1971. The origin of massive icy beds in permafrost, western Arctic coast, Canada. *Canadian Journal of Earth Sciences.* **8**(4): 397-422.

Mackay, J.R. 1972*a*. The world of underground ice. *Annals of the Association of American Geographers.* **62**(1): 1-22.

Mackay, J.R. 1972*b*. Offshore permafrost and ground ice, southern Beaufort Sea, Canada. *Canadian Journal of Earth Sciences.* **9**:1550-1561.

Mackay, J.R. 1989. Massive ice: some field criteria for the identification of ice types. *In* Current Research, Part G, Geological Survey of Canada. **Paper 89-1G**: pp. 5-11.

Mackay, J.R. and Dallimore, S.R. 1992. Massive ice of the Tuktoyaktuk area, western Arctic coast, Canada. *Canadian Journal of Earth Sciences.* **29**: 1235-1249.

McDonald, B.C. and Lewis, C.P. 1973. Geomorphologic and sedimentologic processes of rivers and coast, Yukon Coastal Plain. Environmental-Social Committee, Northern Pipelines, Canada, Report No. **73-39**, 245 pp.

McGillivray, D.G., Agnew, T.A., McKay, G.A., Pilkington, G.R., and Hill, M.C. 1993. Report summary of impacts of climatic change on the Beaufort Sea-ice regime: implications for the Arctic petroleum industry. *Climate Change Digest, Atmospheric Environment Service*. Report No. **CCD93-01**. 17 pp.

McGladrey, K.M. 1984. Herschel Island, Yukon Coast. 1:100 000. Pacific Region, Canadian Hydrographic Service. Project No. 7712/84, Field Sheet No. WA 10167.

McRoberts, E.C. and Morgenstern, N.R. 1974. The stability of thawing slopes. *Canadian Geotechnical Journal.* **11**(4): 447-469.

Milne, Allen. 1973. Oil, ice and climate change: the Beaufort Sea and the search for oil. Childerhose, R.J. (ed). Department of Fisheries and Oceans, Ottawa: The Beaufort Sea Project. 103 pp.

Murray, M.A. and Maes, M. 1986. Beaufort Sea extreme wave studies assessment. *Environmental Studies Revolving Funds*, Report No. 023. Ottawa, 97 pp.

Murton, J.B. 2001. Thermokarst sediments and sedimentary structures, Tuktoyaktuk Coastlands, western Arctic Canada. *Global and Planetary Change.* **28**: 175-192.

Nairn, R.B., Solomon, S., Kobayashi, N., Vidrine, J. 1998. Development and testing of a thermal-mechanical numerical model for predicting arctic shore erosion processes. *In* 7th International Permafrost Conference, Yellowknife, N.W.T., pp. 789-795.

Osterkamp, T.E., Zhang, T. and Romanovsky, V.E. 1994. Evidence for a cyclic variation in permafrost temperatures in northern Alaska. *Permafrost and Periglacial Processes*. **5**: 137-144.

Permafrost Subcommittee, Associate Committee on Geotechnical Research. 1988. Glossary of permafrost and related ground-ice terms. Technical Memorandum **142**, National Research Council of Canada, Ottawa.

Pinchin, B.M., Nairn, R.B. and Philpott, K.L. 1985. Beaufort Sea coastal sediment study: numerical estimation of sediment transport and nearshore profile adjustments at coastal sites in the Canadian Beaufort Sea. *Geological Survey of Canada*, Open File Report No. **1259**. 712 pp.

Pinchin, B.M. and Nairn, R.B. 1987. Beaufort Sea coastal sediment study (continuation): evaluation of inshore wave climate and coastal sediment transport prediction techniques at King Point, Yukon. Toronto, Ontario, Keith Philpott Consulting Limited.

Pollard, W.H. and French, H.M. 1980. A first approximation of the volume of ground ice, Richards Island, Pleistocene Mackenzie Delta, Northwest Territories, Canada. *Canadian Geotechnical Journal*, **17**: 509-516.

Pollard, W.H. and Dallimore, S.R. 1988. Petrographic characteristics of massive ground ice, Yukon Coastal Plain, Canada. *In* 5th International Permafrost Conference, Trondheim, Norway, pp. 224-229.

Pollard, W.H. 1990. The nature and origin of ground ice in the Herschel Island area, Yukon Territory. In: *Permafrost Canada, Proceedings of the Fifth Canadian Permafrost Conference*. Collection Nordicana, Centre d'études nordiques, Université Laval, Montreal, Canada, pp.23-30.

Pollard, W. H. 1991. The investigation of buried snowbank ice in ice-rich permafrost in central and northern Yukon, Canada. *Bulletin of Glacier Research.* **9**: 1-7.

Pollard, W.H. 2000. Distribution and characterization of ground ice on Fosheim Peninsula, Ellesmere Island, Nunavut. Ottawa, Geological Survey of Canada, Bulletin **529**, pp. 207-233.

Rampton, V.N. 1982. Quaternary geology of the Yukon Coastal Plain, Geological Survey of Canada, Bulletin **317**. 49 pp.

Ramseier, R.O., Chudobiak, M.R., Vant, M.R. and Gray, R.B. 1974. Distribution of ice thickness in the Beaufort Sea. Geological Survey of Canada. Interim Report of Beaufort Sea Project Study G3. 9 pp.

Resio, D., Bratos, S. and Thompson, E. 2002. Meteorology and Wave Climate. In: Zeki Demirbilek, *Coastal Engineering Manual, Part II: Coastal Hydrodynamics*. Chapter II-2, Engineer Manual 1110-2-1100, U.S. Army Corps of Engineers, Washington DC.

Sater, John E. (editor). The Arctic Basin: revised edition. Washington, D.C.: The Arctic Institute of North America, 1969. 337 pp.

Shah, V.K. 1978. Protection of permafrost and ice rich shores, Tuktoyaktuk, N.W.T., Canada. *In*: 3rd International Permafrost Conference, Edmonton, AB, Canada, pp. 871-873.

Shaw, J., Taylor, R.B., Forbes, D.L., Ruz, M.-H. and Solomon, S. 1994. Sensitivity of the Canadian coast to sea-level rise. *Geological Survey of Canada*, Open-File Report No. **2825**.

Smith, M.W. and Riseborough, D.W. 1983. Permafrost sensitivity to climatic change. *In*: 4th International Permafrost Conference, Fairbanks, Alaska, USA, pp. 1178-1183.

Smith, M.W. 1988. The significance of climatic change for the permafrost environment. *In*: 5th International Permafrost Conference, Trondheim, Norway, pp. 18-23.

Smith, Walker O. Jr. (editor). Polar Oceanography: Part A – Physical Science. San Diego: Academic Press, Inc., 1990.

Smith, S.L and Judge, A.S. 2003. Natural gas hydrates. Environmental Atlas of the Beaufort Coastlands, Natural Resources Canada. On-line. http://sts.gsc.nrcan.gc.ca/beaufort_dcp/index_e.asp?CaId=8&PgId=41

Solomon, S.M. 1995. Impacts of the September 1993 storm on the Beaufort Sea. *Geological Survey of Canada*, Dartmouth, Nova Scotia, Canada.

Solomon, S.M., Forbes, D.L. and Keirstead, B. 1994. Coastal impacts of climate change: Beaufort Sea erosion study. *Geological Survey of Canada*, Open-File Report No. **2890**.

Solomon, S.M. and Covill, R. 1995. Impacts of the September, 1993 storm on the coastline at four sites along the Canadian Beaufort Sea. *In* Proceedings of the 1995 Canadian Coastal Conference. Vol. 2, pp. 779-796.

Solomon, S.M. and Hart, E. 1999. Storminess in the western Arctic: extending the historical record using Hudson's Bay Company archives. *Environmental Monitoring and Assessment Network Annual Science Meeting.* Victoria, B.C.

Solomon, S. and Gareau, P. 2003. Beaufort Sea coastal mapping and the development of an erosion hazard index. *In* 8th International Permafrost Conference, Zurich, Switzerland, pp. 1091-1096.

Shah, V.K. 1978. Protection of permafrost and ice rich shores, Tuktoyaktuk, N.W.T., Canada. *In* 3rd International Permafrost Conference, Edmonton, AB, pp. 871-873.

Taber, S. 1929. Frost heaving. *Journal of Geology.* **37**: 428-461.

Taber, S. 1930. The mechanics of frost heaving. *Journal of Geology.* **38**: 303-317.

Vigdorchik, M.E. Submarine Permafrost on the Alaskan Continental Shelf. Boulder, CO: Westview Press, 1980. 118 pp.

Walker, H.J. 1988. Permafrost and coastal processes. *In* 5th International Permafrost Conference, Trondheim, Norway, vol.3, pp. 35-42.

Walker, R.G. and Plint, A.G. 1992. Wave- and storm-dominated shallow marine systems (Chapter 12). *In*: Facies Models: response to sea level change. R.G.

Walker and N.P. James (eds.). Memorial University of Newfoundland: Geological Association of Canada. Pp. 219-238.

Washburn, A.L. Periglacial Processes and Environments. London: Edward Arnold Publishers, 1973. 320 pp.

Wolfe, S.A., Dallimore, S.R. and Solomon, S.M. 1998. Coastal permafrost investigations along a rapidly eroding shoreline, Tuktoyaktuk, N.W.T. *In* 7th International Permafrost Conference, Yellowknife, N.W.T., pp. 1125-1131.

World Meteorological Organization. 1978. Present techniques of tropical storm surge prediction. *In*: Reports on Marine Science Affairs. Report No. **13**. 87 pp.

Young, A. Slopes. Edinburgh: Oliver & Boyd Inc., 1972. 288 pp.

Zenkovich, V.P. Processes of Coastal Erosion. New York: Interscience Publishers, 1967. 738 pp.

APPENDIX A:
STORM DATABASE SUMMARIES

A—1 Eid, B.M. and Cardone, V.J. 1992. Top 50 storms 1957-1983.

Date (YYYY-MM-DD)	Duration hours	Max Wind knots	Max Wind km/h	Mean Direction degrees	Max Wave H. metres	Period seconds
1962-07-21	88	50	92.6	290	4.0	5.0
1962-09-03	100	56	103.7	310	9.5	16.0
1962-09-09	51	48	88.9	250	8.0	6.0
1970-09-02	118	45	83.3	110	4.5	12.0
1970-09-12	47	63	116.7	240	5.6	7.0
1971-08-21	72	26	48.2	360	2.9	7.1
1975-08-08	75	40	74.1	280	4.7	10.0
1975-08-26	56	45	83.3	230	5.0	0.0
1976-08-11	72	35	64.8	50	4.3	6.2
1976-09-28	90	32	59.3	70	4.0	6.0
1977-08-25	102	41	75.9	320	3.4	6.9
1977-09-21	38	42	77.8	270	3.0	6.0
1977-10-05	166	45	83.3	130	3.5	5.0
1978-08-22	104	40	74.1	300	3.1	6.7
1978-09-01	240	40	74.1	90	2.7	6.0
1978-09-09	126	38	70.4	30	6.3	8.0
1978-09-19	91	40	74.1	70	7.5	12.0
1978-09-28	99	45	83.3	280	3.5	5.0
1978-10-06	100	50	92.6	50	3.5	7.0
1979-09-11	205	36	66.7	70	4.0	6.0
1979-09-29	246	42	77.8	80	3.5	6.0
1979-10-08	236	40	74.1	110	4.5	6.0
1979-10-21	114	45	83.3	60	0.5	5.0
1980-08-28	120	22	40.7	280	3.3	8.0
1980-08-29	171	40	74.1	130	3.7	6.0
1981-08-01	70	40	74.1	310	4.0	5.0
1981-08-15	60	45	83.3	290	6.0	5.0
1981-08-19	167	35	64.8	310	3.5	6.0
1981-08-28	124	45	83.3	240	4.0	8.0
1981-09-27	275	36	66.7	40	5.0	8.0
1982-07-19	88	35	64.8	350	3.0	6.3
1982-07-26	70	50	92.6	315	5.0	6.4
1982-08-19	93	38	70.4	280	3.5	6.0
1982-09-16	52	41	75.9	230	3.0	5.0
1982-09-19	117	41	75.9	110	4.0	6.0
1982-10-02	192	34	63.0	290	3.0	3.0
1982-10-17	253	54	100.0	270	4.0	5.0
1983-08-29	295	45	83.3	280	5.4	6.0

Date (YYYY-MM-DD)	Duration hours	Max Wind knots	Max Wind km/h	Mean Direction degrees	Max Wave H. metres	Period seconds
1984-07-17	72	35	64.8	250	2.0	5.0
1984-08-10	99	36	66.7	180	2.5	6.0
1984-08-24	96	38	70.4	360	2.5	5.0
1984-09-18	110	38	70.4	90	2.5	5.0
1984-09-28	89	34	63.0	110	4.0	5.0
1985-08-05	77	32	59.3	130	2.0	5.0
1985-09-01	63	34	63.0	110	3.53	5.0
1985-09-12	153	50	92.6	280	6.01	6.0
1986-08-21	90	36	66.7	320	5.1	9.0
1986-09-07	246	32	59.3	120	4.0	8.0
1987-08-24	102	46	85.2	270	6.5	6.0
1988-08-01	93	38	70.4	310	4.3	8.0

A—2 Solomon, S.M., Forbes, D.L. and Keirstead, B. 1994. GSC Open-File Rep. #2890. Major storms based on Tuktoyaktuk (NWT) DEW-line data (revised).

Date (YYYY-MM-DD)	Fetch (km)	Max Wave H. metres	Mean Direction degrees	Duration hours	Max Wind km/h	Min Wind km/h
1959-07-09	18.0	1.2	250	7	58	45
1959-07-27	28.6	1.1	280	7	40	40
1959-08-01	36.5	1.3	295	13	48	37
1959-10-03			295	25	56	37
1959-10-18			270	13	40	37
1959-10-29			50	13	48	37
1960-07-24	71.4	1.7	290	19	47	37
1960-08-15			60	13	37	37
1960-08-20	140.5	2.1	290	31	47	37
1960-09-12			100	7	48	42
1960-09-14	71.4	1.8	295	13	48	40
1960-09-17	168.2	2.1	312.5	73	45	37
1960-09-22			80	13	40	37
1960-09-29	204.0	2.1	320	13	40	37
1961-07-21	81.8	1.6	285	7	40	37
1961-08-01	139.9	1.8	320	13	37	37
1961-08-12	108.7	2.2	305	7	56	37
1961-08-24	114.7	1.9	35	7	45	37
1961-09-13			55	13	42	37
1961-09-29			90	19	40	37
1962-07-04	84.1	1.5	305	7	37	37
1962-07-25			230	19	51	37
1962-07-28	95.8	2.6	305	13	72	37
1962-08-26	114.7	1.8	295	7	40	37
1962-09-03	102.9	2.5	280	19	64	40
1962-09-21	198.6	2.8	295	7	47	47
1962-10-11			50	19	51	40
1962-10-29			260	13	42	37
1963-07-05	45.0	1.6	290	13	47	45
1963-07-27	196.1	3.1	295	73	58	37
1963-08-04	263.7	2.6	320	7	48	37
1963-08-10	236.3	2.1	320	7	37	37
1963-08-23			170	7	50	37
1963-08-26	130.5	2.1	305	7	45	40
1963-08-31			90	7	37	37
1963-10-02	291.9	3.2	340	7	50	47
1963-10-03			150	19	64	37
1963-10-07			90	25	40	37
1963-10-16			335	13	45	40
1963-10-21			70	7	42	37

Date (YYYY-MM-DD)	Fetch (km)	Max Wave H. metres	Mean Direction degrees	Duration hours	Max Wind km/h	Min Wind km/h
1964-07-10			350	25	50	39
1964-07-18			205	13	47	37
1964-08-13			90	7	48	45
1964-08-19	31.8	1.2	320	25	47	37
1964-09-03	38.4	1.6	330	25	60	37
1965-07-05			320	7	37	37
1965-08-06	128.1	2.8	305	13	60	47
1965-08-12	128.1	1.8	305	7	40	37
1965-09-01	195.6	2.0	330	7	37	37
1965-09-04	185.1	1.9	320	7	37	37
1965-09-20	130.9	2.4	305	25	55	39
1965-09-28	216.5	2.5	320	13	47	40
1965-10-12	76.6	1.5	270	7	40	37
1966-09-10			155	7	40	40
1966-09-26			125	13	43	39
1966-10-04			110	7	39	37
1967-07-24	52.0	1.5	320	7	45	40
1967-09-01			70	7	40	37
1967-09-17			72.5	35	55	37
1967-10-03			340	7	55	37
1968-07-09			190	7	40	40
1968-10-03			190	13	50	37
1968-10-24			72.5	73	51	37
1969-07-10			350	7	40	37
1969-08-04			215	13	40	37
1969-08-05	97.1	2.1	305	7	56	37
1969-08-16	94.7	2.2	345	109	60	37
1970-09-05	306.1	2.6	340	13	45	37
1970-09-14	198.6	4.1	297.5	24	71	37
1970-10-01	42.0	1.4	270	7	45	40
1970-10-11	120.7	2.4	280	36	56	37
1970-10-21			280	7	47	39
1971-07-29	109.6	2.2	280	7	47	45
1971-08-03	275.0	2.2	330	13	37	37
1971-08-22	242.3	2.5	325	25	47	37
1971-10-19			345	7	37	37
1972-09-01	321.7	3.4	320	13	51	48
1972-09-11	239.1	2.2	305	13	40	37
1972-09-19	35.8	1.1	260	7	37	37
1972-09-27	278.3	2.5	330	7	45	37
1972-10-16			140	7	40	37
1972-10-29			250	7	37	37
1972-10-30			295	7	45	45
1973-07-13			70	7	37	37
1974-08-19	77.4	2.0	340	13	51	42
1974-09-02	75.0	1.5	330	7	39	37
1974-10-25			90	31	42	37

Date (YYYY-MM-DD)	Fetch (km)	Max Wave H. metres	Mean Direction degrees	Duration hours	Max Wind km/h	Min Wind km/h
1975-08-10	136.7	2.3	290	13	51	40
1975-08-27	123.4	2.5	290	7	56	42
1975-09-25	62.5	1.4	295	13	40	37
1975-10-27			300	91	45	37
1976-07-06	32.6	1.1	290	13	40	37
1976-08-12			35	19	51	37
1976-09-30	367.8	2.3	350	7	37	37
1976-10-18			290	7	40	37
1977-08-27	276.9	2.7	295	19	50	37
1977-09-24			220	7	41	37
1977-10-15			40	13	44	37
1978-07-14			40	13	37	37
1978-09-20			70	7	41	37
1978-10-06			75	55	37	37
1978-10-18			95	7	46	41
1978-10-23			50	7	41	37
1979-07-27			95	7	44	37
1979-08-04	171.0	2.0	300	7	41	37
1980-07-26	152.3	2.2	320	7	48	37
1980-08-17			55	7	46	37
1980-08-30	35.8	1.2	250	7	44	37
1980-09-16	146.8	2.2	315	13	48	37
1980-09-27			92.5	24	39	37
1981-07-29	77.7	1.5	280	7	37	37
1981-08-02	144.7	2.2	310	31	48	37
1981-08-16	123.6	2.1	290	25	48	37
1981-08-21			80	7	37	37
1981-08-30	176.6	2.3	320	49	48	37
1981-09-16	178.2	2.2	295	19	44	37
1981-09-28			35	13	37	37
1981-10-04	268.5	2.8	365	37	52	37
1981-10-29			330	7	37	37
1981-10-31			290	6	37	37
1982-07-27	191.1	2.2	300	7	44	37
1982-08-21	144.4	2.2	300	13	48	37
1982-09-17	175.0	2.8	270	7	52	46
1982-09-20			80	13	44	41
1982-10-02	245.4	2.1	295	7	37	37
1982-10-19			282.5	31	67	37
1982-10-23			60	7	41	37
1983-07-02			80	7	37	37
1983-08-03	103.6	1.9	290	7	46	37
1983-09-02	246.8	2.1	355	7	37	37
1983-09-15	60.6	1.5	330	7	46	37
1983-09-22	53.3	1.4	330	91	43	37
1983-10-04			275	7	37	37
1983-10-07			270	7	44	43

Date (YYYY-MM-DD)	Fetch (km)	Max Wave H. metres	Mean Direction degrees	Duration hours	Max Wind km/h	Min Wind km/h
1984-07-13	71.7	1.4	285	7	37	37
1984-07-18	185.5	2.4	275	19	48	37
1984-08-08			180	7	44	41
1984-08-10	153.5	2.4	310	49	52	37
1984-08-15	80.2	1.9	270	7	48	43
1984-08-25	128.8	2.7	5	37	63	41
1984-10-24			295	31	56	37
1985-07-05	31.2	1.2	280	19	48	37
1985-07-19	21.2	1.1	310	7	48	41
1985-09-15	50.4	1.4	280	73	56	37
1985-09-29	31.2	1.1	250	7	39	37
1985-10-18			280	31	65	37
1986-07-19	52.2	1.4	305	7	41	37
1986-08-21	248.2	3.4	312.5	67	67	37
1986-09-21	224.6	2.3	305	7	44	37
1986-10-01	116.6	1.9	285	7	44	37
1986-10-04			140	7	37	37
1986-10-05	190.1	3.0	315	25	65	37
1986-10-10			235	13	46	37
1986-10-25			280	7	37	37
1987-08-09	295.7	2.6	325	19	46	37
1987-08-23	190.9	2.6	285	7	46	44
1987-08-28	313.6	3.0	300	91	56	37
1987-09-05	200.9	2.7	305	13	56	37
1987-09-08	167.9	2.3	275	13	48	37
1987-10-26			245	7	46	44
1988-07-02			85	7	41	37
1988-07-22	182.1	1.9	290	7	37	37
1988-08-01	105.9	2.2	272.5	67	56	37
1988-08-13	47.1	1.3	270	13	39	37
1988-09-06	169.4	2.0	360	7	41	37
1988-09-16	100.0	1.6	285	7	37	37
1988-10-08	83.2	1.5	285	7	37	37
1988-10-14	32.8	1.3	282.5	73	52	37
1989-07-19			220	7	41	37
1989-08-15	125.7	1.7	300	7	37	37
1989-08-21	131.0	1.9	310	7	41	37
1989-09-16	233.6	2.6	320	67	56	37
1989-09-24			125	7	37	37
1989-09-26	110.3	1.8	290	13	41	37
1989-10-18			327.5	55	48	37
1990-08-27	144.8	2.2	270	7	44	43
1990-09-01	146.0	2.5	297.5	67	56	37
1990-09-07	76.6	1.8	287.5	55	46	41
1990-10-24			55	19	41	37

Date (YYYY-MM-DD)	Fetch (km)	Max Wave H. metres	Mean Direction degrees	Duration hours	Max Wind km/h	Min Wind km/h
1991-08-04	63.3	1.7	340	13	52	37
1991-08-24	51.5	1.5	300	7	44	41
1991-10-08	28.4	1.2	230	13	48	39
1991-10-13			130	31	48	37
1991-10-20			310	79	70	37
1992-09-09	216.0	2.0	5	7	37	37
1992-09-16	91.4	1.9	280	13	50	37
1992-09-22			284	25	46	37

A—3 Environment Canada National Climate Archive (online) 1970-2003. Unpublished major storm compilation based on Tuktoyaktuk (NWT) DEW-line data.

Date (D/M/Y)	Duration (hrs)	Mean Wind Direction (degrees)	Wind Deviation (degrees)	Avg Wind (km/h)	Max Wind (km/h)	Min Wind (km/h)	Wind Speed (m/s)
05/09/1970	27	320	0	45.4	58	42	12.61
13/09/1970	40	290	50	58.5	87	35	16.25
29/07/1971	8			43.6	48	35	12.11
22/08/1971	37			40.1	48	32	11.14
01/09/1972	30			46.6	74	32	12.94
11/09/1972	25			41.8	45	32	11.61
21/07/1973	8			42.8	55	35	11.89
19/08/1974	15			43.4	51	34	12.06
02/09/1974	22			41.3	48	32	11.47
15/09/1974	29			38.9	47	29	10.81
15/10/1974	24			38.1	42	32	10.58
05/07/1975	6			52.3	71	37	14.53
10/08/1975	26			39.3	47	37	10.92
27/08/1975	10			53.3	60	42	14.81
06/09/1975	18			38.8	47	37	10.78
05/07/1976	42			42.6	56	34	11.83
12/08/1976	22			45.8	56	37	12.72
21/08/1976	19			51.5	71	37	14.31
23/08/1976	8			44.9	56	37	12.47
08/09/1976	7			37.9	40	37	10.53
21/09/1976	8			41.9	48	37	11.64
30/09/1976	6			39.3	45	37	10.92
22/06/1977	13	240	30	39.9	48	33	11.08
25/06/1977	8	310	10	37.5	41	37	10.42
28/06/1977	31	320	20	40.0	50	33	11.11
06/08/1977	7	90	10	39.7	41	37	11.03
27/08/1977	25	265	45	43.6	50	33	12.11
15/10/1977	9	40	10	41.1	46	37	11.42
04/07/1978	7	90	10	42.6	48	37	11.83
23/08/1978	15	300	10	43.1	48	41	11.97
25/08/1978	6	280	60	38.8	48	37	10.78
05/09/1978	21	120	30	37.0	37	37	10.28
16/09/1978	9	280	40	40.4	48	37	11.22
19/09/1978	29	90	20	40.9	52	35	11.36
01/10/1978	11	290	20	39.7	43	37	11.03
06/10/1978	8	70	10	40.3	44	37	11.19
08/10/1978	23	70	20	40.6	48	37	11.28
27/07/1979	14	90	20	37.1	41	33	10.31
22/08/1979	13	300	20	38.0	46	33	10.56
03/10/1979	17	100	30	40.5	52	30	11.25
09/10/1979	9	100	0	41.9	46	37	11.64

Date (D/M/Y)	Duration (hrs)	Mean Wind Direction (degrees)	Wind Deviation (degrees)	Avg Wind (km/h)	Max Wind (km/h)	Min Wind (km/h)	Wind Speed (m/s)
02/07/1980	12	90	10	38.3	43	37	10.64
25/07/1980	10	320	10	43.0	50	37	11.94
17/08/1980	6	60	10	38.6	41	37	10.72
30/08/1980	7	250	30	42.6	48	37	11.83
01/09/1980	8	70	10	39.0	41	37	10.83
15/09/1980	22	310	10	43.4	56	33	12.06
26/09/1980	31	100	10	41.5	52	37	11.53
30/09/1980	9	320	10	39.5	46	37	10.97
19/06/1981	12	90	10	37.8	41	37	10.50
19/07/1981	6	300	10	39.7	43	37	11.03
29/07/1981	12	270	30	43.2	56	33	12.00
02/08/1981	44	310	50	42.0	56	19	11.67
09/08/1981	8	290	50	40.6	46	33	11.28
16/08/1981	29	280	20	47.8	74	33	13.28
20/08/1981	25	70	40	41.6	52	33	11.56
29/08/1981	74	310	40	42.7	63	30	11.86
16/09/1981	32	280	40	46.8	56	37	13.00
18/09/1981	10	90	10	46.5	56	37	12.92
19/09/1981	15	290	40	41.1	56	33	11.42
27/09/1981	35	20	50	41.4	48	37	11.50
03/10/1981	42	300	50	48.8	67	37	13.56
19/07/1982	13	270	10	40.9	54	37	11.36
27/07/1982	35	280	40	46.6	81	28	12.94
01/08/1982	7	280	10	40.3	44	37	11.19
03/08/1982	7	300	20	38.1	41	37	10.58
18/08/1982	7	320	10	43.4	48	37	12.06
20/08/1982	36	290	20	44.9	59	26	12.47
16/09/1982	8	280	20	51.8	67	41	14.39
20/09/1982	6	80	10	40.8	44	37	11.33
03/10/1982	7	280	30	37.9	41	37	10.53
13/10/1982	6	340	20	40.1	46	37	11.14
02/07/1983	13	90	0	41.7	48	37	11.58
05/09/1983	8	300	50	40.9	44	37	11.36
15/09/1983	12	320	10	41.5	48	33	11.53
22/09/1983	15	330	20	39.0	48	30	10.83
23/09/1983	8	340	20	37.0	37	37	10.28
24/09/1983	22	320	30	37.6	48	30	10.44
30/09/1983	7	120	10	39.3	43	37	10.92
07/10/1983	15	280	10	40.4	46	33	11.22
18/07/1984	7	310	10	44.7	48	39	12.42
08/08/1984	10	190	10	39.4	44	37	10.94
11/08/1984	14	290	20	41.2	46	30	11.44
25/08/1984	43	330	70	49.1	56	35	13.64
06/07/1985	11	290	20	39.5	48	33	10.97
27/07/1985	7	290	10	38.9	46	37	10.81
16/09/1985	48	270	20	44.5	56	37	12.36

Date (D/M/Y)	Duration (hrs)	Mean Wind Direction (degrees)	Wind Deviation (degrees)	Avg Wind (km/h)	Max Wind (km/h)	Min Wind (km/h)	Wind Speed (m/s)
22/08/1986	8	280	40	45.0	56	37	12.50
03/09/1986	6	280	20	44.8	56	37	12.44
21/09/1986	10	300	10	40.9	50	37	11.36
05/10/1986	12	310	30	53.0	65	35	14.72
28/08/1987	14	290	10	44.4	56	37	12.33
30/08/1987	25	270	20	45.7	56	37	12.69
08/09/1987	6	280	10	42.7	46	37	11.86
30/06/1988	15	80	10	43.6	50	37	12.11
01/07/1988	9	80	10	42.8	48	37	11.89
02/07/1988	8	80	10	45.1	54	37	12.53
01/08/1988	12	290	30	42.8	50	37	11.89
03/08/1988	28	300	40	47.2	56	31	13.11
13/08/1988	7	270	10	39.7	44	37	11.03
08/10/1988	6	290	10	39.2	44	37	10.89
02/07/1989	6	310	10	41.8	44	37	11.61
19/07/1989	6	180	10	40.3	41	37	11.19
16/09/1989	6	290	10	41.0	41	41	11.39
18/09/1989	12	330	30	44.8	48	41	12.44
23/06/1990	14	320	10	40.1	43	37	11.14
27/08/1990	12	270	10	42.7	50	37	11.86
01/09/1990	26	310	40	46.7	63	33	12.97
02/09/1990	20	290	20	42.1	57	37	11.69
07/09/1990	36	280	20	41.0	56	28	11.39
15/09/1990	14	310	10	40.6	44	39	11.28
04/08/1991	18	330	30	44.0	52	37	12.22
23/08/1991	30	310	30	38.4	50	33	10.67
08/10/1991	7	250	10	41.8	44	39	11.61
13/08/1992	9	290	10	42.1	52	35	11.69
22/09/1992	9	290	10	39.7	43	35	11.03
04/10/1992	8	320	10	39.5	43	33	10.97
12/07/1993	16	310	30	38.8	46	33	10.78
24/07/1993	13	310	20	38.3	43	35	10.64
30/07/1993	7	320	10	38.1	41	37	10.58
07/08/1993	11	300	20	43.8	54	33	12.17
09/08/1993	9	290	10	40.4	48	33	11.22
17/09/1993	16	310	10	46.5	56	41	12.92
21/09/1993	38	280	20	53.0	74	37	14.72
27/09/1993	25	250	20	40.8	50	33	11.33
01/10/1993	37	270	30	44.3	65	33	12.31
12/10/1993	29	290	30	42.4	56	35	11.78
18/08/1994	16	280	40	53.9	74	44	14.97
22/08/1994	9	300	10	39.4	46	37	10.94
27/09/1994	9	300	30	41.1	48	37	11.42
24/06/1995	9	300	0	43.9	46	41	12.19
28/08/1995	6	300	30	40.3	43	37	11.19

Date (D/M/Y)	Duration (hrs)	Mean Wind Direction (degrees)	Wind Deviation (degrees)	Avg Wind (km/h)	Max Wind (km/h)	Min Wind (km/h)	Wind Speed (m/s)
27/08/1996	6	290	10	38.2	41	37	10.61
04/10/1996	13	290	20	47.4	57	41	13.17
13/08/1997	8	290	30	40.6	44	37	11.28
08/08/1999	6	110	10	42.3	44	37	11.75
27/08/1999	6	280	10	44.7	52	37	12.42
24/09/1999	36	300	20	40.2	46	32	11.17
27/09/1999	6	300	0	43.0	46	37	11.94
11/08/2000	27	290	30	47.1	70	37	13.08

APPENDIX B: COMPUTER MODEL

PROGRAM CLIFF

```
C       @@@@@@@@@@@@@@@@@@@@@@@@@@@@@@@@@@@@@@

C       COMPUTATION OF CLIFF EROSION DUE TO STORM SURGE
C       FOLLOWING KOBAYASHI'S MODEL

C       @@@@@@@@@@@@@@@@@@@@@@@@@@@@@@@@@@@@@@

C                       MD. AZHARUL HOQUE
C                       CENTRE FOR CLIMATE AND GLOBAL CHANGE RESEARCH
C                       McGILL UNIVERSITY, MONTREAL,QC, CANADA
C
C       @@@@@@@@@@@@@@@@@@@@@@@@@@@@@@@@@@@@@@

C       CALCULATES TEMPORAL VARIATION OF
C               R:      HORIZONTAL RETREAT OF THE CLIFF
C               B:      THICKNESS OF UNFROZEN BEACH SEDIMENT
C               D:      VERTICAL MELTING DEPTH OF THE FROZEN BEACH
SEDIMENT

C       @@@@@@@@@@@@@@@@@@@@@@@@@@@@@@@@@@@@@@

        DIMENSION R(12000), B(1200),D(1200),E(1200)
        COMMON/PARAM/Hrms,Tr,PI,Cw,AKw,ANU,g,a,alpa,gama,fwa,fwc
        REAL nb,nc,linc,Li,Lb,Lc
        DATA g/9.81/,A/0.1/,ALPA/0.001/,GAMA/0.4/,fwa/0.0002/,fwc/0.1/
        PI=4.*ATAN(1.0)

        OPEN(UNIT=11,FILE='CLIFFOUT.DAT')
        OPEN(UNIT=12,FILE='Q&B.DAT')

C       *************** INPUT PARAMETERS ***************
        print*,'storm height in m ?'
        read*,Sm
        print*,'Storm duration in hr ?'
        read*,Ts
        print*,'Hrms value in m ?'
        read*,Hrms
        print*,'Spectral peak period in sec ?'
        read*,Tr

C       STORM SURGE & INCIDENT WAVE CONDITIONS
c       Sm=2.0          !Maximum surge elevation in m
c       Ts=100.0        !Surge duration in hrs
c       Hrms=1.0        !r.m.s. value of the incident wave heights (m)
c       Tr=7.0          !spectral peak period (sec)

C       BEACH PARAMETERS
        Bb=1.0
        Wb=2.0
```

```
BSLOPE=0.1                                  !BSLOPE=TAN(Beach slope angle)
THETAB=ATAN(BSLOPE)                         !Beach slope angle
Db=((4.0*A**3)/9.0)/(BSLOPE**2.)            !Water depth at seaward boundary

Pb=0.60          !Course sediment per unit volume of unfrozen sediment
Vb=0.60          !Course sediment per unit volume of frozen sediment
nb=1.-Vb         !Ice volume per unit volume of frozen beach sediment
AKsb=0.001       !Equivalant sand roughness for frozen beach sediment

C    CLIFF PARAMETERS
Bc=1.0                      !Thickness of unfrozen cliff sediment (m)
Hc=35.                      !Cliff height above MSL (m)
CSLOPE=1.19                 !TAN(CLIFF SLOPE ANGLE)
THETAC=ATAN(CSLOPE)

Pc=0.50          !Course sediment per unit volume of unfrozen sediment
Vc=0.43          !Course sediment per unit volume of frozen sediment
Nc=1.-Vc         !Ice volume per unit volume of frozen cliff sediment
AKsc=0.001       !Equivalant sand roughness for frozen cliff sediment

C    SEWATER AND THERMAL PROPERTIES

Sw=15.0                     !Seawater salinity (<35%)
Tw=5.0                      !Sewater temperature (C)
Tm=-0.06*Sw                 !Melting temperature of ice.

rhoi=920.0       !Density of bubble free ice
Li=330000.0      !Latent heat of melting
Lb=nb*rhoi*Li    !Volumetric latent heat of melting per unit volume of frozen
beach sediment.
Lc=nc*rhoi*Li !Volumetric latent heat of melting per unit volume of frozen cliff
sediment.

AKw=0.0014*Tw+0.564                         !Thermal conductivity
Cw=-2500.0*Tw+4.217*1.0E6                   !Volumetric heat capacity
ANU=(1.787E-6)-(6.25E-8*Tw)+(1.34E-9*Tw**2) !Kinematic viscosity

C    ********** INITIALIZATION **********
T=0.0
St=0.0
B(1)=Bb
R(1)=0.0
D(1)=0.0
E(1)=0.0
Qc=0.0
Qp=0.0
Qm=0.0

W=R(1)+WB+Db/BSLOPE
H=Hc+Db+E(1)-W*BSLOPE
dc=St+dB+E(1)-W*BSLOPE
```

```
      WRITE(11,111)
      111 FORMAT(3X' t(hr)',3X,' St(m) ',3X,' dc(m) ',3X,' R(m) ', *3X,' E(m) ',3X,' D(m)

      WRITE(11,110)T,St,dc,R(1),E(1),D(1)
      110 FORMAT(3X,F6.2,5(3X,F9.6))

C     @@@@@@@@@@@ STARTING OF THE MAIN LOOP @@@@@@@@@@@

      NT=1000
      DELT=Ts*3600.0/NT          !Time increment in sec

      DO 100 I=2,NT+1
      T=(I-1)*DELT/3600.0        !Instantaneous time in Hr
      St=Sm*Sin(PI*T/Ts)

      IF(dc.LE.0.0)THEN
      R(I)=R(I-1)
      Qc=0.0
      GOTO 567
      ENDIF

      CALL HEAT(dc,AKsc,HTCC)          !HTCC:Heat transfer coeff for cliff
      Ru=MIN(dc,Hrms)
      linc=MIN((Ru+dc),(H-Bc))/SIN(THETAC)
      R(I)=R(I-1)+(linc*HTCC*(Tw-Tm)/(Lc*(H-Bc)))*DELT
      Qc=(Pc*Bc+Vc*(H-Bc))*(linc*HTCC*(Tw-Tm))/(Lc*(H-Bc))

      567    W=R(I)+WB+Db/BSLOPE
      Qp=ALPA*Pb*((SQRT(St+E(I-1)+Db)*BSLOPE)-(2./3.)*(A**(3./2.)))

      IF(B(I-1).GT.0.0)THEN
      Qm=0.0
      Qb=Qp
      B(I)=B(I-1)+((Qc+Qm-Qp)/(Pb*W))*DELT
      D(I)=D(I-1)
      GOTO 777
      ENDIF

      drb=(dc+St+db+E(I-1))/2.
      CALL HEAT(drb,AKsb,HTCB)
      D(I)=D(I-1)+(HTCB*(Tw-Tm)/Lb)*DELT
      Qm=Vb*W*HTCB*(Tw-Tm)/Lb

      IF(Qp.GE.(Qc+Qm))THEN
      Qb=Qc+Qm
      B(I)=0.0
      ELSE
      Qb=Qp
      B(I)=B(I-1)+((Qc+Qm-Qb)/(Pb*W))*DELT
      ENDIF
```

```
      777 E(I)=Bb-B(I)+D(I)
      dc=St+db+E(I)-W*BSLOPE
      H=Hc+Db+E(I)-W*BSLOPE
      IF(H.LT.Bc)GOTO 888

      WRITE(6,110)T,St,dc,R(I),E(I),D(I)
      WRITE(11,110)T,St,dc,R(I),E(I),D(I)

      WRITE(12,121)T,Qc,Qm,Qb,B(I)
      121 FORMAT(3X,F6.2,4(3X,F9.6))

100 CONTINUE

      GOTO 999
888 PRINT*,'Calculation stopped at',T,' Hr because of H<Bc'
999 CONTINUE

      CLOSE(11)
      CLOSE(12)

      STOP
      END

C     @@@@@@@@@@@ END OF THE MAIN PROGRAM @@@@@@@@@@@

C     @@@@@@@@@@@@@@@@@@@@@@@@@@@@@@@@@@@@@@@@@@@@@@@

C           SUBROUTINE TO CALCULATE HEAT TRANSFER COEFFICIENT

C     @@@@@@@@@@@@@@@@@@@@@@@@@@@@@@@@@@@@@@@@@@@@@@@

      SUBROUTINE HEAT (dr,AKs,HTC)
      COMMON/PARAM/Hrms,Tr,PI,Cw,AKw,ANU,g,a,alpa,gama,fwa,fwc
      REAL Krdr

C     ******** CALCULATION OF REPRESENTATIVE FLUID VELOCITY ********

      Wr=2.0*PI/Tr
      B=(Wr**2.)*dr/g

C     Calculation of Krdr using Newton Raphson method
      X=0.25
      333     Y=X*TANH(X)-B
      DY=TANH(X)+X*(1.0/COSH(X))**2.0
      XX=X-Y/DY
      IF(ABS(X-XX).GT.1.E-6)THEN
      X=XX
      GOTO 333
      ENDIF
      Krdr=X
```

```
      Hr=MIN(gama*dr,Hrms)
      Ub=PI*Hr/(Tr*SINH(Krdr))

C     ************** CALCULATION OF FRICTION FACTOR **************

      AB=Ub/Wr
      RX=Ub*AB/ANU

C     Calculation of fws for smooth bed using bisection method
C                    The given range of fws: fwa<fws<fwc
      XA=fwa
      XB=fwc
      IF(FR(XA,RX)*FR(XB,RX).GT.0.0)GOTO 55

      44 XMID=(XA+XB)/2.0
      IF(FR(XA,RX)*FR(XMID,RX).GT.0.0)THEN
      XA=XMID
      ELSE
      XB=XMID
      ENDIF
      IF(ABS(XA-XB).GT.1.0E-5)GOTO 44

      fws=(XA+XB)/2.0
      Rss=AKs*Ub/ANU*SQRT(0.5*fws)
      GOTO 66

      55    PRINT*,'There is no root in the given range of fws'
      PAUSE

      66 fwr=EXP(5.213*(AKs/AB)**0.194-5.977)
      Rsr=AKs*Ub/ANU*SQRT(0.5*fwr)

      IF(Rss.LE.5.0)THEN
      fw=fws
      ELSE IF(Rsr.GE.70.0)THEN
      fw=fwr
      ELSE
      Rst=AKs*Ub/ANU*SQRT((fws+fwr)/4.0)
      fw=fws+(fwr-fws)*(Rst-5.0)/65.0
      ENDIF

C     ************** CALCULATION OF THERMAL COEFFICIENT **************
      Ust=Ub*SQRT(0.5*fw)
      RN=Ust*AKs/ANU
      PN=(ANU*Cw)/AKw

      Fsmooth=5.0*(PN-1.+LOG(1.+(5./6.)*(PN-1)))
      Frough=0.52*(RN**0.45)*(PN**0.8)

      IF(RN.LE.5.0)THEN
      F=Fsmooth
```

```
      ELSE IF(RN.GE.70.0)THEN
      F=Frough
      ELSE
      F=Fsmooth+(RN-5.0)*((Frough-Fsmooth)/(70.-5.))
      ENDIF

      HTC=(a*fw*Cw*Ub)/(1.0+F*SQRT(0.5*fw))

      RETURN
      END

C     @@@@@@@@@@@@@ END OF SUBROUTIN HEAT @@@@@@@@@@@@@

C     @@@@@@@@@@@@@@@@@@@@@@@@@@@@@@@@@@@@@@@@@@@@@@@@@

C           FUNCTION FRICTION FOR CALCULATION OF fws

C     @@@@@@@@@@@@@@@@@@@@@@@@@@@@@@@@@@@@@@@@@@@@@@@@@

      FUNCTION FR(fw,RX)
      FF1=1.0/(8.1*SQRT(fw))
      FF2=LOG(1.0/SQRT(fw))
      FF3=LOG(SQRT(RX))
      FR=FF1+FF2+0.135-FF3
      RETURN
      END

C     @@@@@@@@@@@@@@@@@@@@@@@@@@@@@@@@@@@@@@@@@@@@@@@@@
```

APPENDIX C:
HORIZONTAL CLIFF RETREAT PER STORM

Storm Case A

Winds originating between 250° - 50° Beach Width = 2 m

Cliff Height = 35 m Cliff Slope = 50°

Date (D/M/Y)	Duration (hrs)	Wave Height H∞ (m)	Peak Period (s)	Storm Surge (m)	Storm Surge 1.5 multiplier	Horizontal Cliff Retreat R (m)
05/09/1970	27	4.38	9.84	0.84	1.26	0.21
13/09/1970	40	7.27	12.68	0.98	1.46	0.45
29/07/1971	8	4.04	9.45	0.72	1.09	0.02
22/08/1971	37	3.41	8.69	0.82	1.23	0.37
01/09/1972	30	4.61	10.10	0.73	1.10	0.24
11/09/1972	25	3.71	9.06	0.69	1.03	0.16
21/07/1973	8	3.89	9.27	0.82	1.23	0.01
19/08/1974	15	4.00	9.40	0.70	1.05	0.06
02/09/1974	22	3.62	8.95	0.68	1.02	0.13
15/09/1974	29	3.21	8.43	0.66	0.99	0.21
15/10/1974	24	3.08	8.26	0.69	1.04	0.15
05/07/1975	6	5.81	11.33	0.79	1.19	0.01
10/08/1975	26	3.28	8.52	0.72	1.08	0.18
27/08/1975	10	6.03	11.55	0.88	1.32	0.04
06/09/1975	18	3.20	8.41	0.74	1.11	0.09
05/07/1976	42	3.85	9.23	0.72	1.07	0.43
12/08/1976	22	4.45	9.92	0.78	1.17	0.14
21/08/1976	19	5.63	11.16	0.78	1.17	0.10
23/08/1976	8	4.28	9.73	0.75	1.12	0.02
08/09/1976	7	3.05	8.21	0.73	1.09	0.02
21/09/1976	8	3.73	9.08	0.69	1.04	0.02
30/09/1976	6	3.28	8.52	0.75	1.13	0.01
25/06/1977	8	2.99	8.13	0.71	1.07	0.02
28/06/1977	31	3.40	8.67	0.67	1.00	0.24
27/08/1977	25	4.04	9.45	0.82	1.23	0.18
15/10/1977	9	3.59	8.91	0.80	1.20	0.03
23/08/1978	15	3.94	9.34	0.70	1.05	0.06
25/08/1978	6	3.20	8.41	0.73	1.10	0.01
16/09/1978	9	3.47	8.75	0.69	1.03	0.02
01/10/1978	11	3.35	8.60	0.67	1.00	0.03
22/08/1979	13	3.07	8.23	0.65	0.98	0.04
25/07/1980	10	3.93	9.32	0.78	1.16	0.03
30/08/1980	7	3.85	9.23	0.73	1.09	0.02
15/09/1980	22	4.00	9.40	0.70	1.06	0.13
30/09/1980	9	3.31	8.56	0.72	1.08	0.03

Date (D/M/Y)	Duration (hrs)	Wave Height H∞ (m)	Peak Period (s)	Storm Surge (m)	Storm Surge 1.5 multiplier	Horizontal Cliff Retreat R (m)
19/07/1981	6	3.35	8.60	0.70	1.05	0.01
29/07/1981	12	3.96	9.36	0.80	1.20	0.05
02/08/1981	44	3.75	9.10	0.73	1.10	0.47
09/08/1981	8	3.50	8.80	0.79	1.19	0.02
16/08/1981	29	4.85	10.36	0.79	1.19	0.24
29/08/1981	74	3.87	9.25	0.74	1.11	1.05
16/09/1981	32	4.65	10.14	0.80	1.19	0.28
19/09/1981	15	3.59	8.91	0.76	1.14	0.07
27/09/1981	35	3.64	8.97	0.71	1.06	0.31
03/10/1981	42	5.06	10.57	0.81	1.22	0.45
19/07/1982	13	3.55	8.86	0.70	1.05	0.05
27/07/1982	35	4.61	10.10	0.73	1.10	0.32
01/08/1982	7	3.45	8.73	0.67	1.01	0.01
03/08/1982	7	3.08	8.26	0.68	1.02	0.02
18/08/1982	7	4.00	9.40	0.70	1.05	0.02
20/08/1982	36	4.28	9.73	0.71	1.07	0.33
16/09/1982	8	5.70	11.22	0.94	1.41	0.03
03/10/1982	7	3.05	8.21	0.69	1.03	0.02
13/10/1982	6	3.41	8.69	0.67	1.01	0.01
05/09/1983	8	3.55	8.86	0.75	1.12	0.02
15/09/1983	12	3.66	8.99	0.68	1.02	0.04
22/09/1983	15	3.23	8.45	0.75	1.13	0.07
23/09/1983	8	2.91	8.02	0.68	1.02	0.02
24/09/1983	22	3.00	8.15	0.65	0.97	0.12
07/10/1983	15	3.47	8.75	0.67	1.01	0.06
18/07/1984	7	4.24	9.69	0.86	1.29	0.02
11/08/1984	14	3.60	8.93	0.69	1.04	0.05
25/08/1984	43	5.12	10.64	0.83	1.25	0.48
06/07/1985	11	3.31	8.56	0.68	1.02	0.03
27/07/1985	7	3.21	8.43	0.66	0.99	0.01
16/09/1985	48	4.21	9.64	0.73	1.09	0.54
22/08/1986	8	4.30	9.75	0.81	1.21	0.02
03/09/1986	6	4.26	9.71	0.71	1.07	0.01
21/09/1986	10	3.55	8.86	0.73	1.09	0.03
05/10/1986	12	5.97	11.48	0.91	1.36	0.05
28/08/1987	14	4.19	9.62	0.71	1.06	0.05
30/08/1987	25	4.44	9.90	0.72	1.08	0.17
08/09/1987	6	3.87	9.25	0.82	1.23	0.02
01/08/1988	12	3.89	9.27	0.75	1.13	0.04
03/08/1988	28	4.73	10.23	0.79	1.19	0.22
13/08/1988	7	3.35	8.60	0.70	1.05	0.02
08/10/1988	6	3.26	8.49	0.66	0.99	0.01
02/07/1989	6	3.71	9.06	0.69	1.03	0.01
16/09/1989	6	3.57	8.88	0.68	1.02	0.01
18/09/1989	12	4.26	9.71	0.78	1.18	0.05

Date (D/M/Y)	Duration (hrs)	Wave Height H∞ (m)	Peak Period (s)	Storm Surge (m)	Storm Surge 1.5 multiplier	Horizontal Cliff Retreat R (m)
23/06/1990	14	3.41	8.69	0.73	1.09	0.06
27/08/1990	12	3.87	9.25	0.89	1.33	0.05
01/09/1990	26	4.63	10.12	0.79	1.18	0.19
02/09/1990	20	3.76	9.12	0.71	1.07	0.11
07/09/1990	36	3.57	8.88	0.68	1.02	0.32
15/09/1990	14	3.50	8.80	0.67	1.01	0.05
04/08/1991	18	4.11	9.53	0.83	1.24	0.10
23/08/1991	30	3.13	8.32	0.67	1.01	0.23
08/10/1991	7	3.71	9.06	0.75	1.13	0.02
13/08/1992	9	3.76	9.12	0.75	1.13	0.03
22/09/1992	9	3.35	8.60	0.67	1.00	0.02
04/10/1992	8	3.31	8.56	0.67	1.00	0.02
12/07/1993	16	3.20	8.41	0.66	0.99	0.06
24/07/1993	13	3.12	8.30	0.66	0.98	0.04
30/07/1993	7	3.08	8.26	0.71	1.06	0.02
07/08/1993	11	4.07	9.49	0.70	1.06	0.03
09/08/1993	9	3.47	8.75	0.67	1.01	0.02
17/09/1993	16	4.59	10.08	0.85	1.28	0.08
21/09/1993	38	5.97	11.48	0.90	1.35	0.40
27/09/1993	25	3.54	8.84	0.68	1.01	0.16
01/10/1993	37	4.17	9.60	0.81	1.22	0.37
12/10/1993	29	3.82	9.19	0.69	1.04	0.22
18/08/1994	16	6.17	11.68	0.88	1.32	0.08
22/08/1994	9	3.30	8.54	0.83	1.25	0.03
27/09/1994	9	3.59	8.91	0.72	1.08	0.02
24/06/1995	9	4.09	9.51	0.85	1.27	0.03
28/08/1995	6	3.45	8.73	0.74	1.11	0.01
27/08/1996	6	3.10	8.28	0.66	0.99	0.01
04/10/1996	13	4.77	10.27	0.81	1.21	0.05
13/08/1997	8	3.50	8.80	0.82	1.24	0.03
27/08/1999	6	4.24	9.69	0.73	1.09	0.01
24/09/1999	36	3.43	8.71	0.84	1.26	0.36
27/09/1999	6	3.93	9.32	0.70	1.04	0.01
11/08/2000	27	4.71	10.21	0.74	1.10	0.20

Storm Case B

Winds originating between 60° - 160° Beach Width = 4 m

Cliff Height = 20 m Cliff Slope = 25°

Date (D/M/Y)	Duration (hrs)	Wave Height H∞ (m)	Peak Period (s)	Storm Surge (m)	Storm Surge 1.5 multiplier	Horizontal Cliff Retreat R (m)
06/08/1977	7	3.35	8.60	0.67	1.00	0.01
04/07/1978	7	3.85	9.23	0.69	1.04	0.02
05/09/1978	21	2.91	8.02	0.67	1.01	0.11
19/09/1978	29	3.55	8.86	0.73	1.09	0.23
06/10/1978	8	3.45	8.73	0.67	1.01	0.02
08/10/1978	23	3.50	8.80	0.76	1.14	0.15
27/07/1979	14	2.92	8.04	0.65	0.97	0.05
03/10/1979	17	3.48	8.78	0.72	1.08	0.08
09/10/1979	9	3.73	9.08	0.84	1.26	0.03
02/07/1980	12	3.12	8.30	0.66	0.99	0.04
17/08/1980	6	3.16	8.36	0.71	1.06	0.01
01/09/1980	8	3.23	8.45	0.68	1.02	0.02
26/09/1980	31	3.66	8.99	0.69	1.03	0.25
19/06/1981	12	3.03	8.19	0.69	1.04	0.04
20/08/1981	25	3.68	9.01	0.78	1.16	0.18
18/09/1981	10	4.59	10.08	0.74	1.11	0.03
20/09/1982	6	3.54	8.84	0.70	1.05	0.01
02/07/1983	13	3.69	9.04	0.69	1.03	0.05
30/09/1983	7	3.28	8.52	0.83	1.24	0.02
30/06/1988	15	4.04	9.45	0.70	1.05	0.06
01/07/1988	9	3.89	9.27	0.69	1.04	0.02
02/07/1988	8	4.32	9.77	0.72	1.07	0.02
08/08/1999	6	3.80	9.17	0.70	1.05	0.01

Storm Case C

Winds originating between 170° - 240° Beach Width = 6 m

Cliff Height = 5 m Cliff Slope = 10°

Date (D/M/Y)	Duration (hrs)	Wave Height H∞ (m)	Peak Period (s)	Storm Surge (m)	Storm Surge 1.5 multiplier	Horizontal Cliff Retreat R (m)
22/06/1977	13	3.38	8.65	0.81	1.21	0.05
08/08/1984	10	3.30	8.54	0.76	1.14	0.03
19/07/1989	6	3.45	8.73	0.71	1.07	0.01